Defense Threat Reduction Agency
8725 John J. Kingman Road, MS-6201
Fort Belvoir, VA 22060-6201

DTRA-TR-15-12

TECHNICAL REPORT

A Model of Medical Countermeasures for Vesicant Exposure

October 2015

HDTRA1-10-C-0025

Jason Rodriguez, et al.

Prepared by:
Applied Research Associates, Inc.
801 N. Quincy Street
Suite 700
Arlington, VA 22203

Report Documentation Page

Form Approved
OMB No. 0704-0188

1. REPORT DATE	2. REPORT TYPE	3. DATES COVERED
OCT 2015		**15-04-2010 to 14-04-2013**

4. TITLE AND SUBTITLE
A Model of Medical Countermeasures for Vesicant Exposure

5a. CONTRACT NUMBER
5b. GRANT NUMBER
5c. PROGRAM ELEMENT NUMBER

6. AUTHOR(S)

5d. PROJECT NUMBER
5e. TASK NUMBER
5f. WORK UNIT NUMBER

7. PERFORMING ORGANIZATION NAME(S) AND ADDRESS(ES)
Applied Research Associates, Inc.,,801 N. Quincy,Suite 700,,Arlington,,VA, 22203

8. PERFORMING ORGANIZATION REPORT NUMBER

9. SPONSORING/MONITORING AGENCY NAME(S) AND ADDRESS(ES)

10. SPONSOR/MONITOR'S ACRONYM(S)
11. SPONSOR/MONITOR'S REPORT NUMBER(S)

12. DISTRIBUTION/AVAILABILITY STATEMENT
Approved for public release; distribution unlimited

13. SUPPLEMENTARY NOTES

14. ABSTRACT
This paper describes a toxicokinetic/dynamic model of percutaneous exposure to several vesicants. The model also predicts the efficacy of proposed medical countermeasures via a pharmacokinetic/dynamic model of scavenger, cell-cycle inhibitor, PARP inhibitor, protease inhibitor, and anti-inflammatory treatment regimens.

15. SUBJECT TERMS

16. SECURITY CLASSIFICATION OF:			17. LIMITATION OF ABSTRACT	18. NUMBER OF PAGES	19a. NAME OF RESPONSIBLE PERSON
a. REPORT	b. ABSTRACT	c. THIS PAGE			
unclassified	**unclassified**	**unclassified**	**Same as Report (SAR)**	**116**	

DESTRUCTION NOTICE:

Destroy this report when it is no longer needed.
Do not return to sender.

PLEASE NOTIFY THE DEFENSE THREAT REDUCTION AGENCY, ATTN: DTRIAC/ J9STT, 8725 JOHN J. KINGMAN ROAD, MS-6201, FT BELVOIR, VA 22060-6201, IF YOUR ADDRESS IS INCORRECT, IF YOU WISH THAT IT BE DELETED FROM THE DISTRIBUTION LIST, OR IF THE ADDRESSEE IS NO LONGER EMPLOYED BY YOUR ORGANIZATION.

REPORT DOCUMENTATION PAGE

Form Approved
OMB No. 0704-0188

1. REPORT DATE *(DD-MM-YYYY)*	**2. REPORT TYPE**	**3. DATES COVERED** *(From - To)*
00-10-2015	Technical	April 15, 2010 - April 14, 2013

4. TITLE AND SUBTITLE

A Model of Medical Countermeasures for Vesicant Exposure

5a. CONTRACT NUMBER

HDTRA1-10-C-0025

5b. GRANT NUMBER

5c. PROGRAM ELEMENT NUMBER

6. AUTHOR(S)

Jason Rodriguez
Glen I. Reeves
Gene E. McClellan

5d. PROJECT NUMBER

5e. TASK NUMBER

5f. WORK UNIT NUMBER

7. PERFORMING ORGANIZATION NAME(S) AND ADDRESS(ES)

Applied Research Associates, Inc.
801 N. Quincy
Suite 700
Arlington, VA 22203

8. PERFORMING ORGANIZATION REPORT NUMBER

9. SPONSORING / MONITORING AGENCY NAME(S) AND ADDRESS(ES)

Defense Threat Reduction Agency
8725 John J. Kingman Road, STOP 6201
Fort Belvoir, VA 22060-6201

10. SPONSOR/MONITOR'S ACRONYM(S)

DTRA

11. SPONSOR/MONITOR'S REPORT NUMBER(S)

DTRA-TR-15-12

12. DISTRIBUTION / AVAILABILITY STATEMENT

Distribution Statement A. Approved for public release; distribution is unlimited.

13. SUPPLEMENTARY NOTES

This work was sponsored by the Defense Threat Reduction Agency.

14. ABSTRACT

This paper describes a toxicokinetic/dynamic model of percutaneous exposure to several vesicants. The model also predicts the efficacy of proposed medical countermeasures via a pharmacokinetic/dynamic model of scavenger, cell-cycle inhibitor, PARP inhibitor, protease inhibitor, and anti-inflammatory treatment regimens.

15. SUBJECT TERMS

CWAs Vesicants Pharmacokinetics Toxicokinetics Countermeasures

16. SECURITY CLASSIFICATION OF:			**17. LIMITATION OF ABSTRACT**	**18. NUMBER OF PAGES**	**19a. NAME OF RESPONSIBLE PERSON**
a. REPORT	**b. ABSTRACT**	**c. THIS PAGE**	SAR	116	Dr. Christopher Kiley
Unclassified	Unclassified	Unclassified			**19b. TELEPHONE NUMBER** *(include area code)* 703-767-3460

CONVERSION TABLE

Conversion Factors for U.S. Customary to metric (SI) units of measurement.

MULTIPLY →	BY →	TO GET
← TO GET	← BY	← DIVIDE
angstrom	1.000 000 x E -10	meters (m)
atmosphere (normal)	1.013 25 x E +2	kilo pascal (kPa)
bar	1.000 000 x E +2	kilo pascal (kPa)
barn	1.000 000 x E -28	meter^2 (m^2)
British thermal unit (thermochemical)	1.054 350 x E +3	joule (J)
calorie (thermochemical)	4.184 000	joule (J)
cal (thermochemical/cm^2)	4.184 000 x E -2	mega joule/m^2 (MJ/m^2)
curie	3.700 000 x E +1	*giga bacquerel (GBq)
degree (angle)	1.745 329 x E -2	radian (rad)
degree Fahrenheit	$t_k = (t^of + 459.67)/1.8$	degree kelvin (K)
electron volt	1.602 19 x E -19	joule (J)
erg	1.000 000 x E -7	joule (J)
erg/second	1.000 000 x E -7	watt (W)
foot	3.048 000 x E -1	meter (m)
foot-pound-force	1.355 818	joule (J)
gallon (U.S. liquid)	3.785 412 x E -3	meter^3 (m^3)
inch	2.540 000 x E -2	meter (m)
jerk	1.000 000 x E +9	joule (J)
joule/kilogram (J/kg) radiation dose absorbed	1.000 000	Gray (Gy)
kilotons	4.183	terajoules
kip (1000 lbf)	4.448 222 x E +3	newton (N)
kip/inch^2 (ksi)	6.894 757 x E +3	kilo pascal (kPa)
ktap	1.000 000 x E +2	newton-second/m^2 ($N-s/m^2$)
micron	1.000 000 x E -6	meter (m)
mil	2.540 000 x E -5	meter (m)
mile (international)	1.609 344 x E +3	meter (m)
ounce	2.834 952 x E -2	kilogram (kg)
pound-force (lbs avoirdupois)	4.448 222	newton (N)
pound-force inch	1.129 848 x E -1	newton-meter (N-m)
pound-force/inch	1.751 268 x E +2	newton/meter (N/m)
pound-force/foot^2	4.788 026 x E -2	kilo pascal (kPa)
pound-force/inch^2 (psi)	6.894 757	kilo pascal (kPa)
pound-mass (lbm avoirdupois)	4.535 924 x E -1	kilogram (kg)
pound-mass-foot^2 (moment of inertia)	4.214 011 x E -2	kilogram-meter^2 ($kg-m^2$)
pound-mass/foot^3	1.601 846 x E +1	kilogram-meter^3 (kg/m^3)
rad (radiation dose absorbed)	1.000 000 x E -2	**Gray (Gy)
roentgen	2.579 760 x E -4	coulomb/kilogram (C/kg)
shake	1.000 000 x E -8	second (s)
slug	1.459 390 x E +1	kilogram (kg)
torr (mm Hg, 0^0 C)	1.333 22 x E -1	kilo pascal (kPa)

*The bacquerel (Bq) is the SI unit of radioactivity; 1 Bq = 1 event/s.

**The Gray (GY) is the SI unit of absorbed radiation.

Table of Contents

List of Figures

List of Tables

Preface

The research and development work described in this report was conducted under subcontract for Gryphon Scientific, LLC (Gryphon) for the Joint Science and Technology Office (JSTO) of the Department of Defense (DoD) Chemical and Biological Defense (CBD) Program. JSTO is also the Chemical/Biological Technologies (CB) Directorate in the Research and Development (RD) Enterprise of the Defense Threat Reduction Agency (DTRA). Contract HDTRA1-10-C-0025 is titled *Medical Countermeasures for CBR Agents*.

This project was initiated by Ms. Nancy Nurthen, of the Information Systems Capability Development Division (J9-CB) and continued by Dr. Christopher Kiley. It was funded under DTRA Contract Number HDTRA1-10-C-0025 to Gryphon Scientific, LLC, with subcontractor Applied Research Associates, Inc. (ARA). The target application for the product of this contract is under the auspices of the Joint Project Manager for Information Systems (JPM IS) of the Joint Program Executive Office for Chemical and Biological Defense (JPEO-CBD).

Section 1.

Executive Summary

This paper expands on the model of sulfur mustard (HD) exposures and medical countermeasures (MCMs) presented to the Defense Reduction Agency (DTRA) in 2011, (Rodriguez, Reeves, & McClellan, 2011) to a generic vesicant model (GVM). The GVM was developed to predict the effect of inhalation, ocular, and percutaneous exposures in healthy individuals and the efficacy of available and proposed treatments. The baseline models of vesicant exposure use a series of rate equations to describe the following:

- The distribution of vesicants at the injury site and throughout the body.
- The fragmentation of DNA and suppression of glutathione caused by the exposure to vesicants in the nuclei of exposed cells.
- The series of reactions that result in necrotic and apoptotic epithelial cell death at three different exposure sites.
- Systemic oxidative stress.

The MCM models modify the injury equations and capture the therapeutic effects of the countermeasure. In expanding the HD model to the GVM we added parameters for four additional agents, including three nitrogen mustard analogues (HN-1, HN-2, and HN-3), and lewisite. The MCMs included in the framework are the same as those considered for the HD model: bioscavengers, cell-cycle inhibitors, poly(ADP-ribose) polymerase-1 (PARP) inhibitors, protease inhibitors, and anti-inflammatories. We have removed calcium modulators from the framework, as continued research shows that the countermeasures offer no therapeutic effect. Additionally, we included the chelating compound British anti-lewisite (BAL), an antidote against systemic lewisite poisoning.

This page is intentionally left blank.

Section 2.

Introduction and Purpose

Accurate modeling of medical countermeasure efficacy against chemical, biological, and radiological (CBR) agents is essential to understanding the vulnerability of our warfighters on the modern battlefield. In helping calculate the benefit of countermeasures, modeling can inform data-driven purchasing decisions and logistical tradeoffs. In this study, Gryphon Scientific and Applied Research Associates, Inc. (ARA) have developed models to predict the efficacy of medical countermeasures against a variety of agents.

This report (prepared by ARA) is one of ten, describing the medical countermeasure models constructed for this project. This volume focuses exclusively on the methods used to construct the Generic Vesicant Model (GVM), outlines how to use the model, and provides examples of the outputs generated by the model. Other volumes describe models for B. anthracis (volume 1), organophosphates (volume 2), cesium-137 (volume 3), F. tularensis (volume 4), americium-241 (volume 6), botulinum toxin (volume 8), plutonium-238/239 (volume 9), and plague (volume 11). Each volume begins by briefly introducing the agent modeled and the countermeasures available for use against the agent. The overall schematic of each model and the relevant parameters are then discussed, along with a brief explanation of the rationale for selecting each parameter. Lastly, this report discusses the calculations and computational framework of the Berkeley Madonna model and provides examples of modeling outputs. We published the Berkeley Madonna source code in the appendix.

2.1 Summary of Deliverables

Below is a description of the four deliverables assigned for each agent of interest, and a description of what is included in each deliverable. The third numbered item (the "MCM Model" deliverable) is the deliverable presented in this interim report.

2. Modeling Approach

The modeling approach deliverable describes each of the parameters that we anticipate including in our MCM model. For each parameter, a description of the approach for developing and justifying the parameter is presented. The approach developed is based on prior knowledge of the agent and on the general types of data available for each agent, but specific citations are not included as it is a preliminary document.

3. Modeling Parameters

The modeling parameters deliverable defines the value or function for each parameter used to develop the MCM model. Each parameter is supported with a description of the rationale for choosing the parameter, including any scientific evidence used in parameter development or assumptions that were made.

4. MCM Model (This Report)

In addition to the information already developed in the "Modeling Parameters" deliverable, the "MCM Model" includes a description of the model, user inputs, the model calculations, and

the model outputs. For the chemical agents, the report is an accompaniment to a preliminary implementation of the MCM model built in Berkeley Madonna.

5. MCM Model in a Graphical User Interface (GUI)

The MCM models will be implemented in their final version in a graphical user interface. This implementation of the model will include feedback and adjustments made after review of the previous deliverables.

2.2 GVM Description

The basis for casualty and fatality, estimation resulting from vesicant injuries, will be the NATO Planning Guide for Estimation of CBRN Casualties Ratification Draft 1 (AMedP-8 (C) RD.1) (NATO, February 2010). AMedP-8 (C) defines dose and time-dependent sign/symptom profiles for ocular, percutaneous, and inhalation exposures to HD. Since we are expanding this model to four additional vesicants and including the effects of systemic distribution and oxidative stress caused by glutathione suppression, we need to expand our criteria for injury and fatalities beyond the sign/symptom profiles and methodologies defined in AMedP-8 (C). In this document, we will describe our proposed mechanisms for incorporating these agents and injury mechanisms, while keeping with the thrust and goals of AMedP-8 (C). We have compared the toxicity and injury mechanisms of these new agents with the toxicity and injury mechanisms of HD, to make as much use as possible of the AMedP-8 (C) injury profiles. For some agents, such as the nitrogen mustard analogues, the near equivalence of toxicity and effect to that of HD was a simple task, when compared to published toxicity data in Army Field Manual 3.11-9 (FM 3.11-9) (Army, 2005) and the EPA (EPA, Acute Exposure Guideline Levels for Selected Airborne Chemicals: Volume 3, 2003) (EPA, 2007).

This model represents a significant departure from the HD model. We revisited the HD framework and made an almost complete change to the skin injury model in order to develop the GVM. We did this because we quickly realized that to use the HD framework for the GVM, we would need to fit all 13 rate parameters, developed for the HD model, for each individual agent. However, most of the rates that we were modeling are completely independent of the vesicant. For example, the rate of mitosis is a mechanism intrinsically tied to the workings of a cell and will not change when a vesicant is introduced into the system. We revisited the literature we used to develop the HD model and included some new studies. These studies define equations that represent the underlying biological mechanisms in such a way that they are no longer correlated with the insulting agent and, instead, are correlated with generic cellular injury and response. The resulting model is much more elegant, reducing the fits to three vesicant-related rate parameters, only one of which (the rate at which the vesicant binds with and fragments the DNA) changes for each insulting agent. The GVM now has a much stronger foundation in the published data and a well-defined process for modifying parameters as the data becomes available.

Section 3.

Development Environment

The MCM model for vesicant exposure was developed and tested in Berkeley Madonna v8.3.18. Berkeley Madonna is a differential equation solver ideal for modeling rate equations, allowing users to modify inputs, and perform batch runs to test model sensitivity and response. Since the vesicant MCM model is a series of rate equations designed to model DNA fragmentation and the resulting effects, Berkeley Madonna provides a robust environment for model development and testing.

Berkeley Madonna does not export source code into libraries that are useable in C++, Java, or other production languages. Additionally, external programs cannot link into Berkeley Madonna's runtime environment. We have developed a C# differential equation solver that will act as a production code framework for the finalized model. For simplicity of reproduction and equation analysis, we have included the Berkeley Madonna source code at the end of this document. Berkeley Madonna is free to download, but you cannot save the source code without purchasing a copy. However, you can copy and paste the source code into Berkeley Madonna in order to use the model.

On January 15th, 2013, ARA delivered the first version of the C# implementation of this model to DTRA for review. On February 27th, 2013, a revised version was delivered to DTRA, IDA, and Gryphon Scientific. The C# implementation is designed to run on any Windows PC and does not require installation.

This page is intentionally left blank.

Section 4.

Vesicant Injury Mechanics

The model framework for the GVM begins with normal cellular function in the skin and systemic system before vesicant exposure. The model then estimates changes in cellular function, in the event of vesicant exposure. The initial version of this paper included injury to the eyes and the lungs in the model, but ARA agreed to remove those systems from the final model after independent review from the Institute of Defense Analysis (IDA), due to a lack of supportive data to incorporate these models. We have preserved the discussion in Appendix A.

4.1 Normal Cellular Function

The model is based on a cell population with four cellular states, summarized in Table 4-1.

Table 4-1. The Four Cellular States Included in the Model

N_n	Proportion of cells with uninjured DNA
N_i	Proportion of cells with injured DNA
$N_{k,a}$	Proportion of killed, apoptotic (irreparably damaged DNA) cells
$N_{k,n}$	Proportion of killed, necrotic (irreparably damaged DNA) cells

This is a departure from the HD model, which lumped apoptotic and necrotic cells into a generic "killed cells" compartment. The differentiation between apoptotic and necrotic cells is important for two reasons:

1. Necrotic cells result from the severe depletion of NAD+ and ATP, which in turn signals protease and leads to vesication and severe blistering (Kehe, Balszuweit, Steinritz, & Thiermann, 2009) (Kehe & Szinicz, 2005). Since severity of vesication is the metric for injury severity in our model, this is an important distinction. Whereas we won't see large differences in untreated individuals following vesicant exposure, we will see large differences in individuals treated with PARP inhibitors.
2. PARP inhibitors, which have been shown to have no effect on the gross viability of cells or level of vesication (Atkins, Lodhi, Hurley, & Hinshaw, 2000), but have a great effect on the distribution of necrotic and apoptotic cells (Kehe K. , 2008). In the HD model implementation, we saw that our model predicted no therapeutic effect when PARP inhibitors were administered. However, for skin injuries, the therapeutic effect can actually be significant if vesication is minimized.

For this implementation of the model, we only consider percutaneous injuries and systemic injuries. For systemic injuries, we will only consider the systemic concentration of vesicants in this model and correlate the concentration of vesicant to acute lethality using probit analysis from the toxicity data presented in FM 3.11-9 (Army, 2005)

We will routinely use the term "relative concentration" throughout this report. Essentially, the model does not attempt to estimate the actual molar concentration of any chemical, molecule, or cell included in the framework. Instead, it attempts to measure the increase (or decrease) of concentrations for each chemical, molecule, or cell included in the model. In order to achieve this, we set initial conditions, so that any chemical, model, or cell that increases in concentration as a result of vesicant exposure has an initial relative concentration of 0.0. Any chemical, model, or cell that decreases as a result of vesicant exposure has an initial relative concentration of 1.0.

The model assumes that, prior to vesicant exposure, the relative concentrations of normal, healthy cells in the skin are 1.0 and the relative concentration of injured and killed cells is 0.0. These values signify that 100% of the cells in the area of interest are normal, 0% are injured, and 0% are killed. The model does not attempt to estimate actual cell concentrations, rather the fraction of cells above or below the normal percentage. In the event of injury, the relative concentration of normal cells will decrease while fractured and killed cells will increase. During the recovery phase, the relative concentration of normal, healthy cells will approach 1, while the relative concentration of injured cells will approach 0. The relative concentration of killed cells is cumulative and will never return to 1.

In addition to the three cell states, the model also predicts relative concentrations of PARP, NAD, protease, inflammatory cells, glutathione (GSH), ATP, and calcium ions. All of these chemicals are assumed to be present in each cell before vesicant exposure, making their relative concentrations equal to either 1.0 or 0.0, depending on whether their concentration increases or decreases. Following exposure, some of these elements will decrease to zero (NAD, for instance, which depletes during DNA repair) and some of these elements will increase to 1.0 or higher (protease, for instance, which is used to break down killed cells).

4.2 Injury Mechanisms

The differences in vesicant-related skin, eye, lung, and other tissue injuries were discussed in the HD model. We will not discuss the ocular and inhalation injury mechanisms in this paper, as they are not included in the final GVM. We will discuss enhancements to the skin and systemic systems; however, that is meant to augment the discussion in the original HD paper. The types of injured and killed cells considered in the model are listed in Table 4-2.

Table 4-2. Types of Injured and Killed Cells

Variable	Cell Type
N_I	Injured skin cell
$N_{K,A}$	Apoptotic skin cell
$N_{K,N}$	Necrotic skin cell

For systemic injuries, we will only consider the concentration of vesicant in the circulatory system in this model and correlate the concentration to acute lethality, described later.

4.2.1. Skin

The skin and mucous membranes, which cover most of the body and account for over 10% of its mass, provide a protective layer against environmental toxins, injurious substances, and pathogens. The outer layer of the skin (stratum corneum) functions as a barrier and prevents most materials from absorption through the lower epidermal layers into the dermis and deeper tissues, including the systemic circulation (Centers for Disease Control and Prevention (CDC), 2010). Figure 4-1 shows the different layers of the skin. In the GVM, we now account for the distribution of vesicant across these different layers, focusing on the stratum corneum, the basal epidermis, the dermis, and the vascular system.

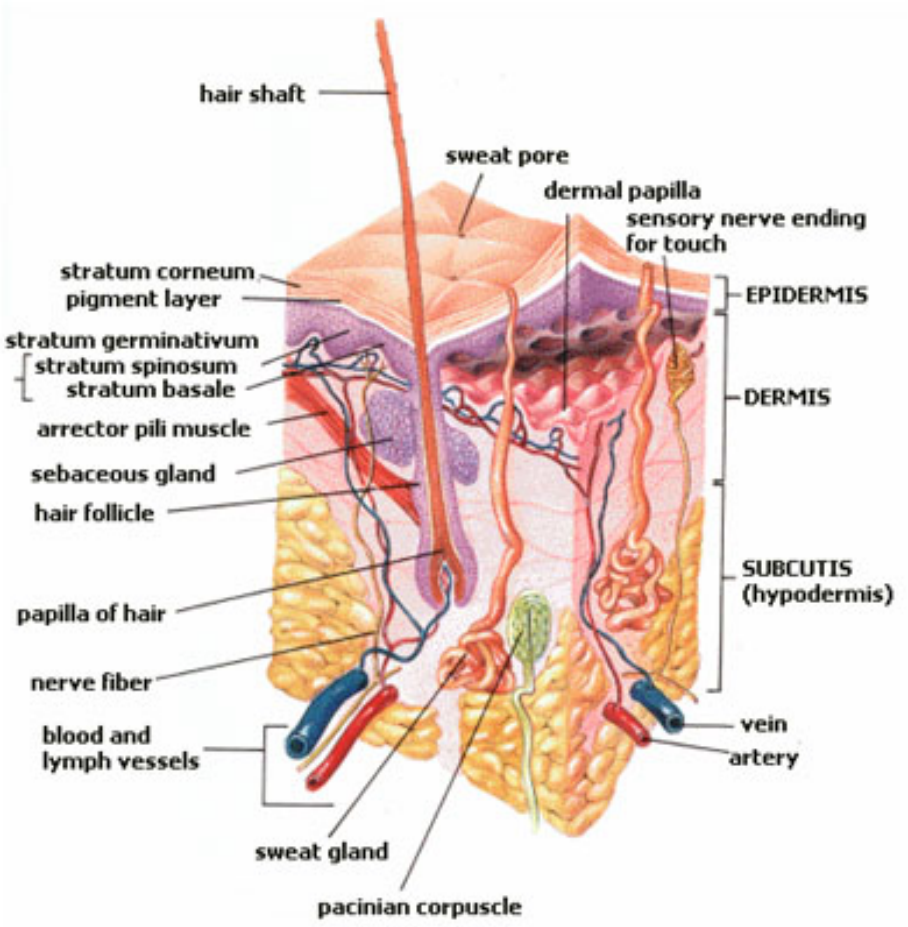

Figure 4-1. Cross-Section of Skin (SEER Training: Layers of the Skin)

As mentioned in the original HD paper, vesication and severe blistering are primarily achieved when vesicants enter the basal epidermis and dermis, alkalizing the healthy DNA and causing necrotic cell death. The toxicokinetic model that we implemented for the GVM and describe in section 4.3 estimates the proportion of HD applied to the skin that ends up in the basal epidermis and the dermis, leading to vesication. Additionally, we included a mechanism that accounts for GSH suppression, which has been shown to increase oxidative stress and acute toxicity. We made another enhancement to the injury mechanism in the skin to differentiate

between apoptotic and necrotic cell death, for reasons stated in the preceding section. Once again, we make this distinction in the basal epidermis and dermis layers of the skin and correlate necrotic cell death to vesication.

The mechanism that differentiates apoptotic and necrotic cell death is still being studied, but sufficient new information was published to allow us to include the differentiation into the model. We found several earlier studies that looked at the effect of N-acetylcysteine (NAC, which is included in our model as a bioscavenger) against both nitrogen mustard (Weltin, et al., 1996) and sulfur mustard (Greenberg, Kamath, Petrali, Hamilton, Garfield, & Garlick, 2006) (Atkins, Lodhi, Hurley, & Hinshaw, 2000) injuries with data that originally led us to believe that apoptosis was the primary injury mechanism for vesication and blistering.

However, more recent papers have shown that necrosis plays a very important role in vesication and is the cause of severe injuries in people exposed to vesicants. Nicotera & Melino (Nicotera & Melino, 2004), who were not working with vesicant exposures, presented evidence that the apoptotic-necrotic switch was a complicated process, originally believed to be tied exclusively to capsases (the HD model we developed even used protease concentrations as a precursor to cell death and vesication), but now shows significant evidence that it is, in fact, tied to ATP depletion. The paper presents a complicated model of ATP regulation, but for our purposes, we can simply focus on relative ATP concentration in order to shift the weighting between apoptotic and necrotic cell death. Figure 4-2, which was taken from Nicotera & Melino's paper, shows the simplified model of apoptosis/necrosis dependence on ATP levels.

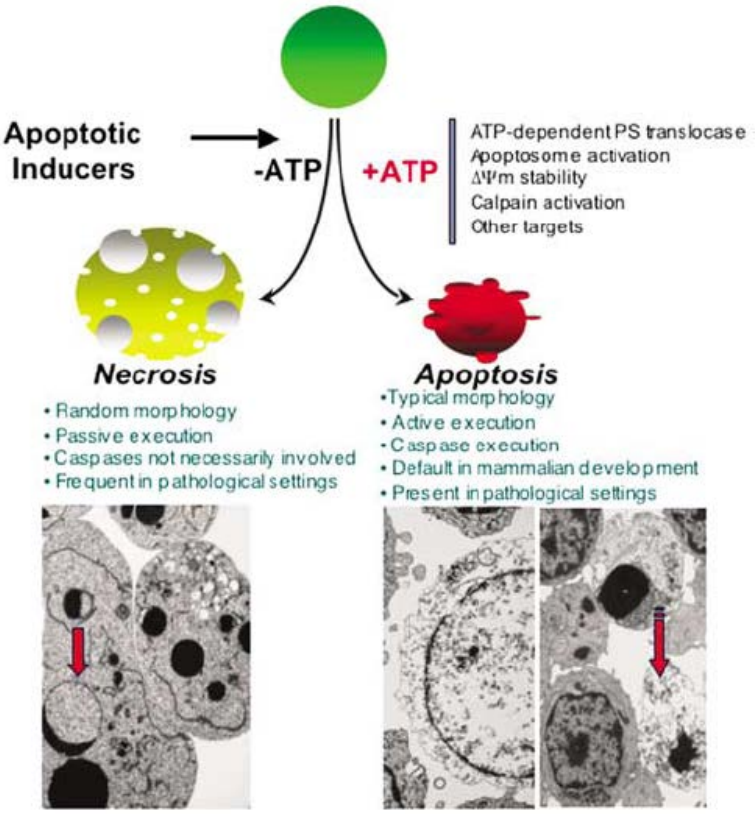

Figure 4-2. Apoptosis-Necrosis Switch by ATP (Nicotera & Melino, 2004)

Tying this into the GVM, our model accounts for NAD+ depletion which, in turn, leads to a depletion of ATP. We did not include ATP in the HD model, but we now include it in the GVM. The vesicant research community has recently published papers that also strengthen the argument for ATP levels being a regulator of necrosis and apoptosis and also determines how the differentiation relates to the type of vesicant injury. Figure 4-3 is from a paper published by Kehe, et. al (Kehe, Balszuweit, Steinritz, & Thiermann, 2009) of a study that aimed to show how NAD+/ATP depletion and necrosis is concentration-dependent, meaning large doses of HD lead to a severe depletion of NAD+ and ATP, which in turn lead to an increase in necrotic cells.

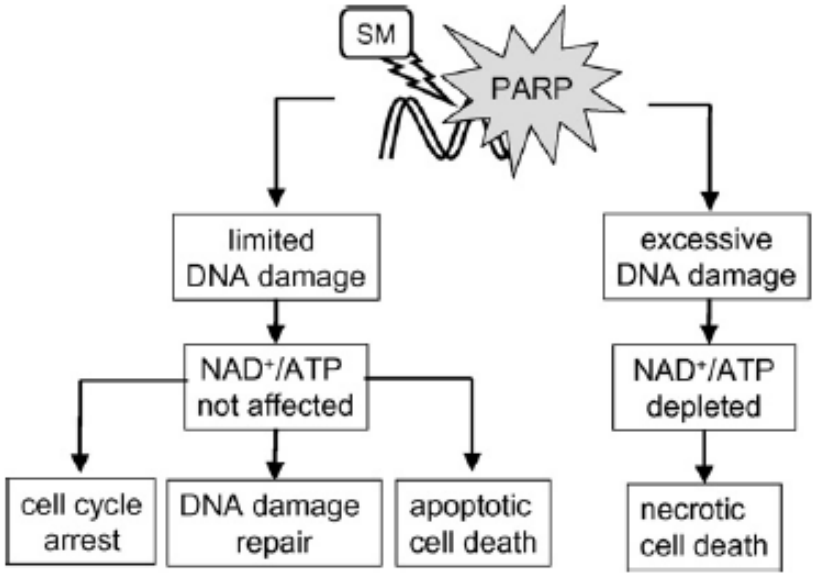

Figure 4-3. Apoptosis and Necrosis Determination Following HD Exposure (Kehe, Balszuweit, Steinritz, & Thiermann, 2009)

Another recent study (Debiaka, Keheb, & Bürkle, 2009) also correlated NAD+ depletion to necrosis and blister formation in HD exposures. Figure 4-4, which was taken from the paper, once again shows how PARP activity leads to NAD+ depletion, necrosis, and eventually inflammation and tissue damage. In the Debiaka, et. al. model, there is an additional pathway to necrosis presented that comes from imperfect DNA repair. This pathway could be considered for future investigation and research in future development of the GVM.

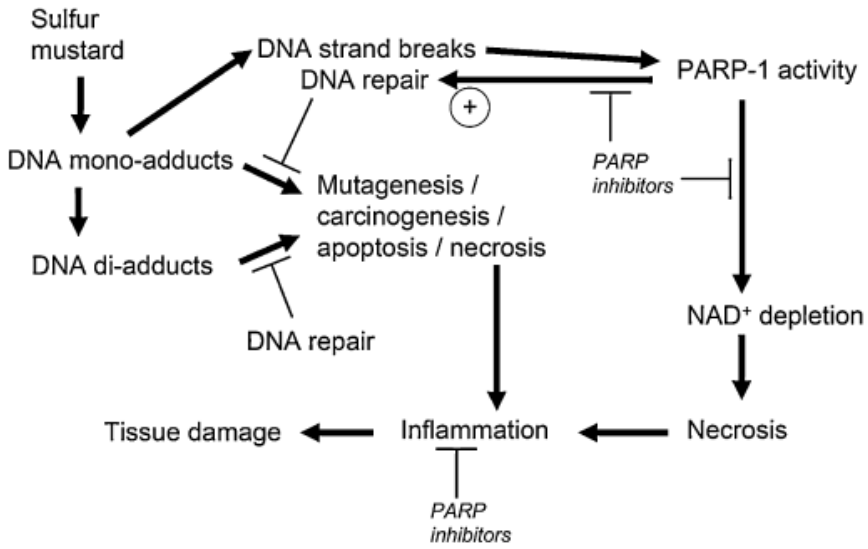

Figure 4-4. Detalied Diagram of Apoptosis/Necrosis Related to HD Injury (Debiaka, Keheb, & Bürkle, 2009)

Also, in a recent study of human exposures (Pita & Vidal-Asensi, 2010), the authors state, "In severe lesions, particularly those due to exposure to the liquid agent, necrosis occurs and they become more susceptible to secondary infections that can complicate the course of the lesion." This statement strengthens the argument that large doses result in blister formation and, eventually, necrosis. In the same paper, the author also states the outer-most layer of some blisters in human injuries is "completely necrotic."

4.2.2. Systemic

The toxicokinetic model also allows us to measure the proportion of vesicant that enters the circulatory system. We are not yet including a model of systemic injury, but we are modeling GSH suppression in following systemic distribution that occurs primarily in the bone marrow, gastrointestinal tract, and the CNS (Pitaa & Vidal-Asensib, 2010). The bone marrow suppression leads to the second cause of death outside of acute respiratory failure. Due to time constraints and a current lack of data, we will not model bone marrow suppression and the subsequent bacterial pneumonia, but will instead tie all of systemic injuries to oxidative stress caused by the systemic dose. The model being used here is likely incomplete, but the mechanism of correlating a percutaneous dose to systemic dose to lethality is well founded. Our first step will be to use the toxicokinetic model to estimate the quantity of applied dose that ends up in the circulatory system. The second step would be to predict the level of glutathione suppression resulting from this systemic dose. The third step would be to use the toxicity values published by ECBC, for all of the vesicants of interest, to correlate systemic dose and glutathione suppression levels to the LD_{50} and probit for percutaneous dose. Although we are missing the finer resolution that a complete systemic model would require, we believe that we have a model that ties systemic dose to lethality. The model will allow us to account for chelating therapy using British anti-lewisite (BAL), which removes lewisite from the circulatory system and will also allow us to better include the beneficial effects of bioscavengers like NAC, which work to increase the level of free GSH in the body.

Section 5.

Vesicant Exposure Model

Unlike with the HD model, we are only considering percutaneous exposures in the GVM. In this section, we will revisit the percutaneous exposure models as we made a change to the original HD model to account for a correction in the MOPP calculation and we also included a toxicokinetic model for percutaneous distribution in the skin and the blood stream. We have preserved the Inhalation and Ocular exposures in Appendix A.

5.1 Percutaneous

For the GVM, we have expanded the HD percutaneous model to include a toxicokinetic model that predicts vesicant concentration at different stratum of the skin and vesicant that enters the circulatory system and is distributed systemically. This is an important feature for vesicants, as the delayed distribution time of the chemical can help the model better predict delayed onset of effects. The percutaneous model will now make use of a compartmental model that was developed by Cutaneous Pharmacology and Toxicology Center at North Carolina State University (Riviere & al., 1994), illustrated in Figure 5-1.

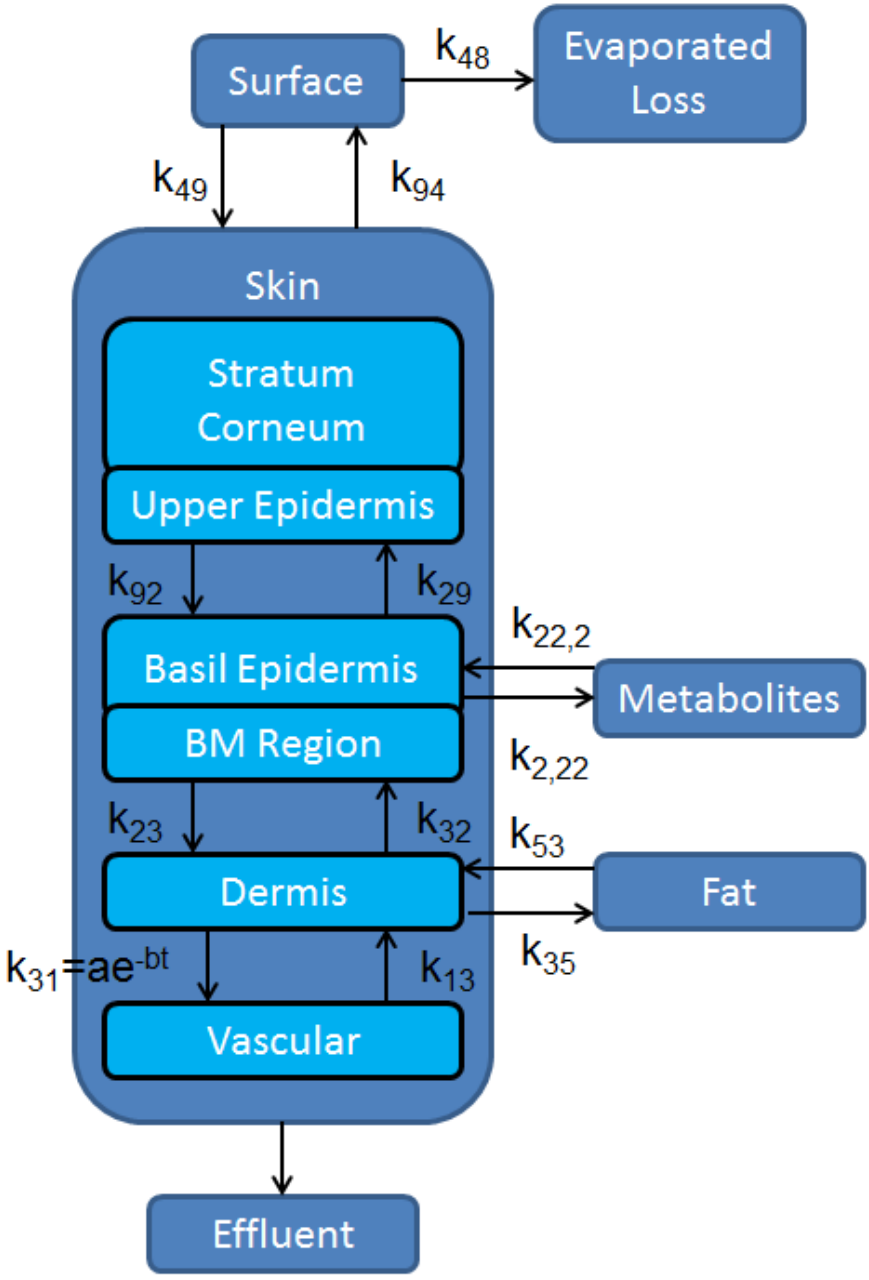

Figure 5-1. Multi-Compartmental Toxicokinetic Model for HD Penetration in the IPPSF (Riviera & al., 1994)

The model was developed using the isolated perfused porcine skin flap (IPPSF) as an analog for human skin. IPPSF was used to study the percutaneous absorption of many different drugs and chemicals (Riviere & Monteiro-Riviere, 1991) (Williams, Carver, & Riviere, 1990). One experiment that documented the absorption of HD using the IPPSF was done by the Cutaneous Pharmacology and Toxicology Center at North Carolina State University in 1997 (Monteiro-Riviere & Inman, 1997). In that study, the morphological similarities between human injuries and HD-induced injury on the IPPSF are very similar. IPPSF is the only human-skin analogue found, to date, that actually produced gross blisters when exposed to HD, much like human

injuries. The model shown in Figure 5-1 has a series of rates that have been derived from experimental data and are given in a Riviere, et al. study (Riviera & al., 1994). The rates are reproduced in Table 5-1.

Table 5-1. Rate Constants for IPPSF HD Deposition Model (Riviera & al., 1994)

Constant	k_{48}	k_{49}	k_{94}	k_{92}	k_{29}	k_{23}	k_{32}	a	b	k_{13}	k_{35}	k_{53}	$K_{2,22}$	$K_{22,2}$
Value (hr)	0.34	0.25	0.23	0.26	0.22	0.24	0.12	0.33	0.0001	0.12	0.0058	0.006	0.12	0.007

The rate constants are used in a series of equations, shown below, that predict the dose of vesicant at each of the compartments. These equations were not defined in the Riviera study, but they take the form of standard rate equations for toxicodynamic processes and we verified the model output (Figure 5-2 - Figure 5-6) against the published results. The equations are shown below.

The concentration of evaporated mustard (*Evap*) off of the surface of the skin (*Surf*):

$$\frac{d}{dt}Evap = k_{48} * Surf \qquad \textbf{(5-1)}$$

The concentration of mustard on the surface of the skin and the relationship between the stratum corneum concentration (*SCorn*):

$$\frac{d}{dt}Surf = k_{94} * SCorn - k_{48} * Surf - k_{49} * Surf \qquad \textbf{(5-2)}$$

The concentration of mustard in the stratum corneum and the relationship between the surface and the basal epidermis concentration (*BEpi*):

$$\frac{d}{dt}SCorn = k_{49} * Surf + k_{29} * BEpi - k_{92} * SCorn - k_{94} * SCorn \qquad \textbf{(5-3)}$$

The concentration of mustard in the basal epidermis and the relationship between the stratum corneum, dermis (*Derm*) and metabolites (*Met*) concentrations:

$$\frac{d}{dt}BEpi = k_{92} * SCorn + k_{32} * Derm + k_{22,2} * Met - k_{23} * BEpi - k_{29} * BEpi - k_{2,22} * BEpi \qquad \textbf{(5-4)}$$

The concentration of mustard in the dermis and the relationship between the basal epidermis, vascular system (*Vas*), and fat (*Fat*) concentrations:

$$\frac{d}{dt}Derm = k_{23} * BEpi + k_{13} * Vas + k_{53} * Fat - a * e^{-b*t} * Derm - k_{32} * Derm - k_{35} * Derm \qquad \textbf{(5-5)}$$

The concentration of mustard in the fat and the relationship between the dermis concentration:

$$\frac{d}{dt}Fat = k_{35} * Derm - k_{53} * Fat \quad \textbf{(5-6)}$$

The concentration of mustard in the metabolites and the relationship between the basal dermis concentration:

$$\frac{d}{dt}Met = k_{2,22} * BEpi - k_{22,2} * Met \quad \textbf{(5-7)}$$

The concentration of mustard in the vascular system and the relationship between the dermis concentration:

$$\frac{d}{dt}Vas = a * e^{-b*t} * Derm - k_{13} * Vas \quad \textbf{(5-8)}$$

This just leaves an equation for effluent mass. We turned to a more recent paper (Riviere & al, 2001) for this calculation and made use of the model:

$$Y(t) = A(e^{-t/\tau_b} - e^{-t/\tau_b}) - e^{-t/\tau_d} \quad \textbf{(5-9)}$$

Where:

1. *Y(t)* is an estimate of the effluent mass. This will be known as the systemic dose, Ds.
2. *A* is the absorbed dose or the mass in the dermis,
3. The first exponential term represents the rate of terminal release of the absorbed chemical, and
4. The second exponential term represents the rate of uptake of the chemical from the skin to the IPPSF

The values of τ_b and τ_d were obtained from Riviera, 2001, and are equal to 39 minutes and 0.7 minutes, respectively. We ran the model with an input surface dose of 3000 µg of HD, as was done in Riviera, 1994, in order to gauge the model output compared to the calculated output. The result of our output is in Figure 5-2 through Figure 5-6. When compared to the output from the referent, we see a near perfect reproduction of the model output (which, in turn, reproduces the experimental data as shown in the referent) for all compartments, except for the effluent mass, which is higher in our model (final mass at 8 hours is equal to 180 µg instead of 110 µg). We attribute this to using an updated effluence model for our implementation, as mentioned above. The next section documents how we use these calculated exposures in the mustard injury model.

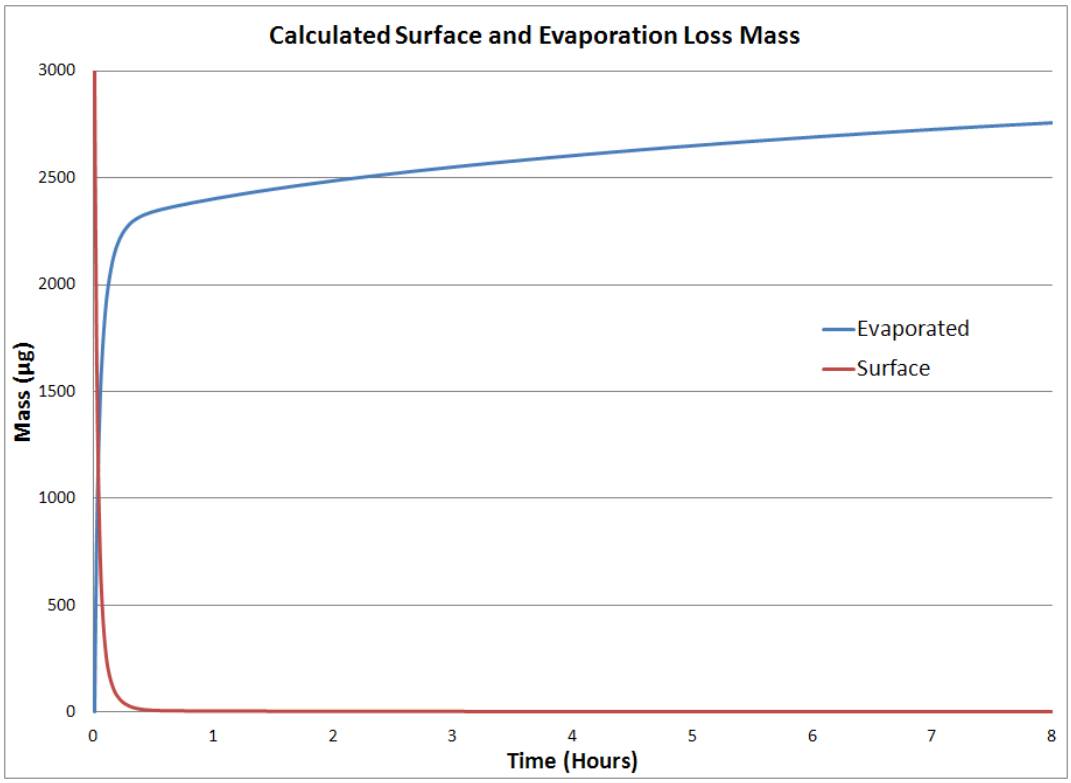

Figure 5-2. Calculated Surface and Evaporation Loss Mass for 3000µg of HD

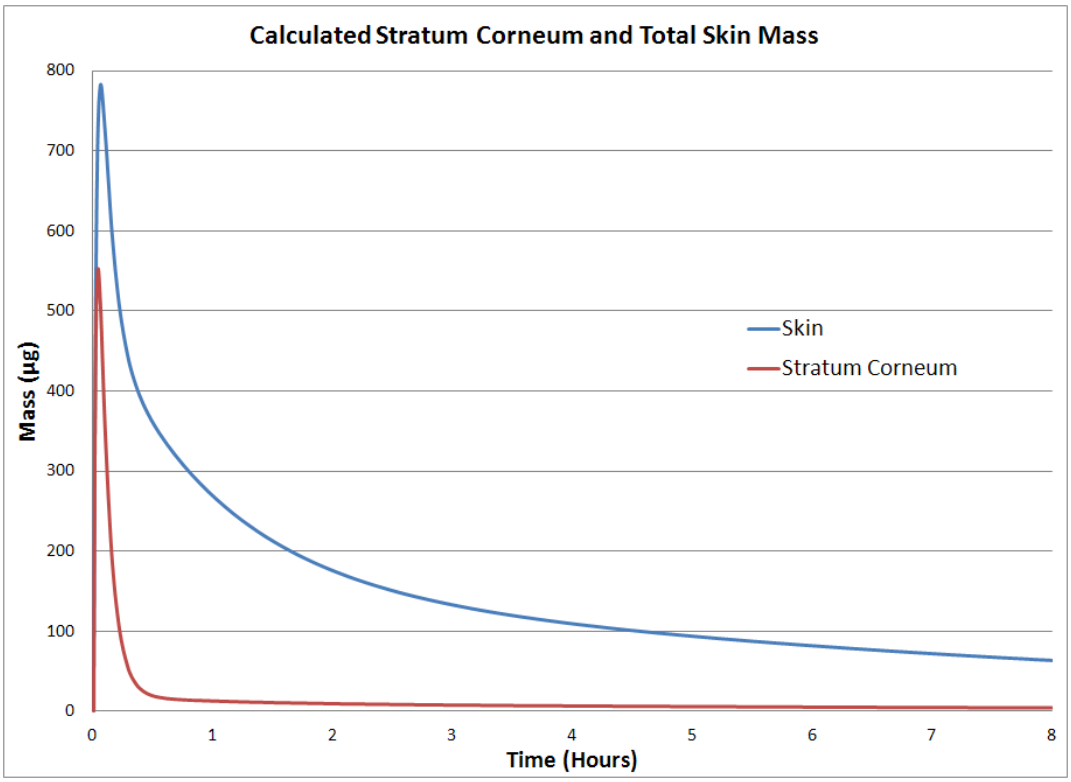

Figure 5-3. Calculated Stratum Corneum and Total Skin Mass for 3000µg of HD

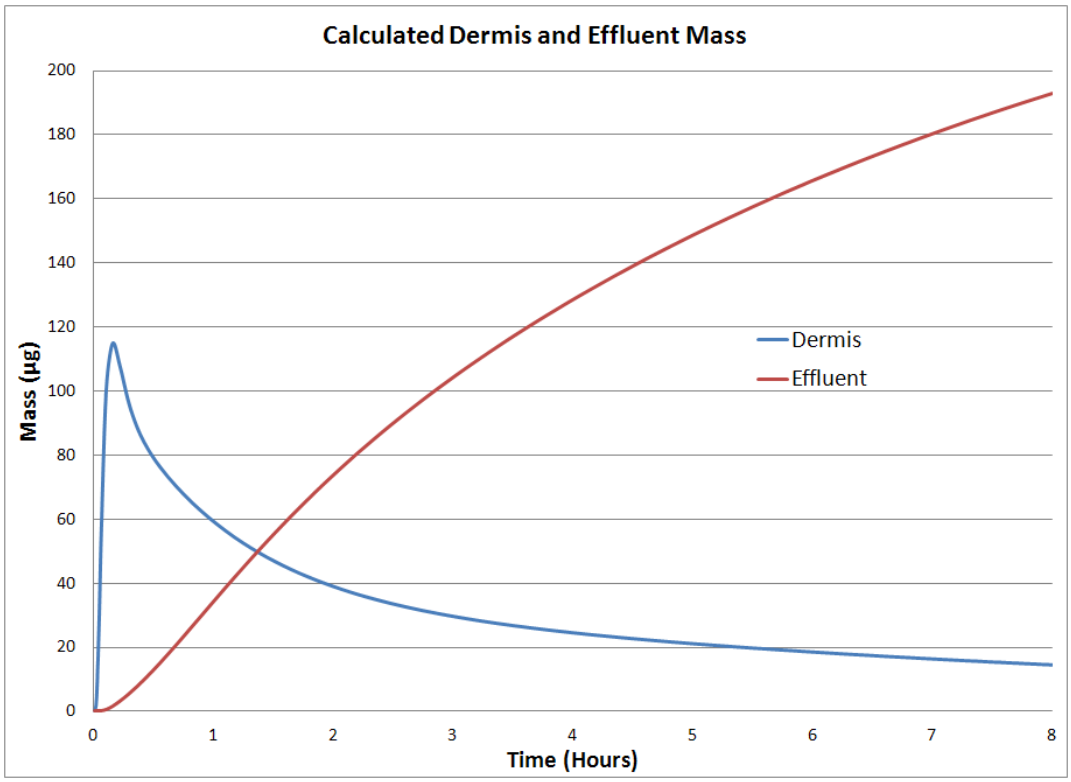

Figure 5-4. Calculated Dermis and Effluent Mass for 3000µg of HD

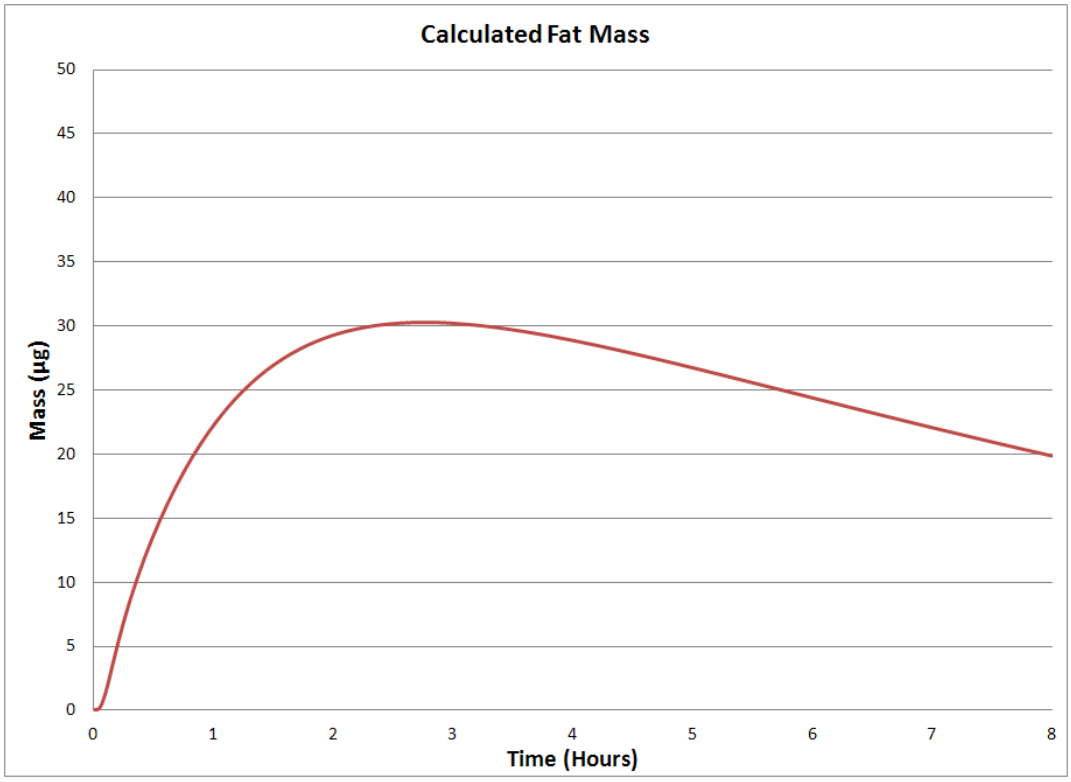

Figure 5-5. Calculated Fat Mass for 3000µg of HD

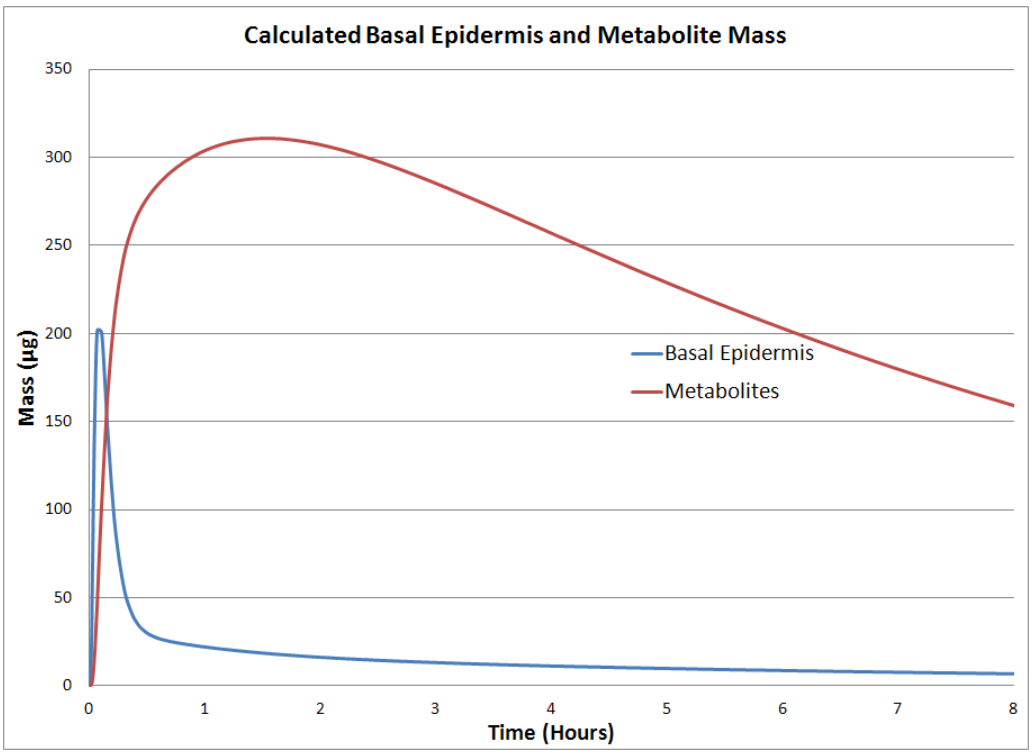

Figure 5-6. Calculated Basal Epidermis and Metabolite Mass for 3000µg of HD

5.2 Using the Calculated Dose in the GVM

For the percutaneous and systemic dose, using the calculated dose modified the HD model's implementation significantly. These changes are discussed in this section.

One note on dose: we assess the dose and the effect at each injury site separately. There are two doses we calculate, summarized in Table 5-2.

Table 5-2. The Two Doses Included in the GVM

Dose	D_s	D_p
Value	Systemic Dose	Percutaneous Dose

The systemic and percutaneous doses have two sink terms, whole DNA in normal cells and free GSH.

For percutaneous dose, the first step is to calculate the combined dose deposited on the skin. This is given by the equation below:

$$\frac{d}{dt}Deposited = \int_0^{T_{mask}} C\,dt * CF + \int_{T_{mask}}^{T_{MOPP}} C\,dt * CF * S_{exposed} \qquad (5\text{-}10)$$

This equation estimates the whole-body percutaneous vapor exposure, up until a mask is donned (T_{mask}). Plus, estimates of the percutaneous vapor exposure to the proportion of the body left unprotected ($S_{exposed} = 0.93$), up until the time at which the rest of MOPP gear is donned (T_{MOPP}). The other term used above is the conversion factor from percutaneous vapor to an equivalent percutaneous liquid dose, CF. In the HD paper we explained that the value is equal to the ratio of the ED_{50} for severe percutaneous liquid exposure to the ECt_{50} for severe percutaneous vapor exposure. This is an agent-specific value that is summarized in Table 5-3. Values for the ED_{50} and ECt_{50} were obtained from FM 3-11.9 (Army, 2005).

Table 5-3. Conversion Factors for Vesicants Included in the GVM

Agent	HD	HN-1, 2, and 3	Lewisite
ED_{50}, Severe Percutaneous, Liquid (mg/man)	600	600	600
ECt_{50}, Severe Percutaneous, Vapor (mg-min/m^3)	500	500	500
CF (m/min)	1.2	1.2	1.2

Equation (5-10) is initialized to be equal to the liquid skin dose in milligrams. The result of this sub-model can be seen in Figure 5-7, where an individual was exposed to 10 mg of liquid vesicant and a constant concentration of 1 mg/m^3 of vapor vesicant, until a mask was donned at 2 minutes and full MOPP gear was donned at 5 minutes. As you can see, the mask makes only an imperceptible change in the accumulating dose for percutaneous dosing.

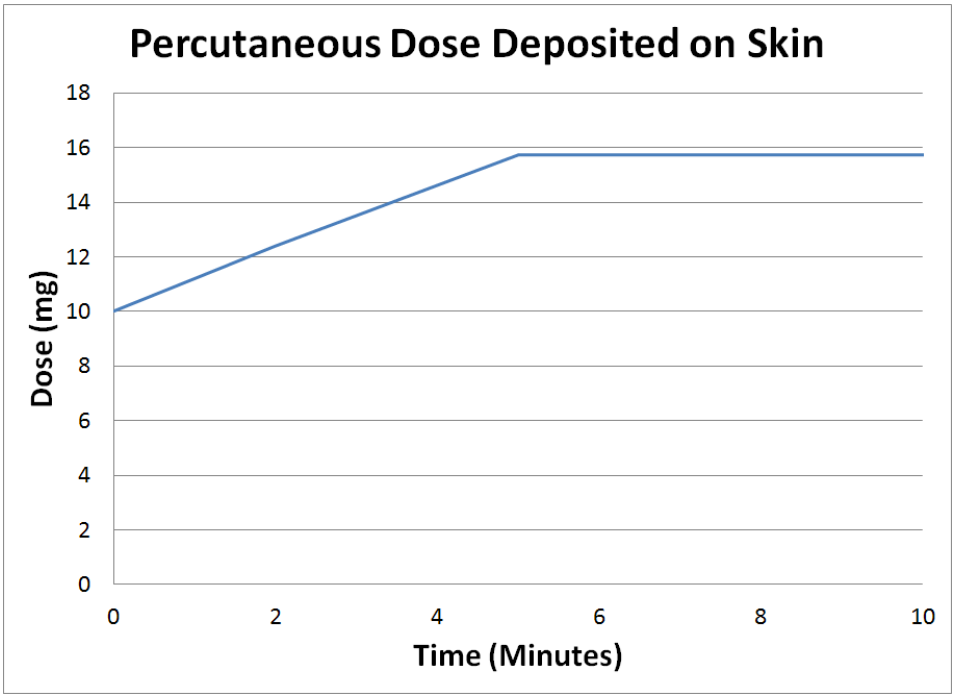

Figure 5-7. Equivalent Percutaneous Dose Deposited on Skin for a Constant Vapor Exposure and Instantaneous Liquid Exposure

The amount of vesicant deposited on the skin (*Deposited*) is then used in the toxicokinetic algorithm by using it as the initial value equation

(5-2), *Surf*.

Figure 5-8 shows the dose at the stratum corneum, basal epidermis, dermis, and vascular compartments, as well as the total skin dose, as a function of time for the inputs used in Figure 5-7, calculated in Berkeley Madonna.

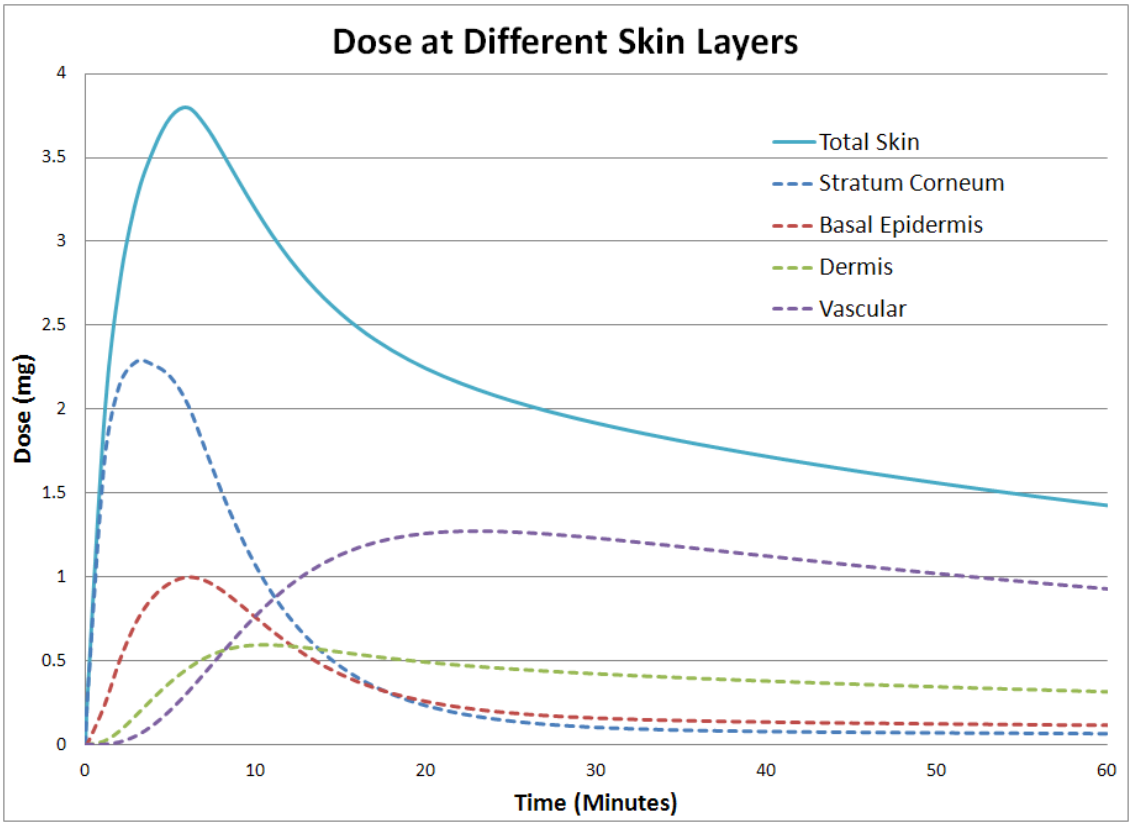

Figure 5-8. Dose Over Time at Four Different Skin Layers

The benefit of the toxicokinetic model is its accounting for the distribution of vesicant across the skin, allowing us to better predict the extent of an injury against a given dose. Vesicants, being lipophilic, can diffuse readily through the intracellular spaces of the stratum corneum, which are filled with lipids such as sebum, oils, waxes, as well as sweat (largely water). From there vesicants can make their way through the intermediate layers into the basal epidermis, where the basal cells (which produce new skin cells, among other functions) are located. Injuring the basal epidermis and the dermis is what ultimately results in vesication, which is the metric for skin injury in our model. For this reason, the percutaneous dose, D_p, is the sum of the Basal Epidermis and Dermis compartment or:

$$D_p(t) = BEpi(t) + Derm(t) \qquad \textbf{(5-11)}$$

It is important to note that, unlike the ocular and inhaled doses, we will not incorporate a sink term for D_p. Toxicodynamic models already account for sink terms when the mass of an agent is calculated at different compartments. For the compartment model used here, radiolabeled HD was administered and monitored at the various skin layers. The dose was fragmenting DNA or suppressing GSH, as it was there. The dose will be incorporated into the model by fragmented DNA and suppressing GSH, while it is present in the basal epidermis or dermis, but it will not persist to injure new, healthy cells until all of the vesicant is used, as was the case in the HD model.

The final dose is the systemic dose, D_s. The systemic dose is the effluent dose calculated by the toxicokinetic model or:

$$D_s(t) = Y(t) - k_G * G * D_s(t) \qquad \textbf{(5-12)}$$

For systemic dose, we are primarily concerned with GSH suppression and acute lethality via the percutaneous route; we ignored these two factors in the HD model. We will include GSH as a sink term for systemic dose and use GSH suppression as the input to the acute lethality calculation that will be explained later in the document.

Section 6.

Vesicant Injury Model Framework

Figure 6-1 shows the injury model framework that was developed for HD. This model was used for ocular, inhalation, and percutaneous exposures. For the GVM, we are modifying this model slightly for ocular and inhalation exposures (Figure 6-1) and we are expanding the injury model framework for percutaneous exposures to include GSH suppression for both percutaneous exposures and systemic injuries (Figure 6-2).

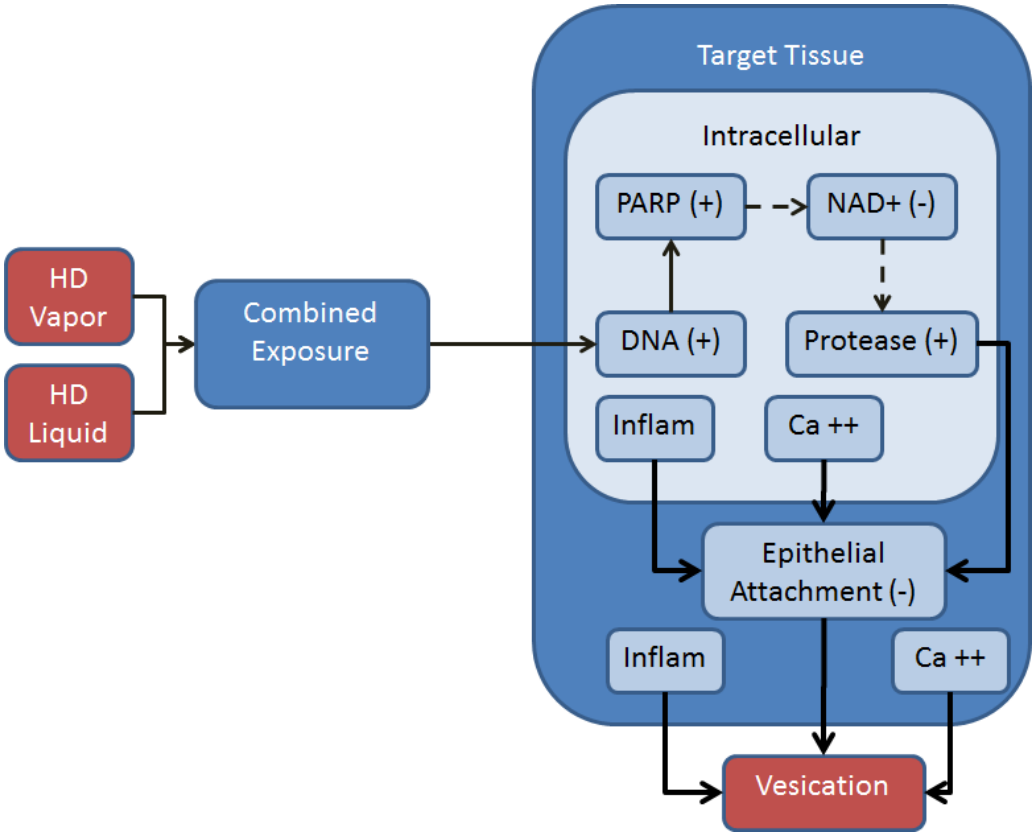

Figure 6-1. Model Framework Developed for HD

For the percutaneous model (Figure 6-2), we made three significant changes to the framework:

1. Differentiating between necrotic and apoptotic cellular death. This will allow us to better estimate the effect of PARP inhibitors, which have been shown to have negligible effects on the percentage of viable cells following mustard exposure, but have been shown (Kehe K., Inhibition of polu(ADP-ribose) polymerase (PARP) influences the mode of sulfur mustard (SM)-induced cell death in HaCaT cells, 2008) to greatly change the ratio of necrotic and apoptotic deaths, thus decreasing the severity of vesication.

2. The addition of ATP and its depletion being the primary signaling pathway for protease.
3. Systemic toxicity that results from the vesicant entering the bloodstream. This will allow us to account for acute lethal percutaneous doses of vesicants as suggested by FM3-11.9.

Relating the compartments in the percutaneous model to the discussion in the previous section on exposure, the vesicant liquid and vapor combine to form the initial surface dosage, which either evaporates or absorbs into the skin. Within the compartment labeled "Combined Skin Exposure" is the toxicokinetic model. The basal epidermis and dermis doses combine to attack the DNA, while the effluent dose enters systemic distribution.

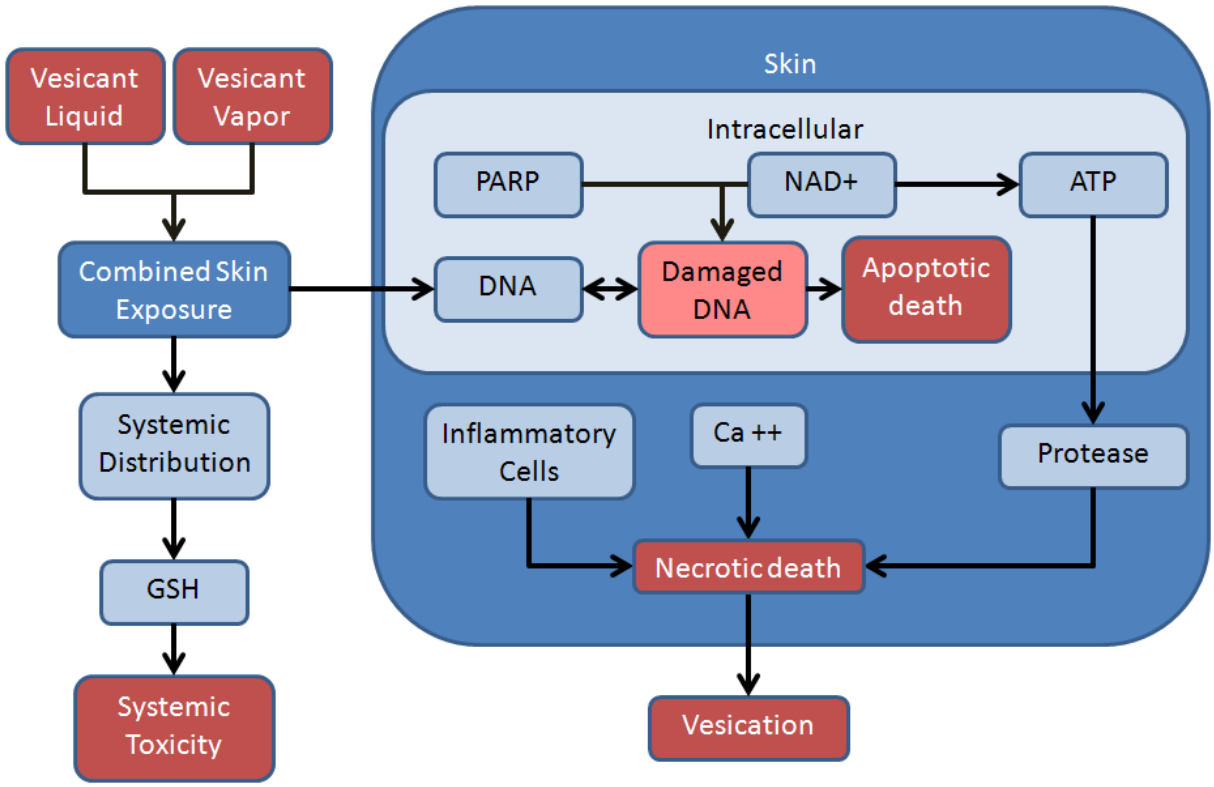

Figure 6-2. GVM Model Framework for Percutaneous Exposures

An additional benefit to the revised framework is an easier discussion on the individual components, as we can now look at each box as subcomponents of the model and provide differential equations for each one. The remainder of this section will present and discuss the system diagrams and equations for each subcomponent. We will also present the data that was used to derive the parameters for the different equations.

6.1 Injury Model Overview

We once again have a significant departure from the HD model. In the HD model, PARP, NAD+, protease, Ca++, and inflammatory cells were modeled the same way as normal, injured, and killed cells – meaning they had source and sink terms and various differential equations to describe their relative concentrations. Revisiting the literature and the framework allowed us to

better understand the complex relationships between these molecules and lead to a better understanding of how they work. We believed we were modeling them incorrectly after further review.

For example, we modeled PARP as a differential equation that was dependent on two terms:

1. PARP could be added to the system at a rate kPARPrel, dependent on the concentration of injured cells.
2. PARP could be removed from the system as it repairs damaged DNA at a rate krep, dependent on the concentration of injured cells and NAD+

There is a fallacy in this equation, as PARP is never truly "removed" from the system, instead it is momentarily used to repair damaged DNA. One solution to this problem would be to introduce a third term that accounts for PARP's reintroduction into the system; however, there is still no way to return PARP back to its baseline value of 0.0, unless we introduce a fourth term that moves PARP back to its baseline concentration. Using Berkeley Madonna to fit two unknown rates to one data set was a difficult task to justify, but fitting four rates to one data set would not result in a good model.

Our solution to this problem was to once again look at the framework and the available data and state several assumptions to better construct our equations:

1. PARP concentration is only dependent on the concentration of injured cells
2. NAD+ concentration is only dependent on the concentration of PARP
3. ATP concentration is only dependent on the concentration of NAD+
4. Protease is only dependent on the concentration of ATP
5. Inflammatory cells and calcium ions are only dependent on the concentration of killed cells

This may seem like a simplification of the model, but it is consistent with the injury mechanism, in turn, consistent with the data, and reduces the fits down to nine equations with three unknowns. Additionally, it keeps with the philosophy of the model: that by incorporating the biochemical processes that lead to injury, we can better study how to disrupt those processes with countermeasures. The new framework implementation is built from the ground up, starting with the biochemical processes (which are independent of agent and exposure) and overlaying the agent and exposure-dependent equations on top of them.

We now present the equations and parameters for the underlying biological processes and the cellular response to these processes.

6.2 Underlying Biological Processes

This section details the equations and data that were used to provide fits for the underlying biological processes: PARP, protease, inflammatory cells, calcium ion signaling, and NAD+ and ATP depletion. We assume that these processes are agent-independent.

6.2.1. PARP, NAD+, and ATP Concentrations

In order to define equations for PARP, NAD+, and ATP we needed data correlating injured cells to each of these parameters. Whereas there are many studies that examine these molecules

independently, we used one study that looked at cell injuries resulting from HD exposure and the effect these injuries have on PARP, NAD+, and ATP levels. This study, performed by Daniel Hinshaw, et al. at the Department of Veterans Affairs Medical Center (Hinshaw, Lodhi, Hurley, Atkins, & Dabrowska, 1999), looked at *in vitro* exposures to human endothelial cells and keratinocytes, to better understand the role that PARP plays in the injury process. In doing so, the researchers managed to look at the extent of injury to the cells and the PARP, NAD+, and ATP levels as a function of time and dose. Whereas this study isn't very recent (published, 1999), it best represents the type of study that can be used to provide data for the GVM. We decided to use the study for this parameter fit as the data is complete and allows us to define the process and the framework for populating our model.

As mentioned, the model studied both endothelial cells and keratinocytes. We focused on the keratinocytes since they make up the majority of the cells found in the basal epidermis and dermis layers that we are interested in. The study looked at extent of injury and PARP, NAD+, and ATP levels against 0, 250, 500, and 1000 μM of HD at 2, 3, 5, and 6 hours post-exposure. Unfortunately, there weren't perfect intersections across all time-points – for instance, cell injury was not measured at 2-hours and PARP, NAD+, and ATP were not measured at 6-hours, but we were still left with enough data to develop a process and initial fits.

Additionally, the study contained three data points (combinations of time and dose) where both injury level and PARP concentrations were measured. PARP was presented in cpm/mg at 2, 3, and 5 hours post-exposure to 0, 250, and 500 μM of HD. Level of injury was presented as % adherence at 3, 5, and 6 hours following 0, 250, 500, and 1000 μM HD exposures. In both cases, we took the ratio of PARP concentration and adherence following exposure against the control values in order to get an estimate in the change of PARP and adherence and then used those values as the relative concentration of PARP and the relative injury level, respectively. Plotting those three points on a graph and setting an intersection point of zero (a value we chose for the baseline PARP concentration) resulted in the curve shown in Figure 6-3.

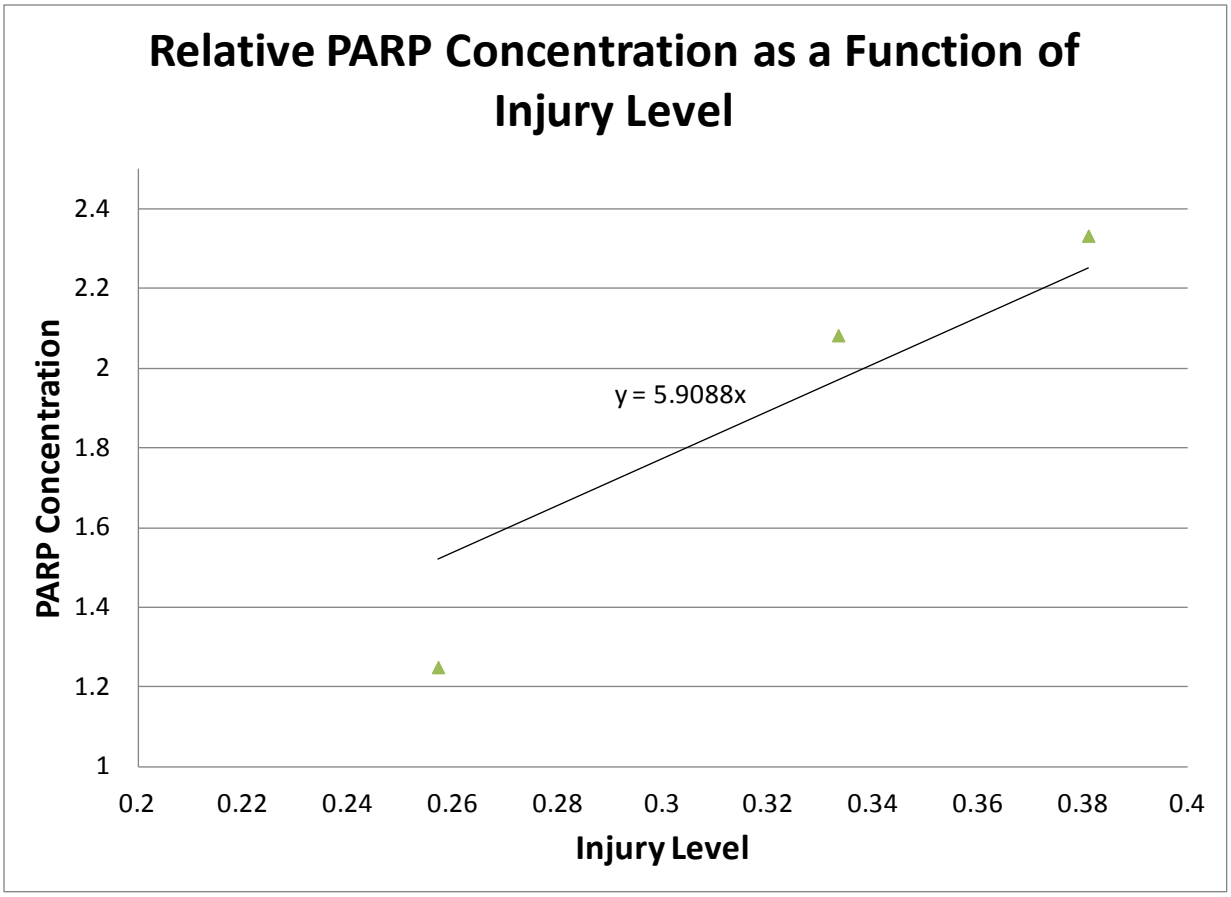

Figure 6-3. PARP Concentration as a Function of Injury Level in Human Keratinocytes Data from (Hinshaw, Lodhi, Hurley, Atkins, & Dabrowska, 1999)

Although a quadratic fit (using Excel) was the best result, we chose a linear fit with an intercept of zero in order to ensure that: 1) an injury level of zero does not result in an undefined or negative value 2) PARP concentrations start at 0.0 and always rise as a function of injury. Therefore, our equation for PARP concentration relative to injured cells is equal to:

$$PARP = 5.91 * N_{I,x} \qquad \textit{(6-1)}$$

For plotting NAD+ as a function of PARP, there were six data points that we were able to use, shown in Figure 6-4, with the corresponding fit. We once again used the relative PARP concentration values described above and applied the same calculation to the NAD+ concentrations (presented in the paper as pmole/mg) in order to determine the relative NAD+ concentration.

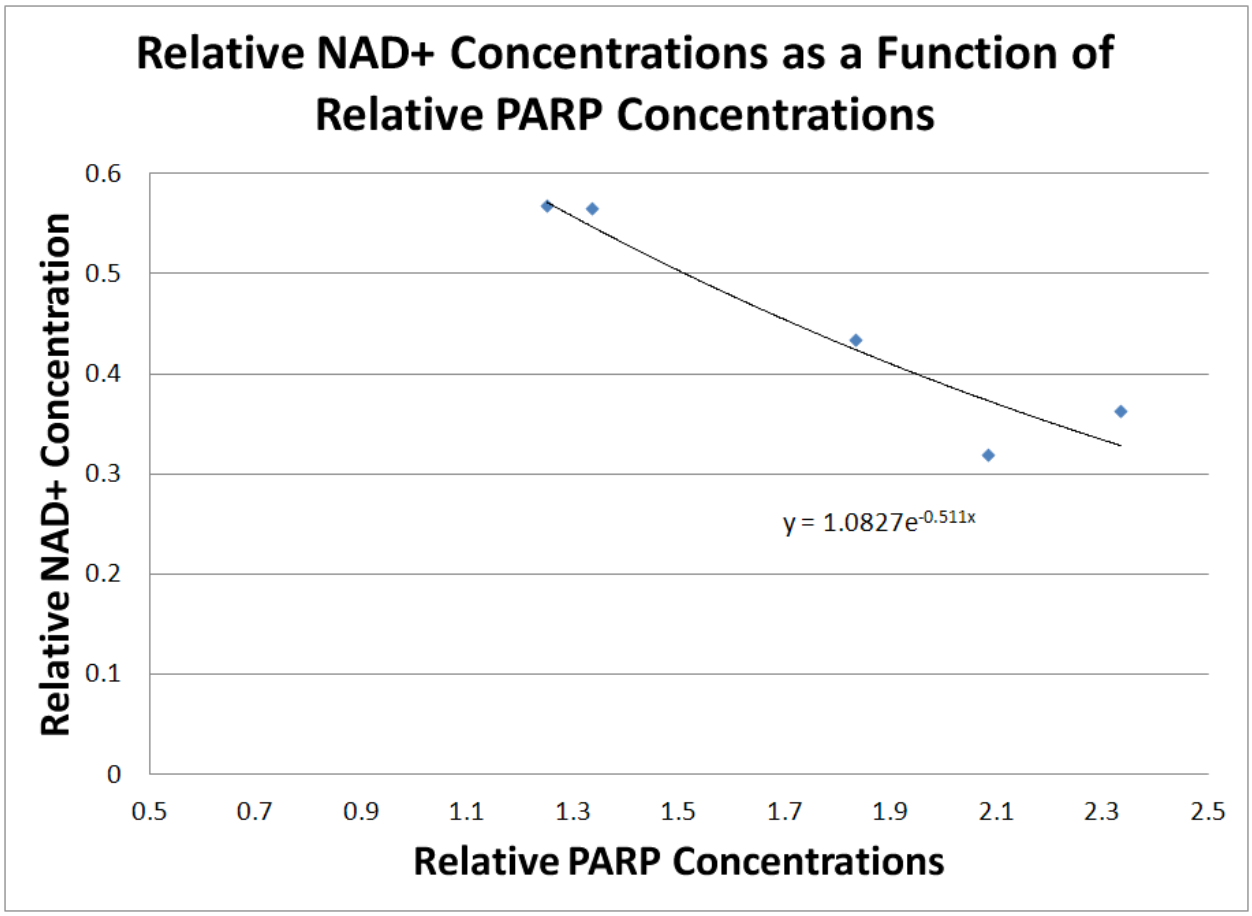

Figure 6-4. NAD+ Concentration as a Function of PARP Concentration in Human Keratinocytes

We chose an exponential to fit the NAD/PARP data, since the NAD+ concentration is supposed to decrease as PARP increases. We needed to ensure that regardless of the PARP value (which has no bound on an upper value), the NAD+ value does not go below zero, as that would lead to complications in the model. Fitting to an exponential function in Excel gives us the following equation:

$$NAD = 1.1 * e^{-0.51*PARP} \qquad (6\text{-}2)$$

For plotting ATP as a function of NAD+, we only have two data points that we can use, as shown in Figure 6-5, with the corresponding fit. We used the relative concentration of NAD+ as described above and applied the same calculation to the ATP levels (which were presented in the paper in nmole/10^6 cells).

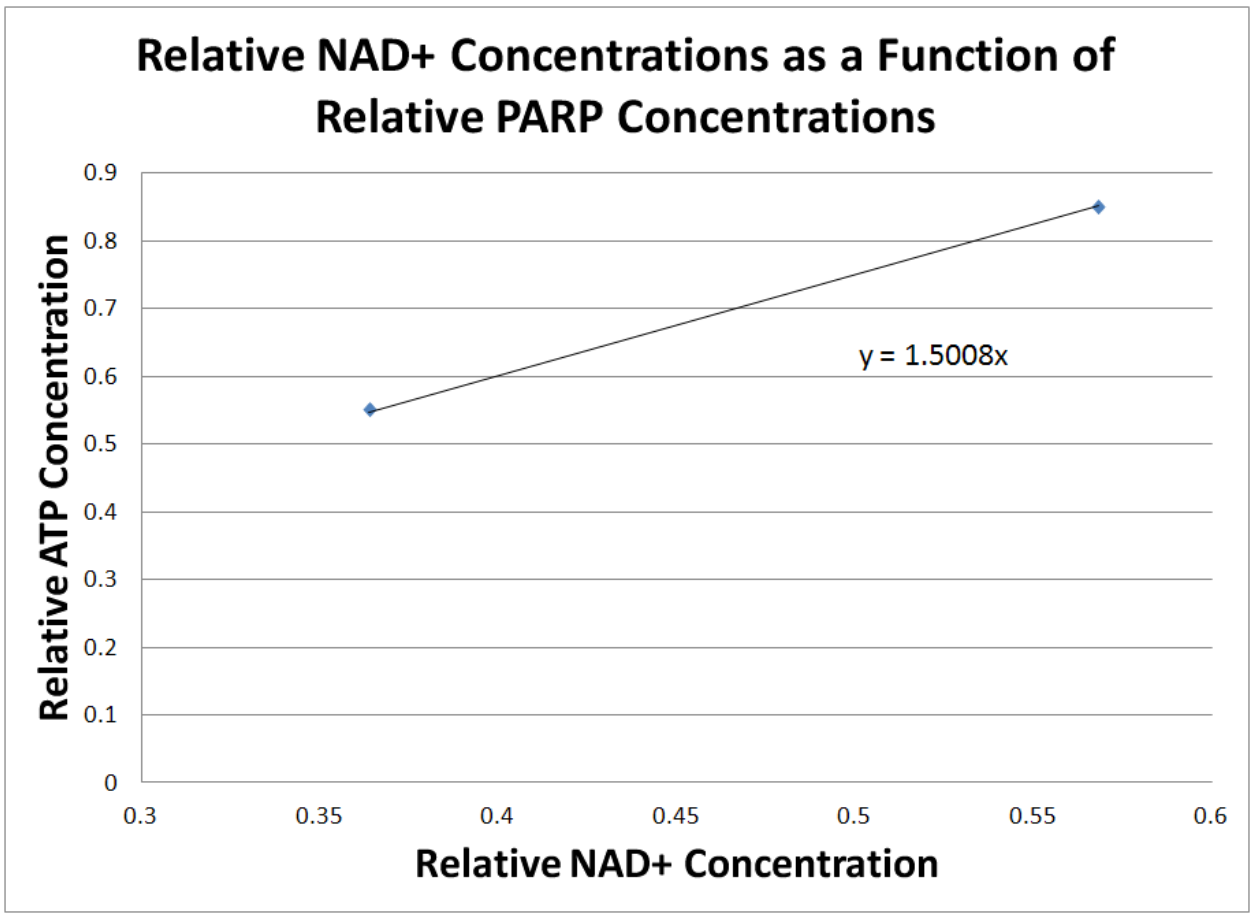

Figure 6-5. ATP Concentration as a Function of NAD+ Concentration in Human Keratinocytes

Since we only have two useable data points, we have no basis for fitting ATP as a function of NAD+ with anything besides a straight line. Since NAD+ cannot go below 0.0, and we set the intercept of the ATP function to 0.0, the relative concentration of ATP will never go below zero. The fit gives us the following equation:

$$ATP = 1.5 * NAD \qquad (6\text{-}3)$$

Figure 6-6 shows the model estimates of PARP, NAD+, and ATP relative concentrations as a function of time, against the entire range of possible injury levels (0.0 to 1.0). The values for NAD and ATP drop significantly as the injury level increases, mimicking the injury mechanism that leads to increased necrotic death, described in the previous section.

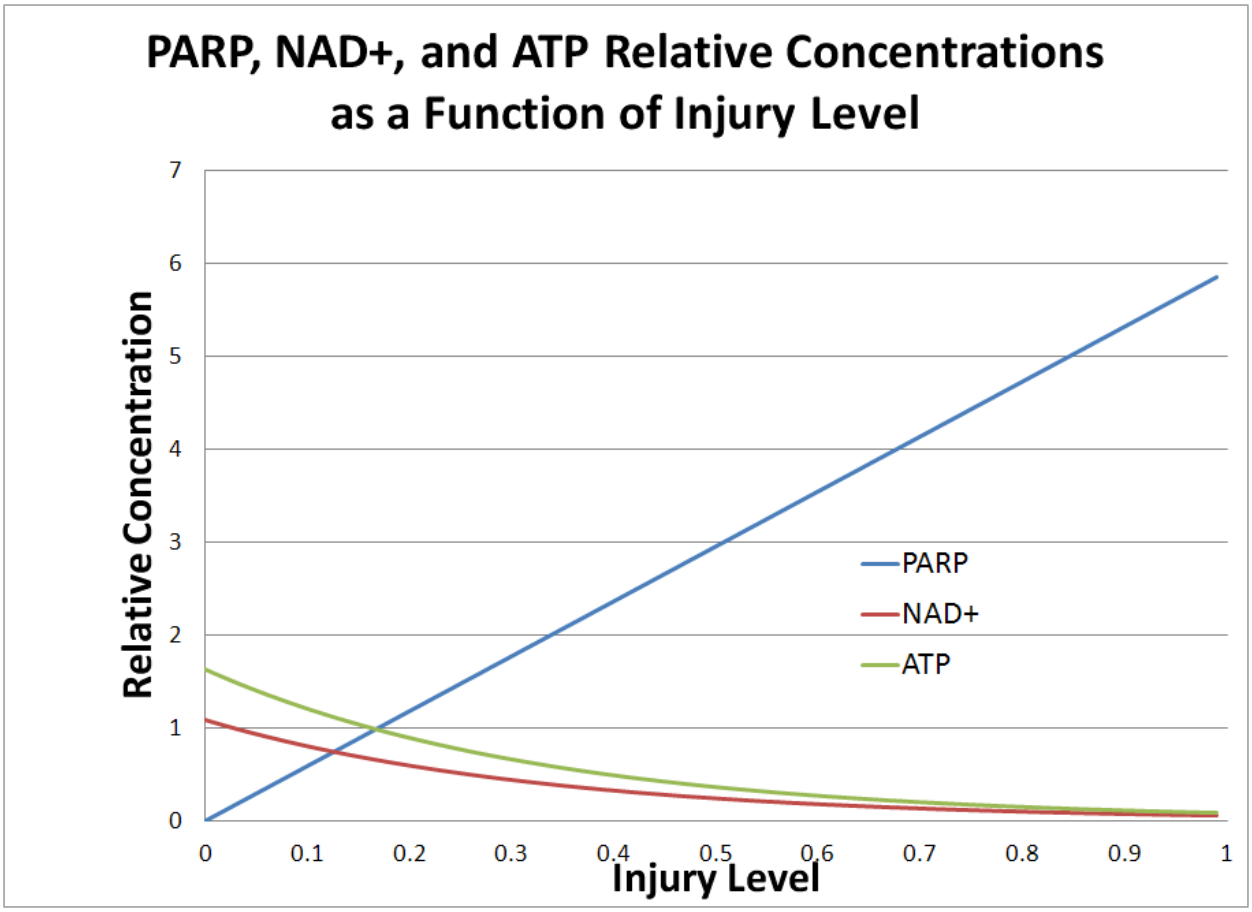

Figure 6-6. PARP, NAD+, and ATP as a Function of Injury

6.2.2. Protease Concentration

At the time of writing this report, we have not yet found a study that looked at both ATP levels and protease activity, although we have found several papers that discussed the correlation between the two (Kehe, Balszuweit, Steinritz, & Thiermann, 2009) (Kehe K., 2008) (Pita & Vidal-Asensi, 2010) (Shakarjian, et al., 2010). We do believe that a more extensive literature search can potentially lead to a paper that explicitly links ATP levels to protease levels, but due to time constraints on this project we needed to make use of the literature we managed to obtain and read so far.

A recent paper (Simbulan-Rosenthal, et al., 2006) modeled protease activity in human keratinocytes following HD exposure and would have been an excellent candidate for fitting the data but the paper had no doses and no time points that intersected with any of the values used in the Hinshaw, et. al. study. A second study (which we used for the protease fit in the HD model) measured protease activity that was collected from mouse ear exposures (Powers J. C., 1999) instead of via *in vitro* human keratinocyte exposure. The problem with using *in vivo* data is that we no longer claim that the processes are agent-independent, as different agents will likely have different diffusion rates in the body. We instead need to make the assumption that exposures from all vesicants will result in the same proteolytic activity as they would following an HD exposure.

We already analyzed the Powers data in the HD model to determine the proteolytic activity increase over the control as a function of time. Table 6-1 shows the derived values of proteolytic activity as a function of time. This is a fold-increase over the control. So, for example, elastase had a 0.04 mOD/min proteolytic activity at hour three in the absence of HD and a 0.102 mOD/min proteolytic activity after HD exposure, which results in a 2.6-fold increase over the control.

Table 6-1. Fold Increase of Proteolytic Activity Following HD Exposure (derived from Powers J. C., 1999)

Time (hr)	Elastase	Tryptase	Chymase	Plasmin	Thrombin	Cathepsin B	Calpain	Cathepsin H
3	2.6	1.2	2.9	4.2	1.5	1.3	1.7	1.3
6	2.1	1.1	1.0	0.2	1.9	1.6	1.7	1.1
12	7.7	1.3	0.9	0.3	1.3	1.1	2.1	1.2
24	19.9	3.2	0.5	4.9	1.5	1.0	2.7	1.1

Our model does not require us to consider the activity of individual proteases. In the HD model, we averaged these values together to obtain one representative curve for proteolytic activity. Since we published that paper, we have learned that capsase-3 is considered to be the most important protease involved in the mustard injury mechanism (Kehe, Balszuweit, Steinritz, & Thiermann, 2009) (Kehe K. , 2008) (Simbulan-Rosenthal, et al., 2006). Described in the table above, caspase-3 activity was not even measured in the experiment.

Therefore, we had to turn to the more recent Simbulan-Rosenthal, et. al. (Simbulan-Rosenthal, et al., 2006) study to plot caspase-3 activity at 16 and 24 hours as a function of dose, to first understand if there is any relationship between caspase-3 activity and dose and then to understand if there is a relationship between caspase-3 activity and time. The data from Simbulan-Rosenthal and the corresponding fit is shown in Figure 6-7 for 16-and 24-hours post-exposure. The equation for caspase-3 activity as a function of dose (D), as defined in Simbulan-Rosenthal at 16 hours, is:

$$\boldsymbol{Caspase - 3 = 0.024 * D - 0.1} \qquad \textbf{(6-4)}$$

And the equation for caspase-3 activity, as a function of dose at 24 hours, is:

$$\boldsymbol{Caspase - 3 = 0.03 * D + 1} \qquad \textbf{(6-5)}$$

As shown in the figure below, there is strong linear relationship between caspase-3 activity and dose at 24-hours post-exposure and a weaker relationship at 16-hours post-exposure. However, the best-fit slopes are at least of the same order of magnitude. Using this equation, we can now predict caspase-3 activity at 16- and 24-hours for a 250, 500, and 1000µM dose of HD, the same dosage used in the Hinshaw study for ATP depletion. The result of this calculation is shown in Table 6-2.

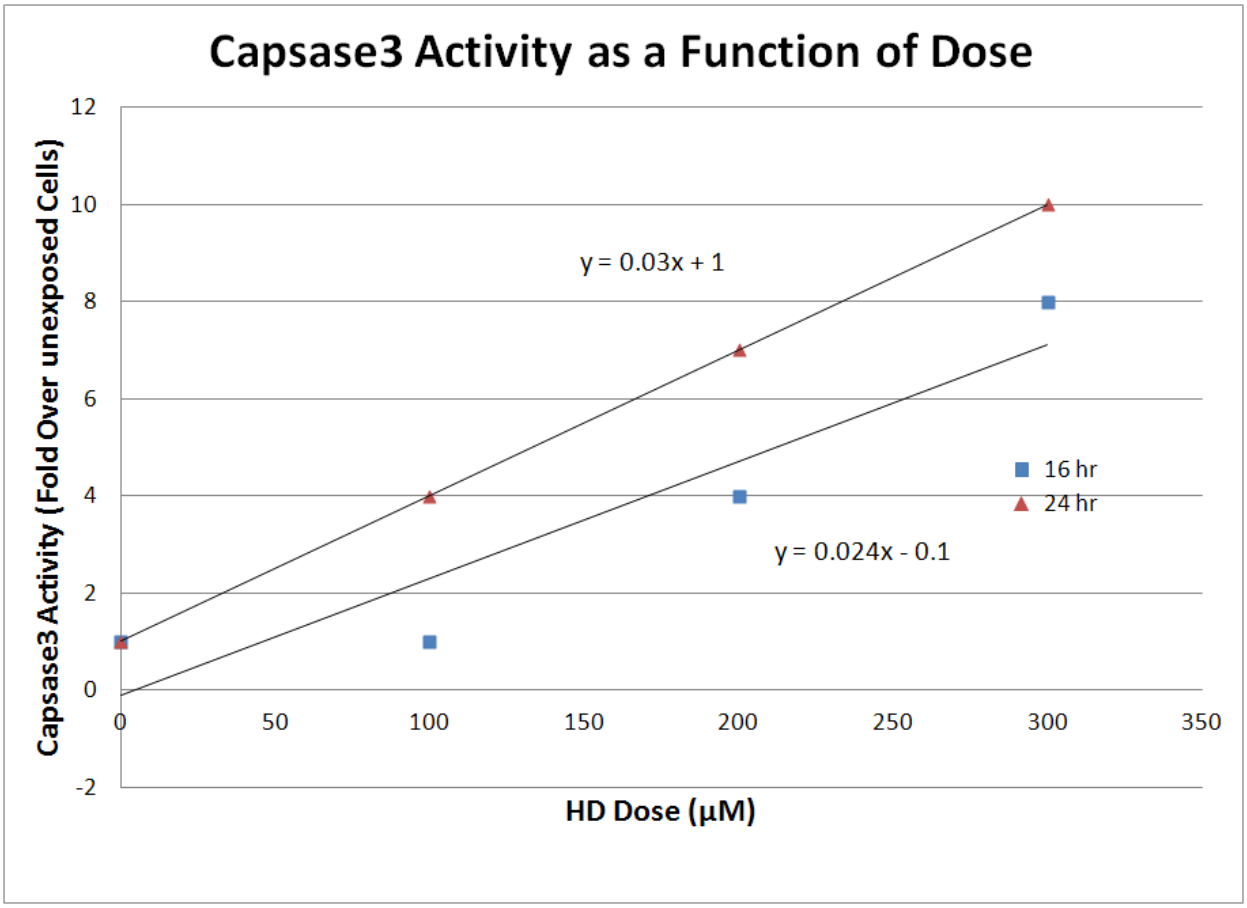

Figure 6-7. Caspase-3 Activity as a Function of HD Dose 16- and 24-Hours Post-Exposure

At these doses, the predicted caspase-3 activity level at 16 and 24 hours are very high. This phenomenon makes sense, as the injury mechanism for vesicants states that, at high doses, ATP depletion is more exaggerated and the level of necrosis increases significantly. Also, the AMedP-8 (C) injury profiles for HD show heavy blistering beginning at the 18-24 hour mark. This is once again verified by this model, since protease activity is what leads to heavy blistering. We still need to make one more step; however, to connect these values to ATP depletion.

Table 6-2. Predicted Caspase-3 Activity Levels for 250, 500, and 1000 µM HD Exposures at 16 and 24 Hours Post-Exposure

	250 µM	500 µM	1000 µM
16 hrs	5.9	11.9	23.9
24 hrs	8.5	16	31

Plotting the values from the above table and fitting the values to a line with an intercept of 1.0 gives the plots shown in Figure 6-8.

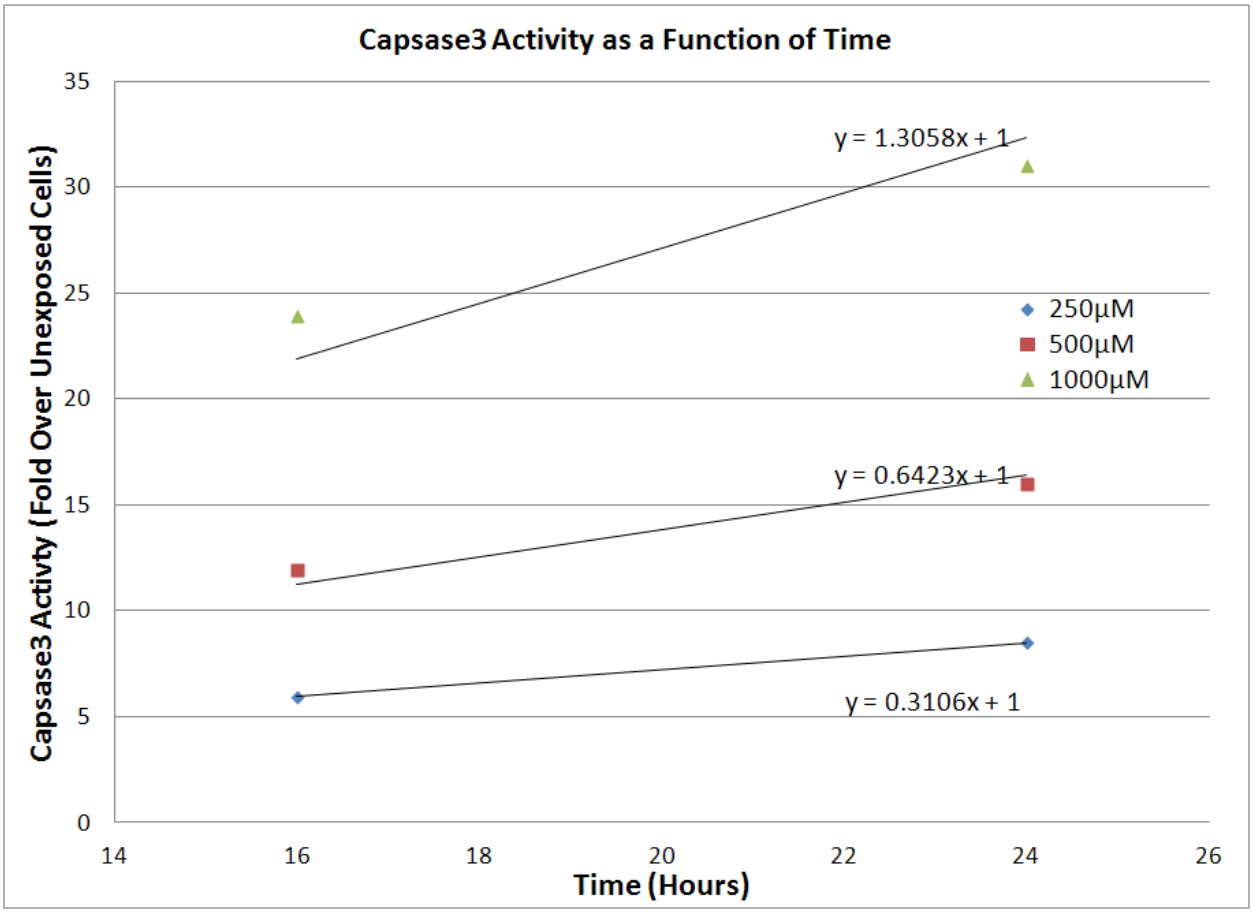

Figure 6-8. Caspase-3 Activity as a Function of Time and HD Dose

We can then use the equations shown in the figure above to predict the caspase-3 activities at 5 hours (the time at which ATP levels were measured in the Hinshaw study) for 250, 500, and 1000 µM exposures. The results of these calculations are shown in Table 6-3, along with the relative ATP concentrations derived from Hinshaw.

Table 6-3. Predicted Caspase-3 Activity at Five Hours for 250, 500, and 1000 µM Exposures of HD

	250 µM	500 µM	1000 µM
Capsase3 Activity (5 hours)	2.55	4.21	7.529
Relative ATP Concentration	0.85	0.55	0.5

Figure 6-9 shows the plot of the table values above and the corresponding fit.

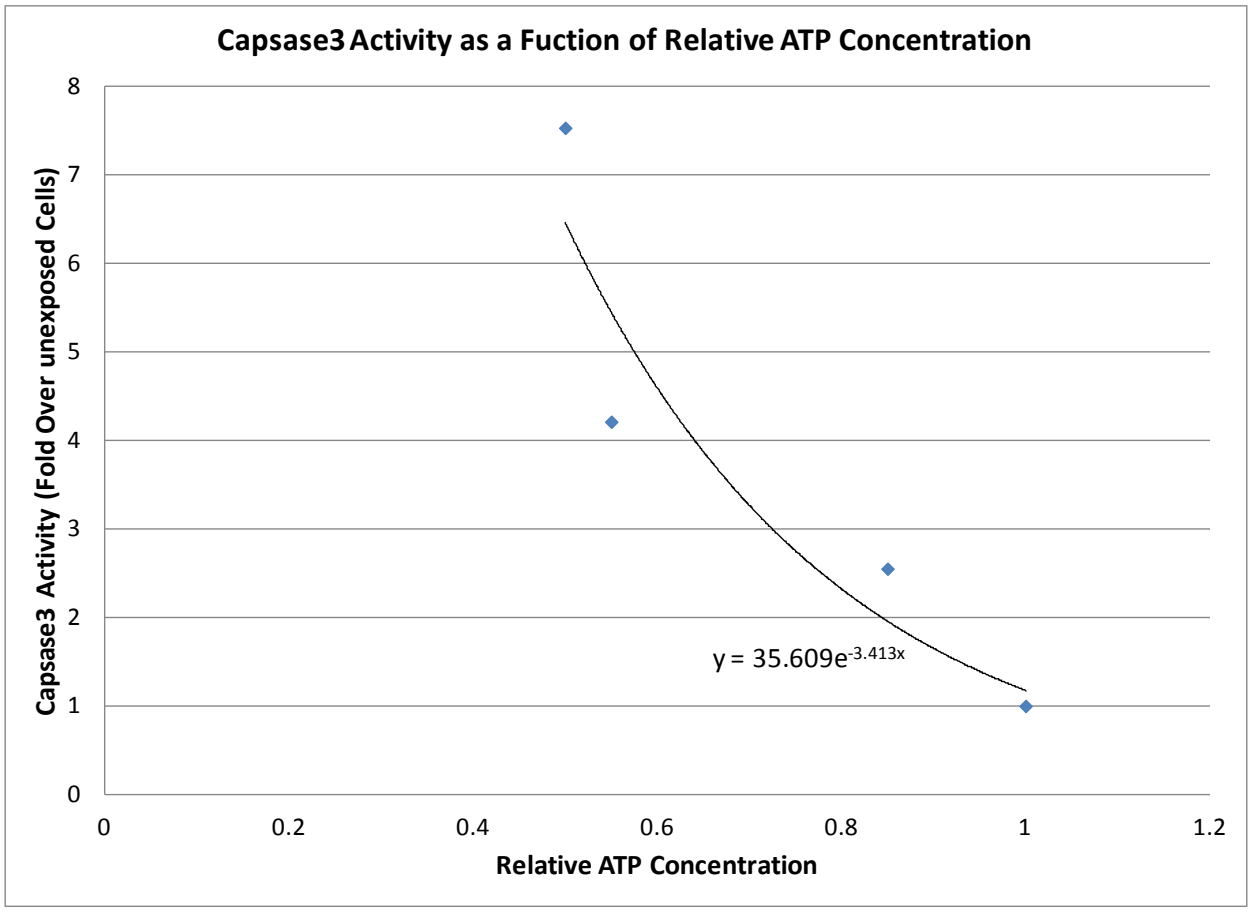

Figure 6-9. Caspase-3 Activity as a Function of Relative ATP Concentration

Using the above analysis of the Hinshaw and Simbulan-Rosenthal papers, we derived an equation for protease that is equal to:

$$\boldsymbol{Protease = 35.6 * e^{-3.4*ATP}} \qquad \textbf{(6-6)}$$

We realize that there were several significant assumptions used to connect the data from these two studies. We believe that a better correlation between ATP and protease can be derived if we had a study that explicitly linked the two.

6.2.3. Inflammatory Response

Once again, we are lacking a comprehensive study of *in vitro* inflammatory response as a result of killed cells and need to derive the necessary data from non-ideal studies. We found one study (Amir, et al., 2000) that measured inflammatory response markers following HD exposures to rabbit eyes. We were able to use the study to make a preliminary correlation between killed cells and inflammatory response. The assumptions being made in using this study are that ocular exposures exhibit similar biochemical processes to skin and lung exposures and that rabbit eyes

exhibit similar biochemical processes to human eyes. For the latter assumption, the belief that biochemical processes are system-independent is an underlying assumption for the entire model. For the former, we do believe that similar experiments using *in vitro* exposures against human cell cultures could likely lead to different models. If better data becomes available, we would revisit the fit. However, our use of the same methodology is described below.

The Amir et al. study measures inflammatory markers (protein levels) in the anterior chamber 6- and 48-hours post-exposure of vapor HD against the eye. Additionally, the study reports the size of ocular lesions (which can be correlated to killed cells) on days 1-7 post-exposure. The primary goal of the study was to measure the effects of anti-inflammatories against the ocular lesions and corneal weight, but we will only use the data in this section to estimate the correlation between the level of blistering (ocular lesions) and the level of inflammatory markers (protein).

Our first step was to fit the level of corneal erosions (reported in the study as the clinical score) as a function of time, for a dose of 390µg/L over 2 minutes (the dose used in the study). The resulting plot and fit is shown in Figure 6-10.

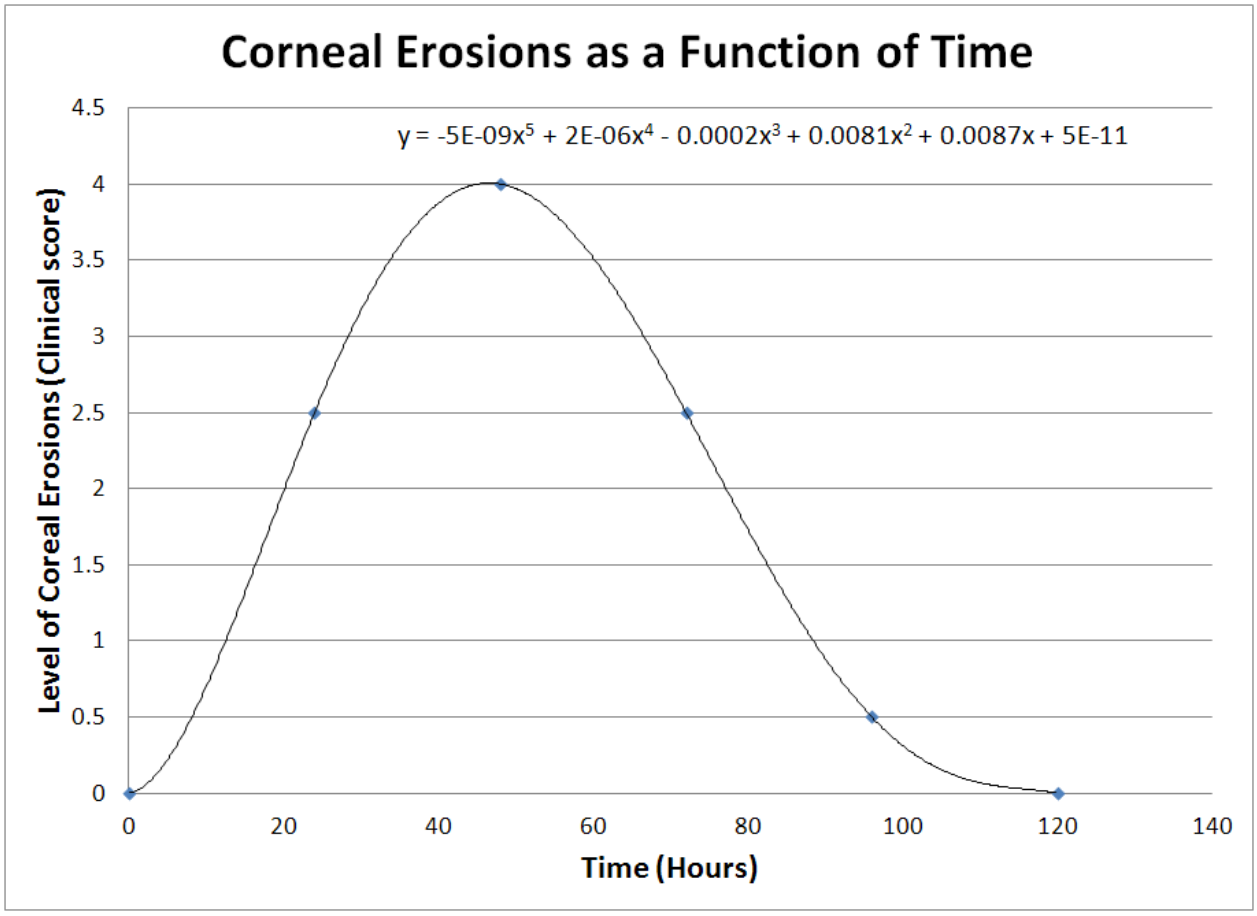

Figure 6-10. Level of Ocular Injury as a Function of Time

In order to get a good fit to the data we needed to use a fifth-order polynomial. The equation for ocular injury as a function of time is therefore:

$$Injury = -5E-9 * t^5 + 2E-6 * t^4 - 0.0002 * t^3 + 0.0081 * t^2 + 0.0087 * t + 5E-11 \quad (6\text{-}7)$$

The next step is using Equation 5-7 to estimate the extent of corneal erosions at 30 minutes, 6 hours, and 48 hours; these times are at which the study measured protein levels indicative of inflammatory response. The curve and resulting fit can be seen in Figure 6-11.

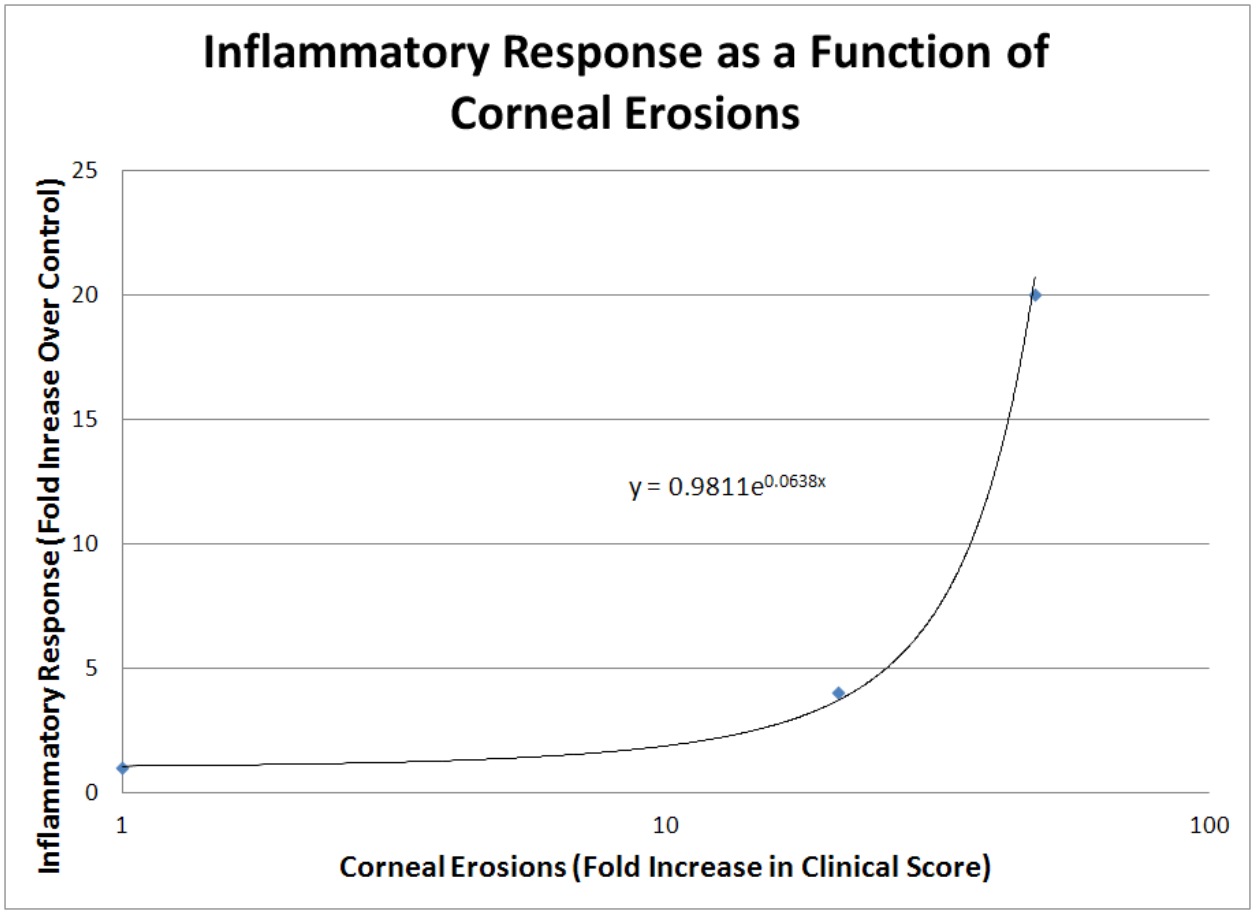

Figure 6-11. Inflammatory Response as a Function of Fold Increase of Corneal Erosions

The fit would certainly benefit from more data points, but the curve has the shape we expect and is a good starting point for our model. We see that rapid onset of injury results in a significant increase in inflammatory cells. As the injured cells decrease, the inflammatory response will decrease accordingly. This would lead to a rapid increase in inflammatory response, followed by a rapid drop-off as injured cells are vesicated. Correlating this to the AMedP-8 (C) injury bands for HD, injury severity reaches a maximum in all cases before 48 hours. We infer that the inflammatory response should trend back towards zero as there are no more injured and dead cells to vesicate. In order to account for this phenomenon, we substituted

the exponential term with the relative concentration of injured cells. Our equation for inflammatory cells as a function of injured cells is therefore:

$$\boldsymbol{Inflam} = .\mathbf{98} * \mathbf{exp}(\mathbf{N_i^2}) \qquad \textit{(6-8)}$$

6.2.4. Calcium Ion Concentration

When we developed the HD model we stated that there was no evidence that calcium modulation reduced the toxicity of HD injuries. One of the studies (Sawer & Hamilton, 1999) that supported this statement looked at the effect that the calcium chelator BAPTA-AM and calcium inhibitor thapsigargin have on cell viability following HD exposure. The study found that there were no beneficial therapeutic effects from either of these potential countermeasures. Since writing our final report on the HD model, we have come across one paper that may suggest a therapeutic effect of calcium modulators (Ray, Benton, Anderson, Byers, & Petrali, 2000), although not in a way that is consistent with our model. The findings of Ray et al. suggest that calcium modulators may actually work by slowing cellular proliferation and metabolic rates. Thus, the rate of apoptotic cell death slows, but not necrotic cell death, as we have stated in our model.

There are the remaining questions of whether or not the dosing of calcium modulators required for a therapeutic effect is toxic in an organism, or whether or not slowing the rate of apoptotic cellular death would actually stop the formation of blisters that follow large exposures of vesicants. The author references having begun experimentation in animals using BAPTA-AM, but we have not found a follow-up report with the results.

Pending future data, we still consider calcium ions and calcium modulation to not be integral components of vesicant injury. We have defined a simple equation for calcium ions that is independent of injury and dose and will have no effect on the model output:

$$\boldsymbol{Ca} = \mathbf{1} \qquad \textit{(6-9)}$$

In our model, calcium ions will be held at a constant concentration. If further research begins to show a better understanding of calcium ions' role in vesication or the therapeutic effects of calcium ions, we will revisit this assumption.

6.2.5. Glutathione (GSH) Suppression

We found two excellent papers that studied the effects several vesicants have on glutathione levels in various compartments of the body.

The first study (Sharma, Vijayaraghavan, & Agrawal, 2010) looked at the effects HD, HN-1, HN-2, and HN-3 have on body weight, spleen weight, white blood cells, red blood cells, liver enzymes, GSH, oxidized glutathione (GSSG), liquid peroxidation (MDA), and DNA damage. The effects are followed in percutaneous exposure to mice ears with and without treatment. This is a model study in the type of data that can best be used for the GVM, because it considers different vesicants, different compartments, and different countermeasures. Additionally, by focusing on systemic effects, it allows us to model GSH suppression via systemic dose. The first point to make after reviewing this paper is that HN-1, HN-2, HN-3, and HD all result in approximately a 60% decrease in GSH levels in the liver. This fact further strengthens two of our assumptions: the underlying biological process disruptions are largely agent-dependent and our

assumption, the three nitrogen mustard analogues are as toxic as sulfur mustard. In this study, GSH suppression was only measured in the liver, but a second study (Lomash, Deb, Rai, Jadhav, R.Vijayaraghavan, & S.C.Pant, 2011) gives some insight into why.

The Lomash et al. study examined the effect of HD on body weight, liver, kidney, and spleen weight, white blood cells, red blood cells, hemoglobin, GSH levels in the blood and liver, GSSG and MDA levels in the liver, and even the occurrence and severity of injury in the liver, kidneys, spleen, and skin. The purpose of this extensive study was to design an *in vivo* model that produced skin lesions without producing systemic toxicity. As a result, the study gave significant insight into the role of GSH suppression in vesicant injury. This paper benefits our model by providing evidence that GSH plays a significant role in systemic toxicity. Small exposures of HD (5mg/kg) result in little to no systemic toxicity, but still produce significant skin lesions, whereas larger exposures of HD (10mg/kg) result in systemic toxicity in almost all animals exposed (and also produces significant skin lesions). The second insight gleaned from this study is that GSH levels in the blood are not significantly changed when challenged with a 5 mg/kg or 10mg/kg percutaneous dose. However, GSH levels in the liver are significantly changed when challenged with a 10 mg/kg dose, but not with a 5 mg/kg dose. This leads us to believe that it is GSH-suppression in the target organs that results in systemic toxicity and not in the blood. This study would have helped further if the researchers measured GSH suppression in the bone marrow and spleen, as we would potentially be able to create a toxicodynamic/kinetic model of vesicant distribution and effect. For now we have to group all of the important organs into one compartment and apply the systemic dose to that compartment. The only data that we can correlate dose-to-effect is in the liver. Since this is a new research area (the two papers were published in 2010 and 2011, respectively), we are hopeful that continued research allows us to better refine this model.

Another benefit of the study, is that we can extrapolate the findings to human exposures using the toxicokinetic model we are implementing in the GVM.

First we need to calculate the systemic dose that results from a 5 mg/kg and a 10mg/kg percutaneous exposure in a 70-kg man (350 and 700mg, respectively). Using that as input to the toxicokinetic algorithm, we get the two estimates of systemic dose as a function time, shown in Figure 6-12.

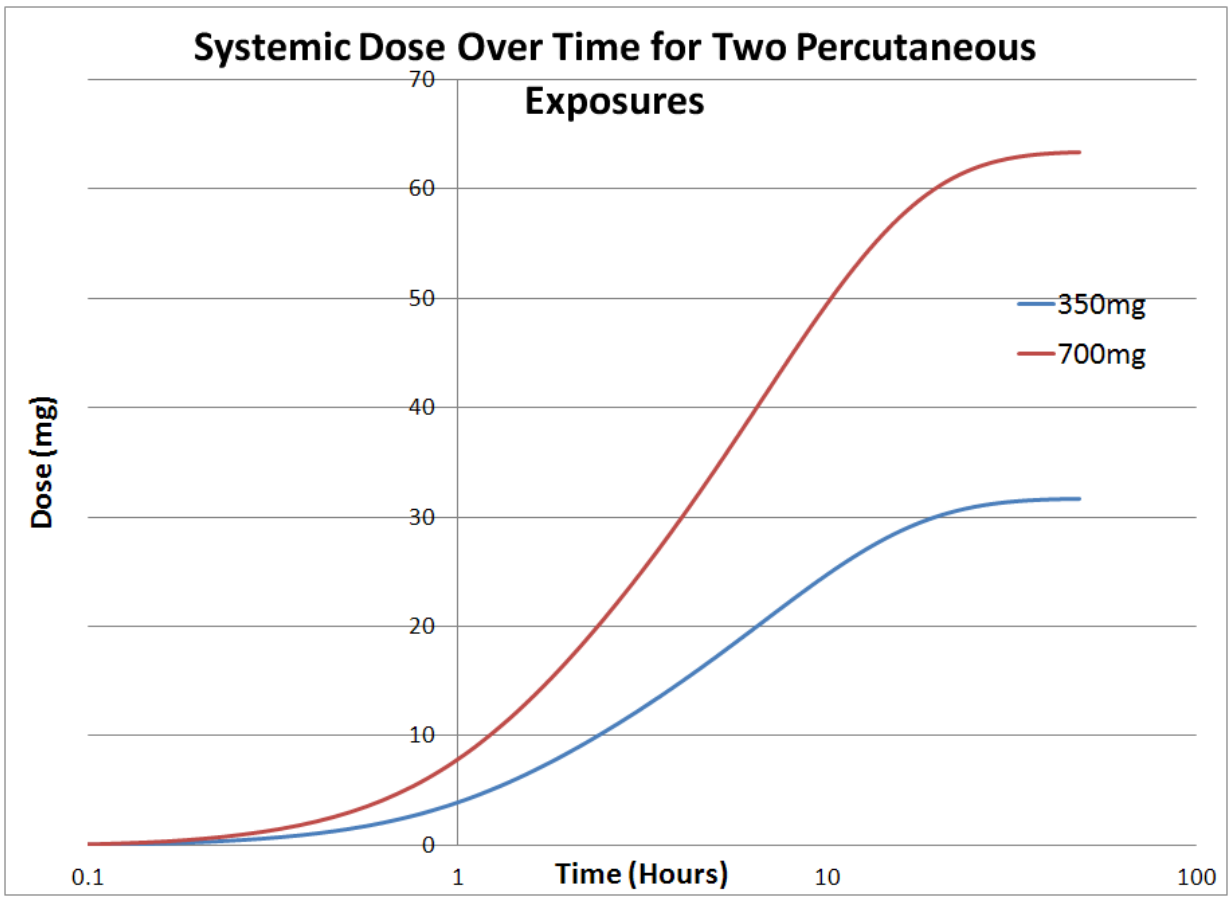

Figure 6-12. Systemic Dose Over Time for a 350mg and 700mg Percutaneous Exposure

The Sharma et al. study measured GSH levels in the liver on days 4 and 8. As shown in the figure above, most of the systemic dose enters the circulation system before day 2. The Lomash et al. study measures GSH levels in the liver and kidneys on days 3 and 7. Table 6-4 tabulates the data from the two studies (Sharma et al.) using a percutaneous dose of 8.1 mg/kg.

Table 6-4. GSH Supression in the Liver for Three Different Doses

Percutaneous dose	5 mg/kg	8.1 mg/kg	10 mg/kg
3 days	1	-	0.8
4 days	-	0.4	-
7 days	1	-	0.8
8 days	-	0.4	-

One issue is immediately apparent: Sharma et al. study measured a greater level of GSH suppression in the liver for an 8.1 mg/kg dose than the Lomash et al. study measured, using a 10 mg/kg dose. This is likely due to one big difference between the two studies: For the Sharma et al. study the mice were exposed on their backs; however, for the Lomash et al. study the mice were exposed on their ears. This tends to be an issue when working with percutaneous hazards;

effects tend to be exposure-site dependent. In this case we can postulate several reasons for the drastic difference between the two exposure sites:

1. Differences in thickness between back tissue and ear tissue
2. Differences in fat content between the back tissue and the ear
3. Differences in the paths required to get to the target tissue, especially if there are multiple sinks or metabolites en route

Regardless of the reason, the issue highlights one of the problems with modeling percutaneous exposures. For this implementation, we assume that a human exposure would resemble the ear exposure (Lomash et al.), considering we are modeling to a 70-kg warfighter who would most likely not have an exposed back. From a mathematical standpoint, the Lomash study also gives us two data points to include in the model. The plot and corresponding fit are shown in Figure 6-13. The equation for GSH suppression as a function of systemic dose is:

$$GSH = 1.25 * e^{-0.007 * D_s} \qquad (6\text{-}10)$$

We chose to fit GSH using an exponential curve, so that the LD50 for percutaneous exposures results in a positive value for GSH suppression. For example, using our model, a 1400 mg exposure of HD (the LD50 for percutaneous exposures) produces a 126mg systemic dose and a GSH level of 0.51. We will discuss how we tie GSH suppression to lethality in the coming sections.

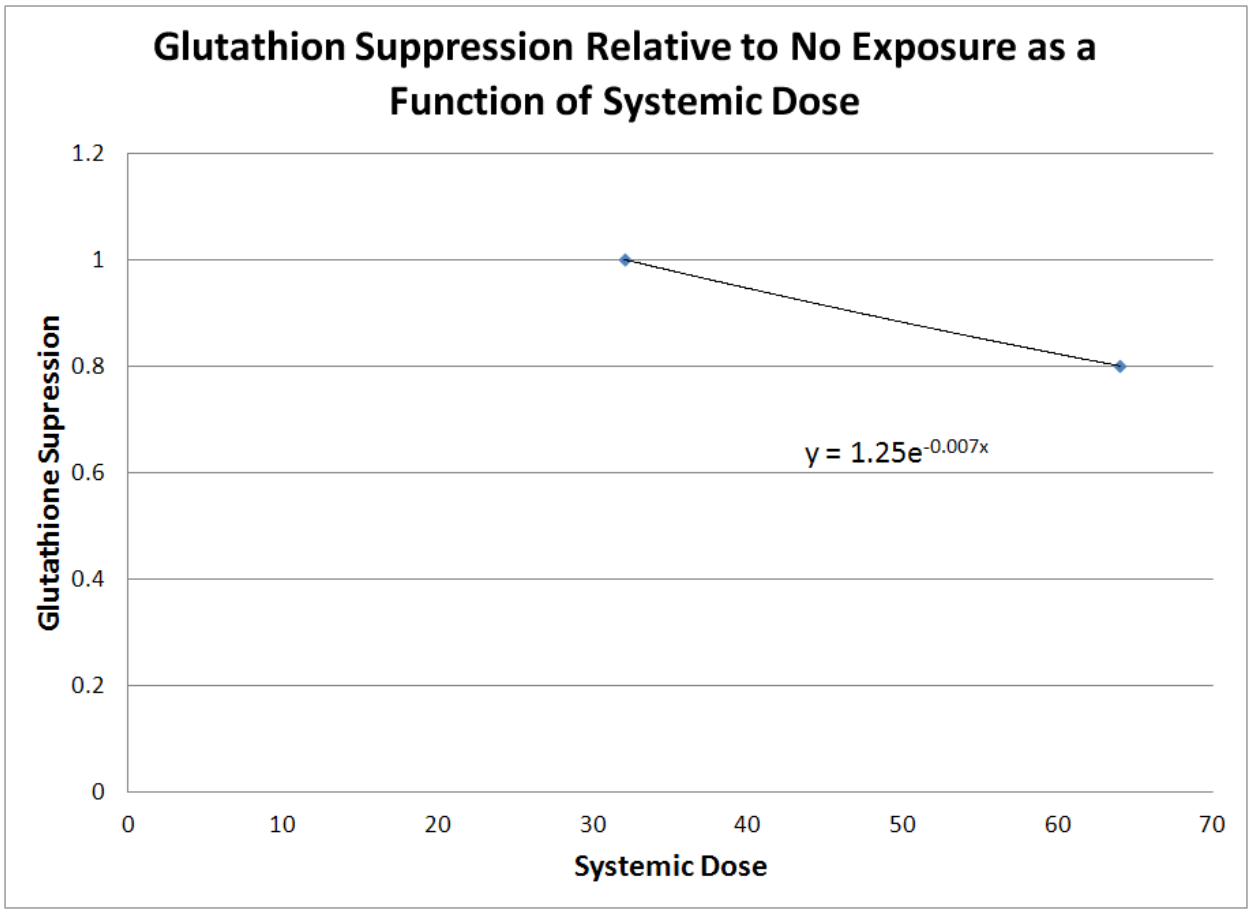

Figure 6-13. GSH Suppression as a Function of Systemic Dose

6.3 The Effect of Biological Processes

Now that we have defined the models that act as the foundation of the GVM, we can overlay the effects that perturbing these processes have on cells. There are four primary categories for cells in our model: normal healthy cells, injured cells, necrotic cells, and apoptotic cells. We will first define the equations and then complete the fits.

6.3.1. Proportion of Healthy Cells (N_N)

The proportion of healthy cells in the basal epidermis and dermis is given by the variable N_N. It describes the proportion of cells at an injury site that have undamaged DNA with respect to vesicant injury.

At equilibrium (pre-exposure), we assume the value of N_N is equal to 1.0, meaning all of the cells at the injury site have not been damaged by vesicant exposure. N_N is modified by:

1. The rate of mitotic cell division, which we assume to be proportional to the rate of programmed cell death. Therefore, pre-exposure, the rate of mitotic division results in no net gain of healthy cells. Post-exposure, the rate of mitotic cell division will result in an increase in the value of N_N, until equilibrium is once again reached.

2. The rate of DNA alkalization from vesicant exposure. A cell with damaged DNA is moved into the cohort N_I, which represents the proportion of cells with injured DNA.
3. The rate of DNA repair. A cell with damaged DNA can once again move back to the N_N cohort, provided there are significant levels of PARP and NAD+ to repair the DNA. Although research has shown that PARP and NAD+ can incorrectly repair DNA, we are not modeling that mechanism or its effect in this implementation of the model.

We can now draw a system diagram for percutaneous injuries that accounts for liquid and vapor vesicant, as shown in Figure 6-14.

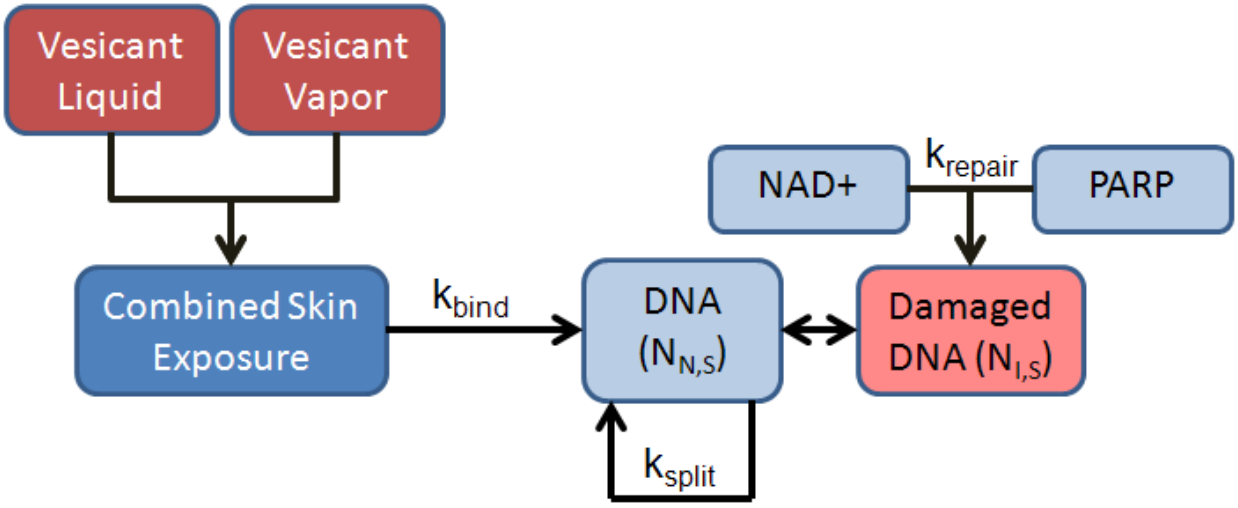

Figure 6-14. Proportion of Healthy Cells in the Skin (N_N)

The equation that describes the above diagram is:

$$\frac{d}{dt}N_N = k_{split} * (1 - N_N) * N_N - k_{bind} * D \quad * N_N + k_{repair} * PARP \quad * NAD \quad * N_I \qquad \textbf{(6-11)}$$

Where:

1. D is the dose in the skin, given in milligrams and described in Section 5,
2. k_{split} is the rate of mitotic division given in min^{-1},
3. k_{bind} is the rate vesicant binds with the DNA in healthy, normal cells in min^{-1},
4. k_{repair} is the rate of DNA repair given in min^{-1}, and
5. NAD and PARP are the relative concentrations of NAD+ and PARP in the skin, respectively, and are defined by the equations in Section 5.2.1.

6.3.2. Proportion of Injured Cells (N_I)

The proportion of injured cells is given by the variable N_I. It describes the proportion of cells at an injury site that have fragmented DNA with respect to vesicant injury.

At equilibrium (pre-exposure), we assume the value of N_I is equal to 0.0, meaning none of the cells at the injury site have been damaged by vesicant exposure. N_I is modified by:

1. The rate of mitotic cell division, which we assume to be proportional to the rate of programmed cell death. For injured cells, mitotic division causes the cell to die. For the percutaneous model, this specifically places the cell in the apoptotic compartment.
2. The rate of DNA alkalization from vesicant exposure. A cell with damaged DNA is moved into the injured cohort.
3. The rate of DNA repair. An injured cell can once again move back to the N_N cohort, provided there are significant levels of PARP and NAD+ to repair the DNA.
4. The rate of necrotic cell death. For the inhalation and ocular model, the principle behind this rate in the GVM is the same as the HD model; an injured cell dies at a constant rate, provided it wasn't repaired by PARP and NAD+. For the percutaneous model, this rate of necrotic cellular death is tied to the depletion of ATP, which increases the concentration of protease, as described in section 5.2

We can now draw a system diagram for percutaneous injuries that accounts for liquid and vapor vesicant, as shown in Figure 6-15.

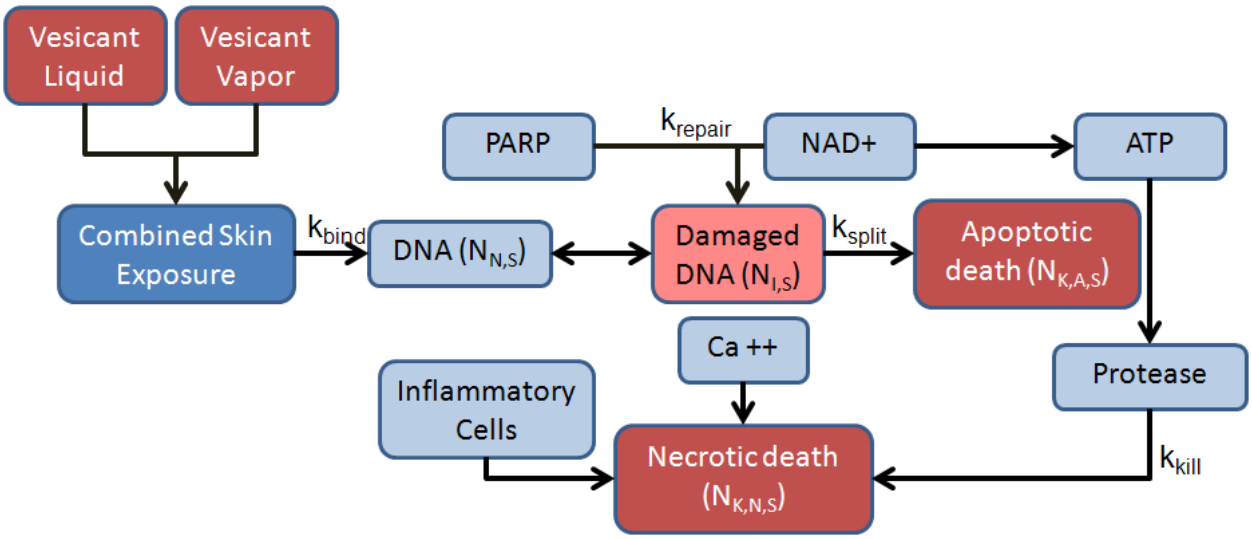

Figure 6-15. Proportion of Injured Cells in the Skin (N_I)

The equation that describes the above diagram is:

$$\frac{d}{dt}N_I = k_{bind} * D \quad * N_N - k_{split} * (1 - N_I) * N_I - k_{repair} * PARP * NAD * N_I - k_{kill} * Prot * Ca * Inflam * N_I \qquad (6\text{-}12)$$

Where:

1. D is the percutaneous dose, given in milligrams,
2. k_{split} is the rate of mitotic division given in min^{-1},

3. k_{bind} is the rate DNA vesicant with the DNA in healthy, normal cells in min^{-1},
4. k_{repair} is the rate of DNA repair given in min^{-1},
5. k_{kill} is the rate of DNA death given in min^{-1},
6. NAD, PARP, Prot, Ca, and Inflam are the relative concentrations of NAD+, PARP, protease, calcium ions, and inflammatory cells, respectively, as described in Section 5.2

6.3.3. Proportion of Apoptotic Cells ($N_{K,A}$)

The proportion of cells undergoing apoptotic cell death is given by the variable $N_{K,A}$. It describes the proportion of cells at an injury site that die as a result of damaged DNA attempting mitotic cell division. We only consider apoptotic cell death for percutaneous injuries in this model. The only data we've come across that could support an apoptotic/necrotic model and give weight to the benefit of differentiating has been done in skin cultures and via percutaneous exposures on animals. It is possible we may have enough data to justify an apoptotic/necrotic model for the eyes and lung, at some point, but have yet to find it at the time of writing this report.

At equilibrium (pre-exposure), we assume the value of $N_{K,A}$ is equal to 0.0, meaning none of the cells at the injury site have been killed via apoptotic cellular death, ***resulting from vesicant exposure***. This is an important distinction, as the primary mode of cellular death is via the apoptotic pathway. The only factor that contributes to apoptotic cell death in our model is:

1. The rate of mitotic cell division, which causes injured cells to die in our model. For the percutaneous model, this specifically places the cell in the apoptotic compartment.

We can draw a system diagram for apoptotic cell death, as shown in Figure 6-16.

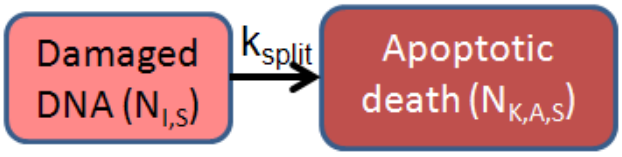

Figure 6-16. Proportion of Apoptotic Cells in the Skin ($N_{K,A}$)

The equation that describes the above diagram is:

$$\frac{d}{dt}N_{K,A} = k_{split} * (1 - N_I) * N_I \qquad (6\text{-}13)$$

Where:

1. k_{split} is the rate of mitotic division given in min^{-1}, and
2. N_I is the proportion of injured skin cells

6.3.4. Proportion of Necrotic Cells ($N_{K,N}$)

The proportion of cells undergoing necrotic cell death is given by the variable $N_{K,N}$. It describes the proportion of cells at an injury site that die as a result of damaged DNA being repaired by PARP. Thus, NAD+ is depleted, which, in turn, depletes ATP stores.

At equilibrium (pre-exposure), we assume the value of $N_{K,N}$ is equal to 0.0, meaning none of the cells at the injury site have been killed via necrotic cellular death. The factors that contribute to necrotic cell death in our model are:

1. The rate of mitotic cell division in injured ocular and lung cells. Attempted mitotic division in injured skin cells results in apoptotic cell death.
2. The rate of cell death due to ATP depletion.

We can now draw a system diagram for necrotic cell death in the skin, as shown in Figure 6-17.

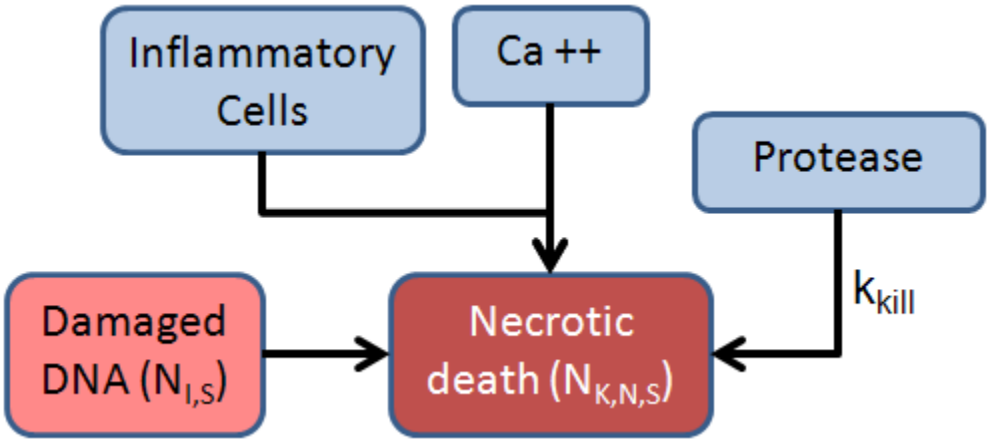

Figure 6-17. Proportion of Necrotic Cells in the Skin ($N_{N,K}$)

The equation that describes the above diagram is:

$$\frac{d}{dt}N_{K,N} = k_{kill} * Prot * Inflam * Ca * N_I \qquad \textit{(6-14)}$$

Where, k_{kill} is the rate of necrotic cell death given in min^{-1}.

6.4 Fitting Cell Concentration Equations

We are getting to the point in the model where we will need to start differentiating between the different agents, primarily for the value k_{bind}, which defines the rate at which vesicant binds with and fragments DNA. This is an agent-dependent variable. However, we are still making the assumption that the other three rates, k_{split}, k_{repair}, and k_{kill}, are still agent-independent for reasons specified below:

- k_{split} is the rate of mitotic cell division, a biological process that changes with the level of injury, regardless of how the injury was caused.

- k_{repair} is the rate at which PARP repairs fractured DNA and is independent of how the DNA became injured.
- k_{kill} is the rate at which protease breaks down injured cells in the absence of ATP and is independent of how the ATP was depleted or the cell was injured.

Due to this assumption, we fit all four parameters using HD as a baseline and then made the necessary adjustments to k_{bind} for the other agents.

6.4.1. The Rate of Mitotic Division (k_{split})

We discussed the rate of mitotic division in the HD paper. For that model, we let the rate of cellular division ultimately be a fit parameter. However, for the GVM, we set the rate of mitotic division at $0.004hr^{-1}$ in order to match the value in the literature (Murray, Mathematical Biology, Volume 2, 1993). We assume that this rate is the same for all three exposure sites of interest. We are assuming that this rate is constant for all exposure sites.

6.4.2. The Repair Rate, Kill Rate, and HD Binding Rate for Percutaneous Exposures

After setting the rate of mitotic division to a rate found in the literature we are left with three equations and three unknowns, an easy problem to solve using an equation solver like Berkeley Madonna. As mentioned, we first calibrated the model to HD, as this would give us values for the repair rate and kill rate in each of the four systems. We can then calibrate the binding rate to each of the remaining agents. For all fits we are trying to capture the rate of injury and repair documented in AMedP-8 (C). For the HD model we attempted to match AMedP-8 (C) severity scales to the proportion of injured and killed cells, but for the GVM we assume that is an unnecessary step. The AMedP-8 (C) severity scales have no real correlation to magnitude of injury (i.e., a Severity Scale of 2 is not necessarily "twice as a severe" as a Severity Scale of 1). Mapping a quantitative value to a qualitative description of illness is not a valid mechanism.

For the GVM we define an Injury function, which is the complement of the normal, healthy cell concentration:

$$Injury = 1 - N_{N,x} \qquad \textbf{(6-15)}$$

In doing so, we are stating that the level of injury is directly related to the concentration of normal, healthy cells. If an exposure site has a 1.0 concentration of normal, healthy cells the model predicts that there is no injury. If an exposure site had a 0.5 concentration of normal, healthy cells the model predicts that only half of the exposure site is operational. We fit the Injury equation, so that it has a similar peak and duration as AMedP-8 (C) severity scales.

6.4.3. Skin Injury

In order to give an example of the fitting process, we focus on percutaneous exposures. The top dose band for percutaneous exposures in AMedP-8 (C) is for exposures greater than 180 mg-min/m^3. As shown in Figure 6-18 (green line), an individual reaches Severity Level 1 at 2 hours, Severity Level 2 at 5 hours, and Severity Level 3 at 24 hours. Severity Level 3 is the injury peak. On the recovery side, an individual goes back down to a Severity Level 1 at 504 hours and is fully recovered at 588 hours. Constraining the equation for Injury to meet these criteria, we got

the parameters for percutaneous exposure to HD that are shown in Figure 6-18. These values were derived using the curve fitting function in Berkeley Madonna.

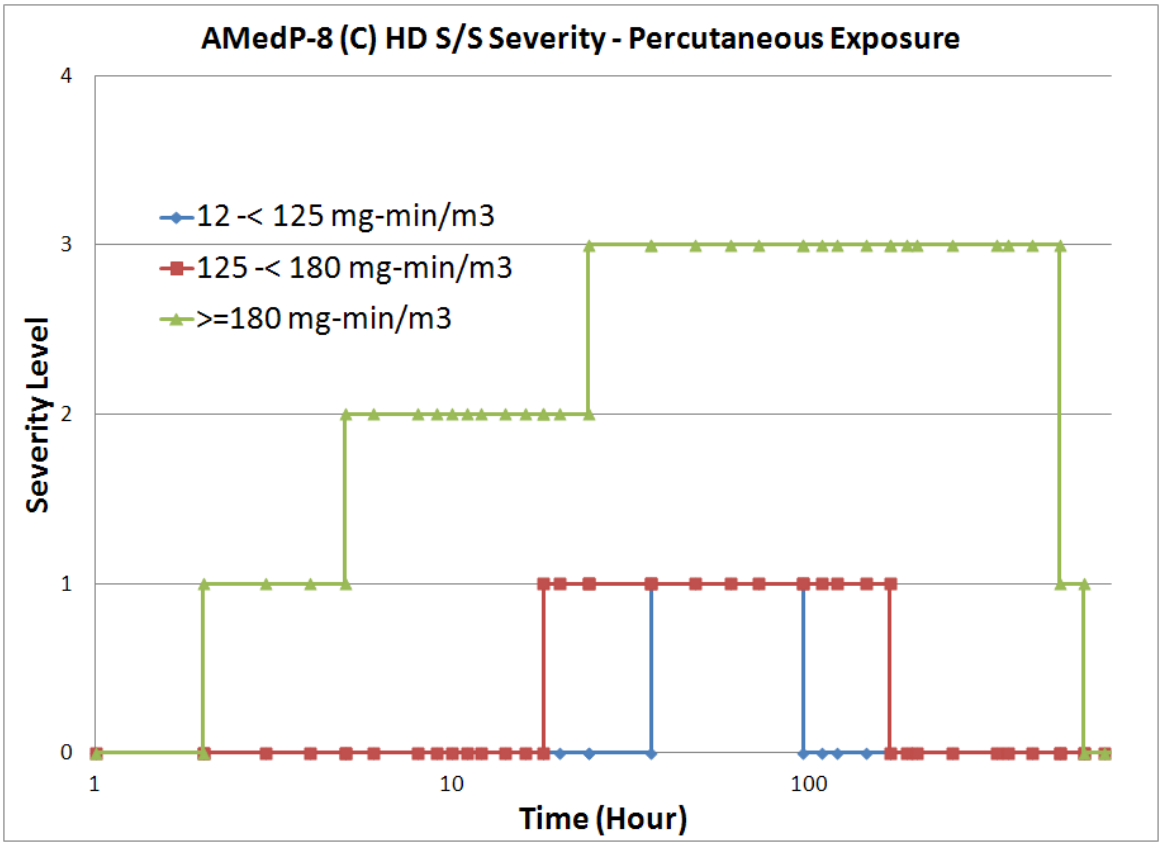

Figure 6-18. AMedP-8 (C) HD S/S/ Severity for Percutaneous Exposures

Table 6-5. HD Percutaneous Values for k_{bind}, k_{repair}, and k_{kill}

k_{bind} (hr^{-1})	k_{repair} (hr^{-1})	k_{kill} (hr^{-1})
0.04	0.003	0.003

Using the values in the table above, we get the results shown in Figure 6-19.

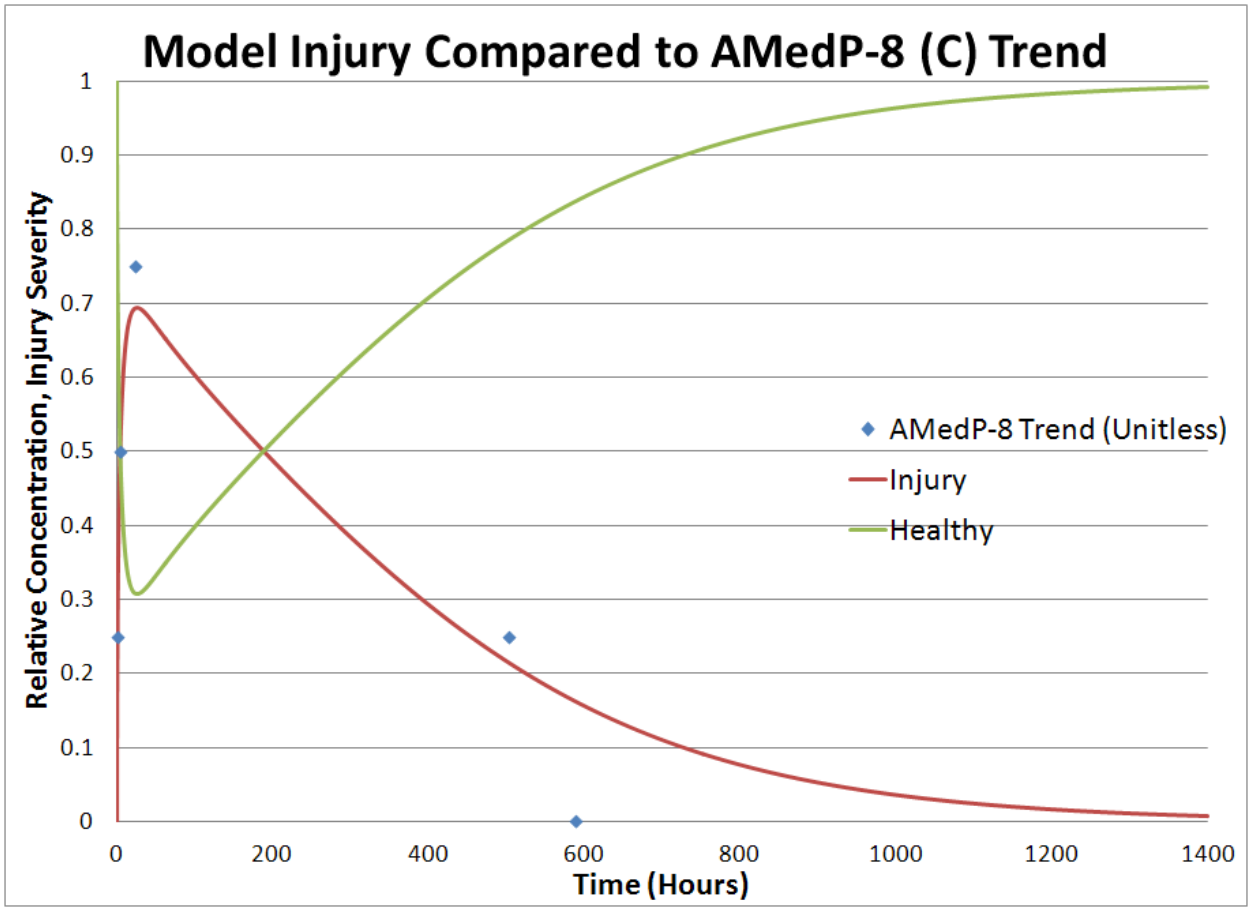

Figure 6-19. Percutaneous Model Output for HD Compared to AMedP-8 (C)

Note how the model peaks at the exact time as the injury profile. Recovery is also consistent with the AMedP-8 (C) output. For the severe percutaneous dosage we get a maximum value of 0.7 for the Injury function, meaning 70% of the cells in the dermis and basal epidermis are injured.

Figure 6-20 shows the concentrations of ATP, PARP, NAD+, and protease, following a 180 mg/m^2 exposure. Note the rapid increase in PARP that leads to a rapid decrease in NAD+ and ATP, which causes a rapid increase in protease.

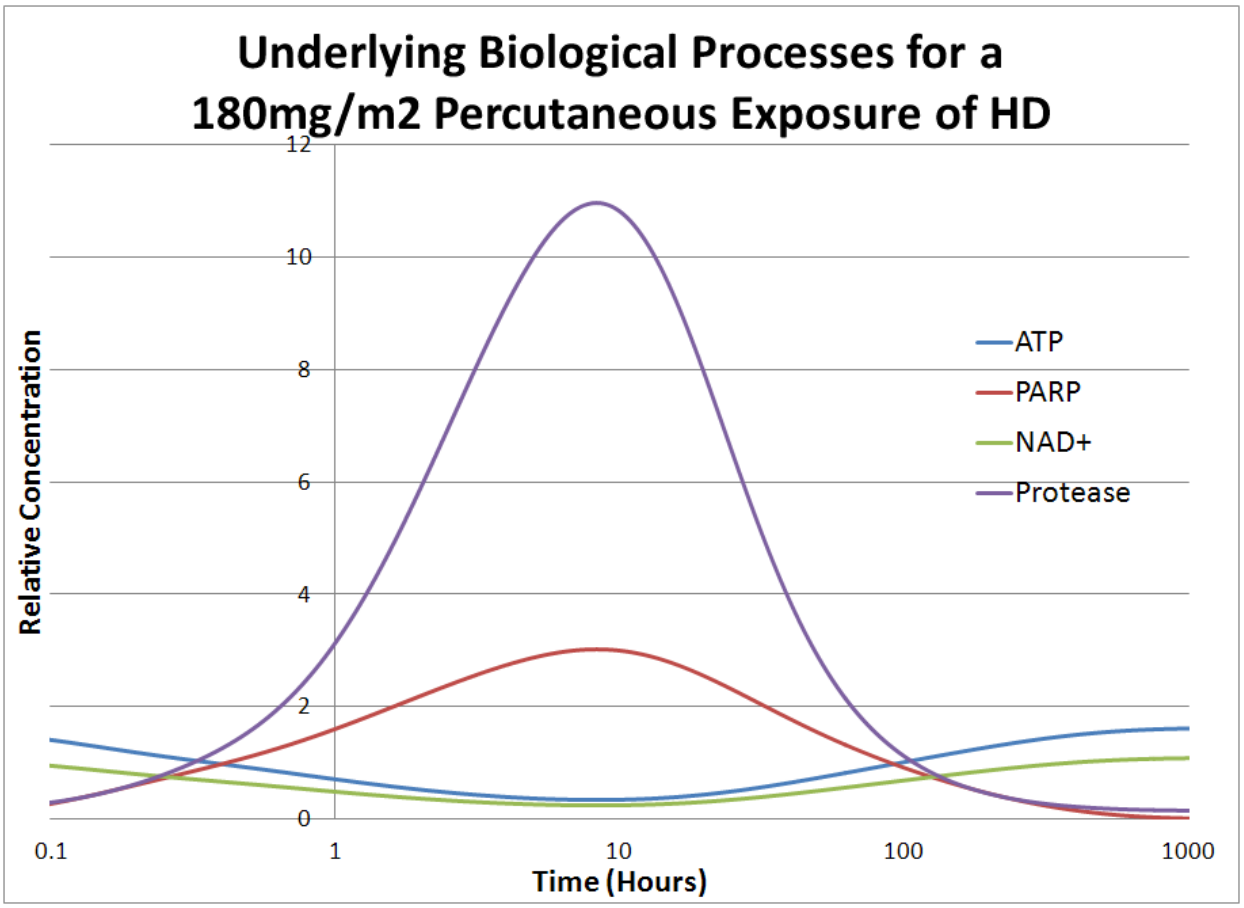

Figure 6-20. ATP, PARP, NAD+, and Protease Concentrations for a 180mg/m2 Percutaneous Exposure to HD.

Figure 6-21 shows the percentage of necrotic and apoptotic cells, following a 180mg/m^2 exposure of HD. Note that at these high exposures, the majority of injured cells become necrotic, indicating a severe injury. The model equations were designed in such a way that would make apoptotic cell death the primary mechanism for low exposures and necrotic cell death the primary mechanism for high exposures. Figure 6-22 shows this phenomenon. A 10mg/m^2 exposure leads to a higher percentage of apoptotic cell death. As the exposure increases, the apoptotic pathway begins to apex, while the necrotic pathway becomes the dominant pathway.

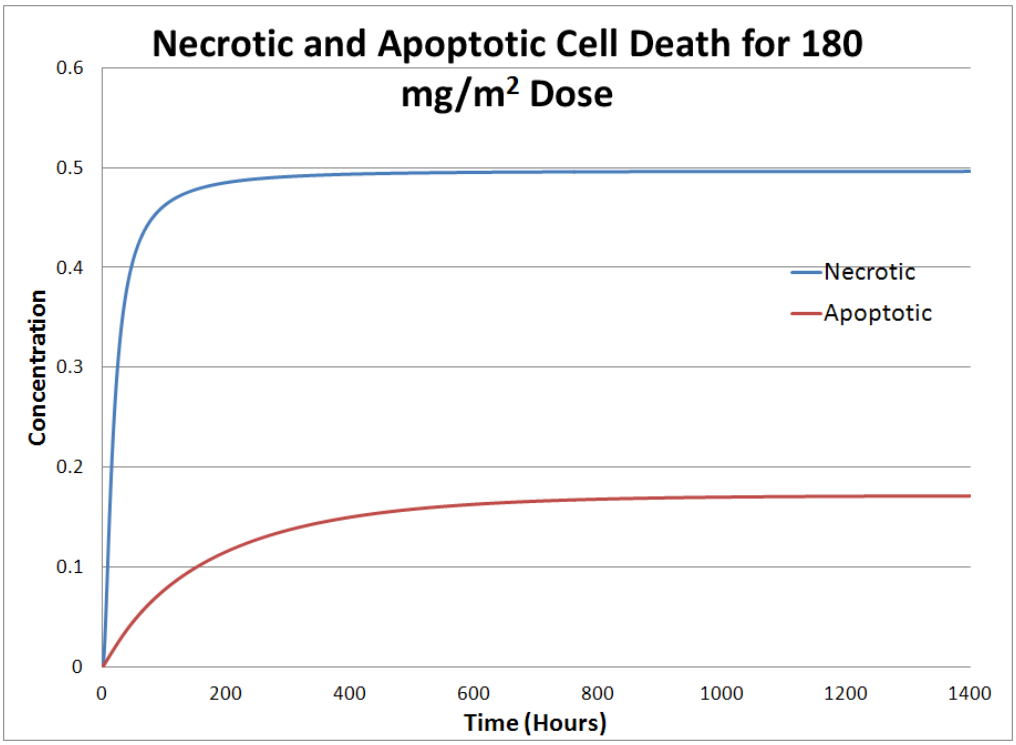

Figure 6-21. Relative Concentration of Necrotic vs. Apoptotic Cell Death for a 180mg/m^2 Percutaneous Exposure to HD.

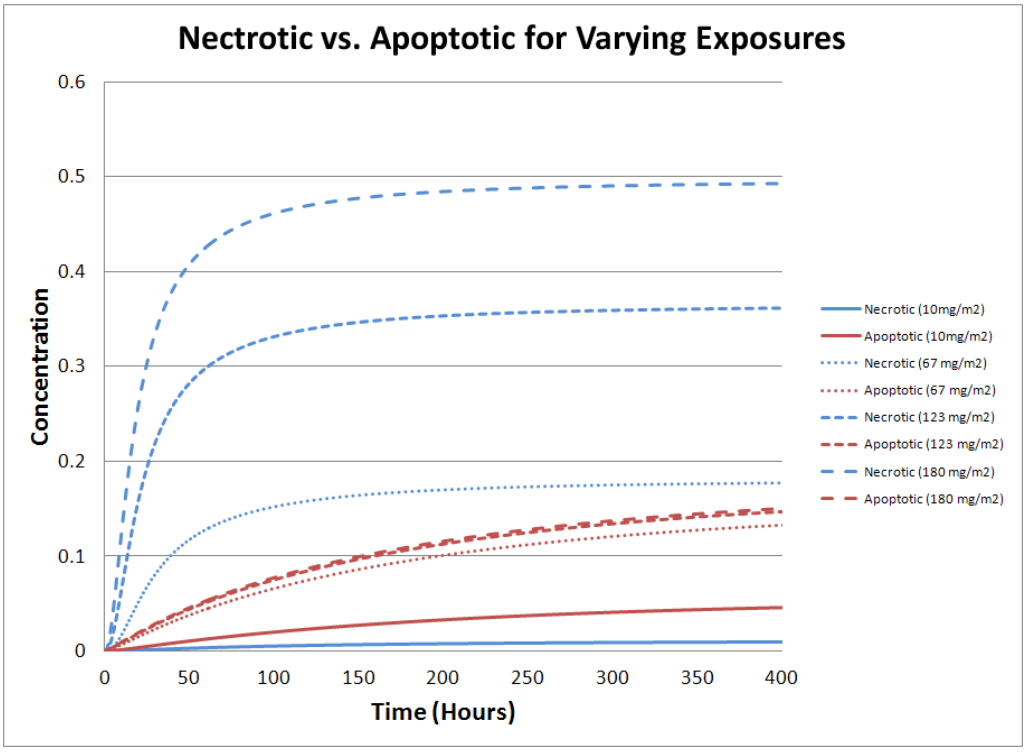

Figure 6-22. Relative Concentration of Necrotic vs. Apoptotic Cell Death for Four Different Percutaneous Exposures of HD.

6.4.4. HN-1, HN-2, HN-3, and Lewisite Binding Rate

The difficulty in modifying the binding rates for these four agents is the fact that FM 3-11.9 reports that they have the same toxicities as HD. This leaves us with two choices:

1. Assume that all five agents have the same exact binding rates.
2. Use the published EPA AEGL values (which are different for some of the agents) to scale these binding rates.

We decided to go with the second option, since the AEGL values represent a more recent review of agent toxicity. The AEGL values for the five vesicants are shown in Figure 6-23.

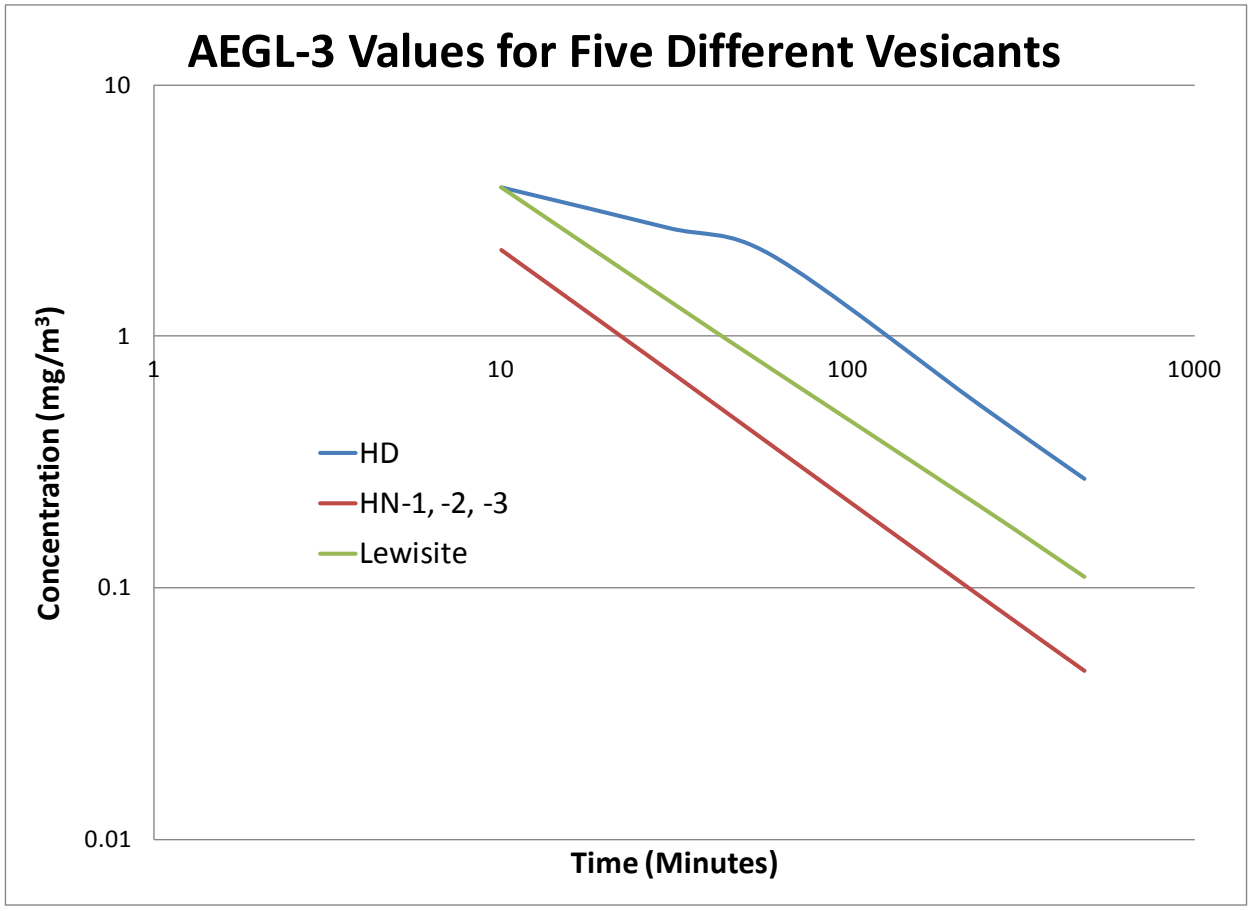

Figure 6-23. AEGL-3 Concentrations for HD, HN-1, HN-2, HN-3, and Lewisite

For the purpose of this model, we are most concerned with the 10-minute AEGL-3 concentrations. Lewisite and HD have equivalent 10-minute AEGL-3 values, adding support to a decision to assume that lewisite and HD have equivalent binding rates. HD and lewisite do deviate from each other with longer exposures, but we do not yet have a mechanism to account for this deviation. It is possible that the difference could come from the variances in the toxicokinetics of the two agents; perhaps, lewisite metabolizes more rapidly than HD. Due to time and data constraints, we were not able to account for this difference in this implementation of the model.

The AEGL documentation does state that being exposed to a 2.2 mg/m^3 concentration of nitrogen mustard for ten minutes will have an equivalent effect as being exposed to a 3.9 mg/m^3 concentration of HD for ten minutes, making nitrogen mustard more toxic than HD. We do not believe this difference can be ignored. In order to account for this difference using the binding rate, we ran the inhalation model using a 3.9 mg/m^3 exposure for ten minutes. This resulted in a peak injury level of approximately 0.31. We wanted to derive a binding rate for nitrogen mustard that resulted in the same injury level as a 2.2 mg/m^3 exposure. This was achieved with a binding rate of 0.6 hr^{-1}. Since this binding rate represents an increase of 1.5 for inhalation exposures, we made the assumption that the binding rate for the other three injury sites are also 1.5 times greater. All of the rate parameter values are summarized in Table 6-6.

6.5 Summary of Rate Parameters

Table 6-6. Summary of all Rate Parameter Values

	Ocular	Inhalation	Percutaneous
k_{split}	0.004	0.004	0.004
k_{bind}, HD	0.4	0.35	0.04
k_{bind}, HN-1, -2, and -3	0.6	0.6	0.06
k_{bind}, lewisite	0.4	0.4	0.04
k_{repair}	10	10	0.003
k_{kill}	5.8	2	0.003

6.6 Calculating Casualties

Since the vesicant model was calibrated using AMedP-8 (C) severity profiles, we need to make use of the dose bands presented in the reference document when calculating casualties. We correlate the dose bands, defined in AMedP-8 (C) to the proportion of killed cells (necrotic cells, particularly, for percutaneous exposures), to determine the severity level for a given exposure. For example, Table 6-7 shows the range of AMedP-8 (C) dose bands and the corresponding proportion of necrotic cells that are calculated in the model. To calculate an individual's severity profile from AMedP-8 (C), you would calculate the proportion of necrotic cells for a given dosage and see where the values lies in relation to Table 6-7.

Table 6-7. AMedP-8 (C) Percutaneous Dose Ranges Compared to Proportion of Necrotic Cell Ranges Following Percutaneous Exposure

AMedP-8 (C) Dose Range	Proportion of Necrotic Cells Range
12 - < 125 mg-min/m^3	0.01 -<0.37
125 - < 180 mg-min/m^3	0.37 - < 0.5
> 180 mg-min/m^3	> 0.5

So if an individual is exposed to 100 mg-min/m^3 of HD, he would have a proportion of necrotic cells equal to 0.39. This value falls in between 0.37 and 0.5 and therefore, the individual's sign/symptom severity profile follows the 125 - <180 mg-min/m^3 profile from AMedP-8 (C). As we'll show in the next section, certain countermeasures will reduce the proportion of necrotic cells and could potentially move an individual into a lower AMedP-8 (C) dose band.

Using the same method detailed above, we calculated the proportion of killed cells dose range for ocular (Table 6-8) and inhalation (Table 6-9) exposures.

Table 6-8. AMedP-8 (C) Ocular Dose Ranges Compared to Proportion of Killed Cell Ranges Following Ocular Exposure

AMedP-8 (C) Dose Range	Proportion of Killed Cells Range
4 - < 26 mg-min/m^3	0.05 -<0.21
26 - < 50 mg-min/m^3	0.21 - < 0.38
50 - < 70 mg-min/m^3	0.38 - <.51
70 - < 100 mg-min/m^3	0.51 - < 0.73
> 100 mg-min/m^3	> 0.73

Table 6-9. AMedP-8 (C) Inhalation Dose Ranges Compared to Proportion of Killed Cell Ranges Following Inhalation Exposure

AMedP-8 (C) Dose Range	Proportion of Necrotic Cells Range
50 - < 70 mg-min/m^3	0.16 -<0.22
70 - < 100 mg-min/m^3	0.22 - < 0.3
100 - < 150 mg-min/m^3	0.3 - < 0.45
150 - < 250 mg-min/m^3	0.45 - < 0.8
250 - < 1200 mg-min/m^3	0.8 - < 1.0
> 1200 mg-min/m^3	> 1.0

6.7 Calculating Fatalities

In AMedP-8 (C), a fatality is someone who spends 15 minutes at Severity Level 4. This would make everyone who receives an inhalation dose greater than 250 mg-min/m^3, a fatality. Using the criteria for casualty calculation, we can adopt the same methodology in the GVM for inhalation exposures. If an individual spends greater than 10 minutes with a proportion of necrotic cells greater than 0.8, the individual becomes a fatality.

For systemic effects, however, we must make use of the GSH suppression level, since an LD_{50} for percutaneous exposures (1400 mg/man) will lead to complete necrosis of the injury site as would significantly lower doses. Therefore, necrosis at the injury site is not a good metric for systemic lethality in the GVM. AMedP-8 (C) uses > 1400 mg per man as the fatal percutaneous band. This value is equivalent to the LD_{50} in FM 3-11.9. Since we don't have any other systemic dosage bands in AMedP-8 (C), we decided to make use of the toxicity data for percutaneous exposures for calculating the incidence of lethality via systemic injuries.

FM 3-11.9 specifies an LD_{50} of 1400 mg per man and a probit slope of 7 for HD, HN-1, HN-2, HN-3, and lewisite. Using these values to calculate 20 doses between the LD01 (651 mg/man) and the LD99 (3010 mg/man) and using those doses as inputs into the GVM results in a range of GSH suppression levels from 0.17 to 0.81. Figure 6-24 shows the plot of incidence of fatality as a function of GSH suppression, along with the corresponding fit to a log-normal distribution (dashed line).

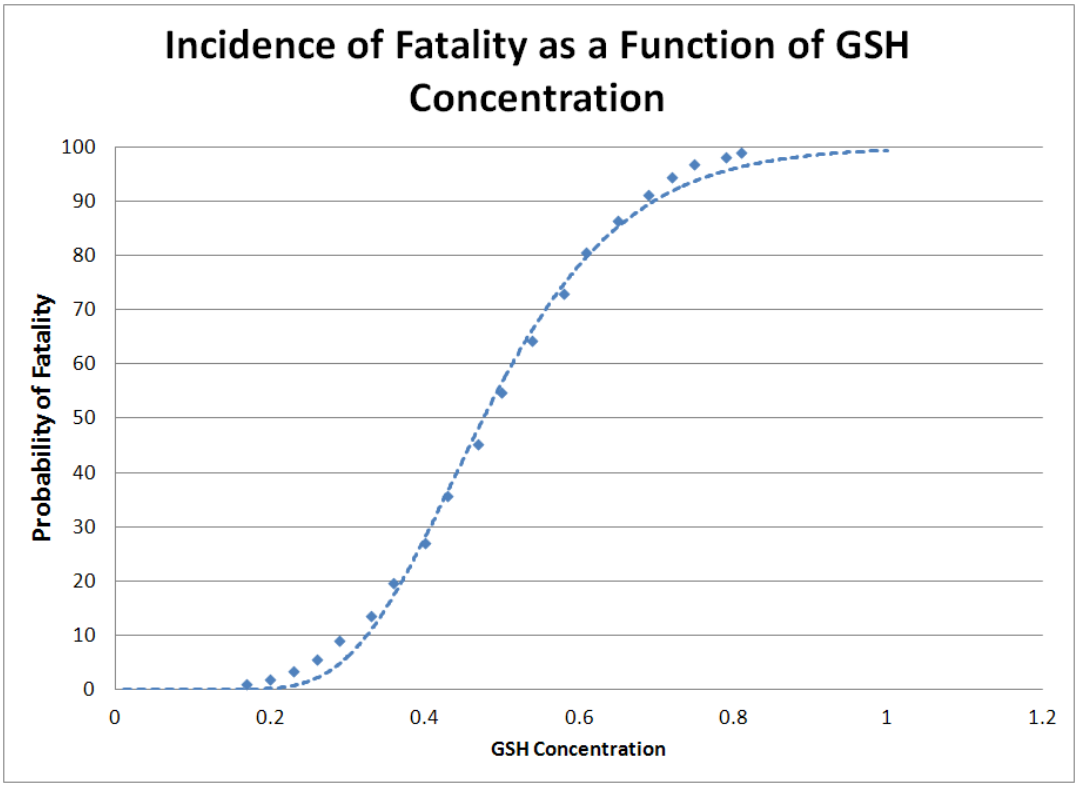

Figure 6-24. Incidence of Fatality as a Function of GSH Concentration Following Systemic Exposures.

The equation for the log-normal distribution of Probability of Fatality for a given GSH suppression level is:

$$Probability\ of\ Fatality = \frac{1}{2}\mathrm{erfc}\left(\frac{-\ln(1-\mathrm{GSH})+\mu}{\sigma * \sqrt{2}}\right) \quad \textbf{(6-16)}$$

Where:

1. erfc is the complementary error function,
2. GSH is the concentration of GSH,
3. μ is the mean, equal to 0.74, and
4. σ is the standard deviation, equal to 0.29.

In order to calculate whether or not someone becomes a fatality, you would first calculate their GSH level, use it in the above equation to get the Probability of Fatality, and then compare that value to a random draw. For example, if a person were to calculate a Probability of Fatality of 0.5, and random draw greater than 0.5, would result in that person becoming a fatality.

This page is intentionally left blank.

Section 7.

Vesicant Countermeasure Model Framework

We are including the same medical countermeasures in the GVM that were proposed by USAMRICD, with the exception of calcium modulators. As mentioned earlier in this paper, we are excluding calcium modulators because they have not been shown to have a therapeutic effect *in vitro*. The countermeasures proposed by USAMRICD are listed in Table 7-1.

Table 7-1. Proposed Medical Countermeasure Development Areas (Smith W. J., 2009)

Biochemical Event	Pharmacologic Strategy	Example
DNA alkylation	Scavengers	N-acetyl cysteine
DNA strand breaks	Cell cycle inhibitors	Mimosine
PARP activation	PARP inhibitors	Niacinamide
Proteolytic activation	Protease inhibitors	AEBSF is a sulfonyl fluoride compound
Inflammation	Anti-inflammatories	Indomethacin, capsaicin, hydrocortisone

The five countermeasures we will focus on have the following mechanisms of action:

1. **Scavengers** – Act as a sink for vesicants before DNA strand breakage can occur (Bobb, 2005). Used as a prophylactic, an intracellular scavenger such as NAC increases the level of gluthathione (GSH) within cells, a compound that HD has a natural affinity for. HD reacts with the GSH and is rendered inert. This effect appeared in cancer patients that use HD as chemotherapy. When used in conjunction with NAC, low levels of HD have a diminished effect. This prompted research into NAC as a chemoprotectant against HD and it has been found to significantly reduce lung injury in rats, when used as both a prophylactic and post-exposure countermeasure.
2. **Cell cycle inhibitors** – Stops the proliferation of cells by stopping DNA replication (Krude, 1999). Mimosine, for example, stops the replication of DNA in the G1 phase, before the strands fork. This treatment delays the production of new cells, allowing DNA repair to take place, and also stops injured cells from attempting to replicate, resulting in a killed cell.
3. **PARP inhibitors** – Inhibits poly(ADP-ribose) polymerase (PARP), an enzyme responsible for DNA repair. It was observed that PARP inhibitors are capable of arresting DNA fragmentation that is associated with mustard injuries (Meier, 1998).
4. **Protease inhibitors** – Blocks protease from breaking down the epithelial attachment. AEBSF specifically targets proteases that cut peptide bonds in proteins. The inhibition process using AEBSF is irreversible, allowing DNA to repair itself and return the body to a stable baseline.

5. **Anti-inflammatories** – Multiple anti-inflammatories have been shown to reduce the signs and symptoms associated with mustard exposure. They work to slow erythema, but their effect decreases over time (Yourick, 1995). However, delaying the onset of erythema allows for treatment that repairs the fragmented DNA.

In addition to these five countermeasures, we are also including a model for British anti-Lewisite (BAL). BAL is a chelating agent that is very effective at removing lewisite (and other heavy metals) at the injury site (Vilensky & Redman, 2003) and systemically.

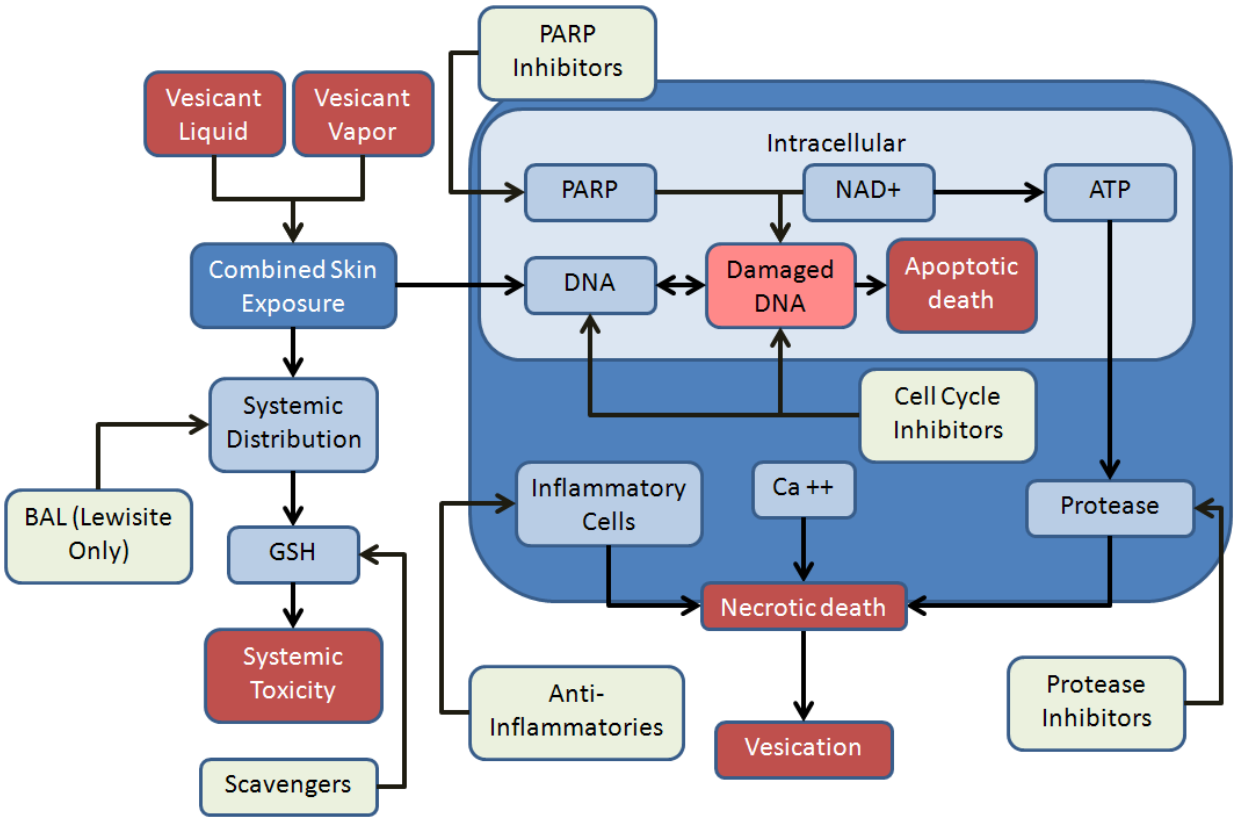

Figure 7-1. System Diagram for Vesicant Countermeasures

This section will document the models and data for each of the countermeasures. An additional benefit to the revised injury model mechanism for the GVM is we no longer have to derive rates of action for each of these countermeasures. In all cases, the countermeasures work to reduce the concentration of the compartment that it is acting on. Since these individual compartments are no longer based on differential equations, the countermeasures can now act as dose-dependent scaling factors that work to reduce the concentration in the compartment. One exception to this rule is the cell-cycle inhibitors, which will effectively reduce the level of mitotic cell division to zero. Each of the proceeding sections will discuss how the countermeasure model is different than the model proposed for HD and provide new model equations based on the reviewed literature.

7.1 Scavengers

In the HD model, we derived two rates that described the efficacy of scavengers against HD exposure: the rate at which scavengers sequester HD in the lungs, the rate at which scavengers sequester HD in the skin. We based our derivations on a study performed by K. Atkins, et. al. (Atkins, Lodhim, Hurley, & Hinshaw, 2000) that studied the efficacy of N-acetylcysteine (NAC) against HD exposures in epithelial cells. We will turn to this study again for discussion on how to incorporate scavengers into the model. Table 7-2 summarizes the result from the Atkins et al. study.

Table 7-2. Efficacy of IntracellularSscavenger NAC against HD (Atkins, 2000)

	Control			500 μM HD		
	% Viable	% Apoptotic	% Necrotic	% Viable	% Apoptotic	% Necrotic
Untreated	90.3±3.1	3.6±2.1	6.1±2.8	50.4±4.0	33.1±5.0	16.3±4.5
0.2 mM BSO	91.0±3.0	2.7±0.6	6.3±3.1	35.7±8.4	32.7±10.3	31.7±17.8
50 mM NAC	92.3±3.6	2.5±1.0	4.3±2.6	69.3±1.7	21.2±4.3	9.5±4.4
BSO + NAC	92.7±4.0	2.0±1.0	5.3±3.2	51.7±4.7	37.0±5.7	11.3±1.2
2.5 mM GSH	88±0.0	3.6±2.1	6.1±2.8	72.7±5.9	15.7±5.5	11.7±4.2
5.0 mM GSH	88.0±5.5	4.8±2.5	9.8±5.6	75.4±5.6	11.3±1.3	11.3±4.2
10.0 mM GSH	83.0±4.0	4.0±1.7	13.3±3.0	66.7±6.4	10.7±3.2	23.0±3.6

The study measured the viability of exposed cells (a value that correlates directly with the percentage of normal, healthy cells), and the percentages of apoptotic and necrotic cells following treatment. For a 500μM exposure of HD, untreated cells had 50.4% viability with 33.1% of cells being apoptotic and 16.3% of cells being necrotic. 50mM of NAC increased the percentage of viable cells to 69.3% while decreasing the percentage of apoptotic and necrotic cells to 21.2% and 9.5%, respectively. This is equivalent to a protection factor of approximately 1.5 for a 1:10 dosage of NAC.

However, a second study (Sharma, Vijayaraghavan, & Agrawal, 2010) did not result in the same level of efficacy for NAC. This study looked at NAC efficacy (along with other GSH-producing countermeasures) in mice exposed to a LD50 of nitrogen mustard and sulfur mustard. In that study, a dose of 185 mg/kg of NAC was applied following an 8.1 mg/kg dosing of HD (at comparable dosage of nitrogen mustard) and showed no statistically significant change in the percentage of viable cells at the injury site.

Obviously, the results from these two studies are drastically different. One potential reason for the discrepancy is the efficacious benefit of NAC was overpowered by the high dosing of vesicant. If we consider that NAC stimulates GSH production in the cell, it is possible to postulate a point at which even the maximum rate of increased GSH production is insignificant, compared to the dose of vesicant at the cellular level.

A second possibility is that the mechanism of NAC administration in the Sharma et al. study (oral dosing) does little to affect the level of injury, but instead affects the incidence of lethality by decreasing the level of oxidative stress. However, in the Sharma study, there was very little decrease in the GSH level in the liver following NAC administration.

A third possibility is that NAC is not efficacious against percutaneous exposures. The Atkins et al. study was performed on lung epithelial cells and the Sharma et. al. study was performed via percutaneous administration of vesicants. This possibility is strengthened by looking at a study performed by Om Kumar et al. (Kumar, Sugendran, & Vijayarghavan, 2001). In this study, the researchers looked at the effect that three scavengers (trolox, quercetin, and pure GSH) have on lethality in HD-exposed mice. Unfortunately, NAC was not included in the study. All three scavengers showed a dramatic increase in survival time for mice that were exposed via inhaled HD (100% of mice died on day 7 without treatment; 12.5%, 12.5%, and 25% died on day seven following trolox, quercetin, and GSH, respectively) and no significant change in survival time when mice were exposed percutaneously.

Given the result of these three studies, we assume that NAC (and other scavengers) are most efficacious in the lungs. Knowing that scavengers work to reduce the dose of vesicant available to attack the DNA of normal, healthy cells, we use NAC to modify the inhaled dosage $N_{N,I}$. In the Atkins et al. study, a 1:10 dosage, of NAC vs. agent, results in a 39% increase in viable cells. That seems like a drastic increase in cell viability, but the Kumar et al. study showed the level of efficacy that scavengers like NAC are capable of achieving. We incorporate NAC into the model by accounting for its dose-reducing properties in the equation for D_i.

$$\frac{d}{dt}D_i = \int_0^{T_{mask}} C\,dt * b - NAC_{reduction} * k_{bind} * N_{N,i} * D_i \qquad \textit{(7-1)}$$

Since we don't have the necessary data to support a dose-dependent model of NAC efficacy, or found a study that sampled multiple dosings of NAC, or a study of NAC being used for anything outside of prophylaxis, we had to assume that pre-exposure administration of NAC leads to a 39% increase in viable cells in the lungs, as shown in Atkins, et. al. Therefore, the value for $NAC_{reduction}$ is 1.0 if no NAC is administered and 1.39 if NAC is administered. Note that the proposed application of NAC against vesicant injuries is as a pre-exposure prophylaxis, so this model is consistent with current doctrine. If NAC is ever proposed as a post-exposure antidote for vesicant exposures, we will revisit this model. However, given the rapid action of vesicants in the lungs and the fact that NAC has not been shown to be beneficial against percutaneous injuries, we find the likelihood if it being designated an antidote relatively small.

In order to see what NAC does in the GVM, we varied the inhaled dose of HD from 250 mg-min/m3 (the lower bound of the first dose band that causes acute lethality) to 250 mg-min/m3 and calculated the value for $N_{K,I}$. The results are shown in Table 7-3.

Table 7-3. Fraction of Killed Cells With and Without NAC

Dose (mg/man)	250	260	270	280	290	300	310	325	340	350
$N_{K,I}$ (without NAC)	0.8	0.83	0.87	0.91	0.96	1	1	1	1	1
$N_{K,I}$ (with NAC)	0.56	0.58	0.61	0.63	0.66	0.69	0.72	0.75	0.79	0.83

For the high, lethality-causing doses, NAC significantly lowers the proportion of cells. As a reminder, the value for inhalation lethality is anything over 0.8. The $N_{K,I}$ range for the most severe, non-lethal AMedP-8 (C) dose band is 0.45 – 0.8. With NAC, the model predicts that an individual would survive a dose of up to 340 mg-min/m^3, but they will still exhibit severe effects.

7.2 Cell-Cycle Inhibitors

When we developed the cell-cycle inhibitor model for HD, we underwent a thorough literature review and developed a pharmacokinetic and dynamic model for cell-cycle inhibitors. The models ended up predicting that cell-cycle inhibitors did more harm than good as the injury progressed, despite published studies showing a slight overall beneficial effect of cell-cycle inhibitors. At the time, we reported that the discrepancy could come from a lack of modeling for apoptotic vs. necrotic death. Since cell-cycle inhibitors work to slow mitotic division, they would work to stop the apoptotic pathway in the percutaneous model. For low doses, this would result in a lower concentration of apoptotic cells, but at the risk of having a higher proportion of necrotic cells. So, even if the overall proportion of killed cells decreases, cell-cycle inhibitors would work to actually increase the level of necrotic cells, thereby increasing the concentration we use as a metric for injury severity.

We believe our model captured the concentration and efficacy of cell-cycle inhibitors, which we reused in the model for the GVM.

The method for incorporating cell-cycle inhibitors into the HD model was to multiply the terms that account for mitotic cell division, by a scaling function *f(CC),* which is equal to:

$$f(CC) = \begin{matrix} 0, CC \leq CC_{dose} \\ CC_{eff}, CC > CC_{dose} \end{matrix} \quad \textbf{(7-2)}$$

Where CC_{dose} is the efficacious dose of the cell-cycle inhibitor (for mimosine we derived a value of 0.1 ng/mL) and C_{eff} represented the efficacy of the cell-cycle inhibitor (for mimosine we derived a value of 1.0, meaning it was completely effective in stopping mitotic division). CC was the calculated concentration of cell-cycle inhibitor in ng/mL, which is given by:

$$CC = D_{CC} * y * e^{-zt} \quad \textbf{(7-3)}$$

Where DCC is the user-inputted administered dose, and *y* and *z* were constants fit to 20 and 0.49, respectively. Since cell-cycle inhibitors are to be used sparingly, due to potential adverse side effects, we modified the above equations to account for time of administration as well as administered dose.

$$CC = \begin{matrix} D_{CC} * y * e^{-zt}, t > t_{admin} \\ 0, t \leq t_{admin} \end{matrix} \quad \textbf{(7-4)}$$

Where t_{admin} is the time the cell-cycle inhibitor was given in hours.

The model accounts for the effect of cell-cycle inhibitors by multiplying the mitotic cell division terms in the healthy cell and injured cell equations by 1-f(CC). The relative concentration of normal, healthy cells therefore becomes:

$$\frac{d}{dt}N_N = \big(1 - f(CC)\big) * k_{split} * (1 - N_N) * N_N - k_{bind} * D \quad * N_N + k_{repair} * PARP \quad * NAD \quad * N_I$$

And the relative concentration of injured cells becomes:

$$\frac{d}{dt}N_I = \big(1 - f(CC)\big) * k_{bind} * D \quad * N_N - k_{split} * (1 - \mathrm{N_I}) * N_I - k_{repair} * PARP * NAD * N_I - k_{kill} * Prot * Ca * Inflam * N_I$$

Since CC_{eff} is equal to 1, the implementation effectively states that the cell-cycle inhibitors are completely effective as long as they are present in the body above some threshold.

The model now more accurately predicts the therapeutic effects of cell-cycle inhibitors against vesicants. Figure 7-2 shows the model prediction for cell-cycle inhibitor effectiveness against the concentrations of necrotic (blue) and apoptotic (red) cells as well as the overall concentration of killed cells (green) with and without (dashes) 100mg of mimosine. As the figure shows, cell-cycle inhibitors have a very small effect on the overall level of killed cells, decreasing the proportion of apoptotic cells, and increasing the proportion of necrotic cells.

The model even does a good job of matching the published protection factors of mimosine. In a study performed by ICD (Smith W. S., 1993), the researchers reported a 4% increase in viable cells at 24 hours following pre-exposure mimosine dosing, whereas our model predicts a 3.3% decrease in killed cells at 24 hours (0.152 without mimosine and 0.147 with mimosine); however, the study does not differentiate between apoptotic and necrotic deaths.

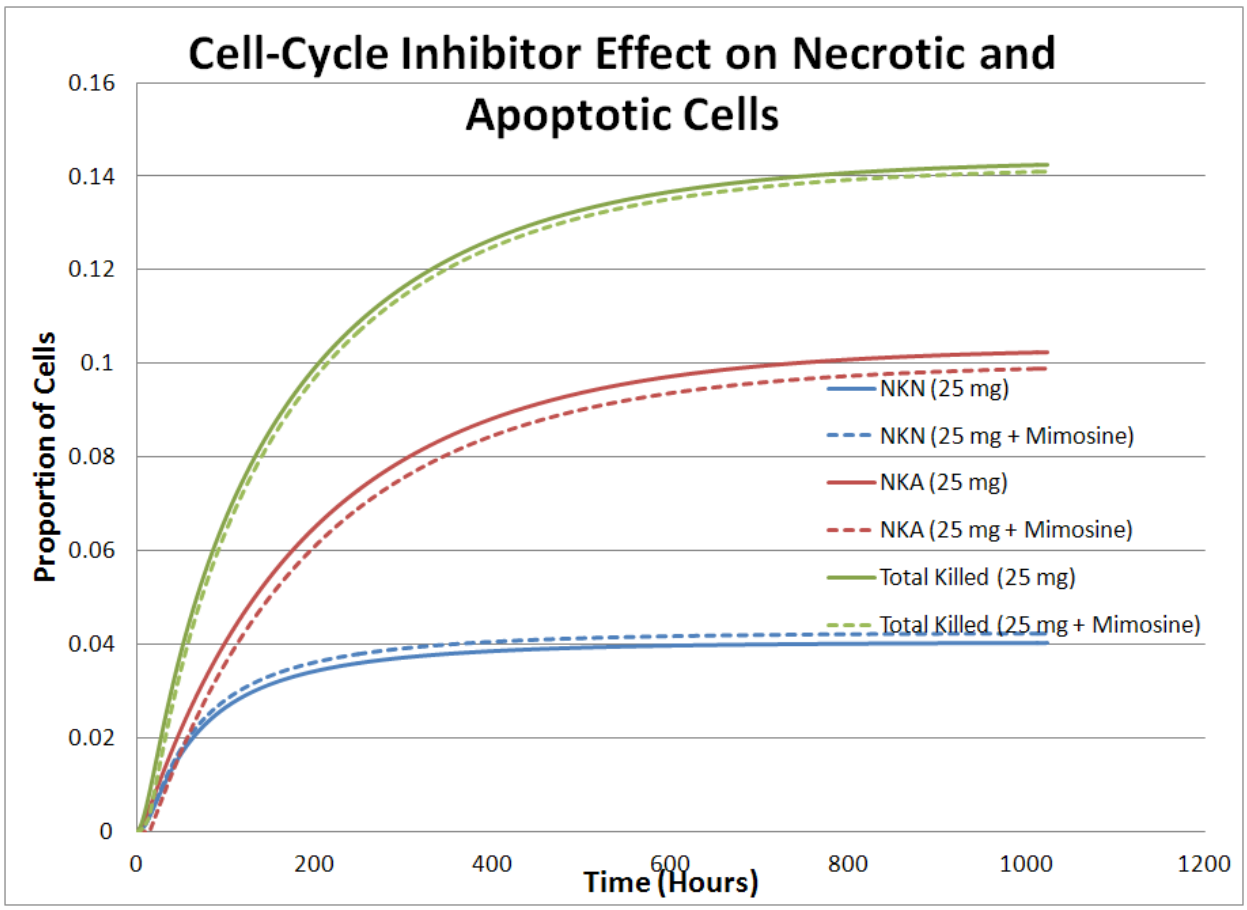

Figure 7-2. Cell-Cycle Inhibitor Effect on Nectrotic and Apoptotic Cells Following Percutaneous Exposure to Vesicants

Figure 7-3 shows the model prediction for cell-cycle inhibitor effectiveness for five different dosing times. Notice how the cell-cycle inhibitor is predicted to be more efficacious as the dosing time gets later. This agrees with the model's framework, as cell-cycle inhibitors provide a window of protection against apoptotic cell death. As that window is shifted towards the time at which injury levels are at their highest (12-48 hours according to the model), the cell-cycle inhibitor would have the greatest effect against cells dying via attempting mitotic division. As the dosing time is delayed further, however, the cell-cycle inhibitors will begin to lose efficacy according to our model. This trend is also noted in the literature. In the Smith et. al. study, mentioned above, the efficacy of cell-cycle inhibitors against HD was measured when mimosine was dosed at 3, 5, and 21-hours post-exposure. The efficacy at 24 hours for the three dosings was measured to be 17%, 15%, and 15% respectively, compared to the 4% when the cells were dosed before exposure.

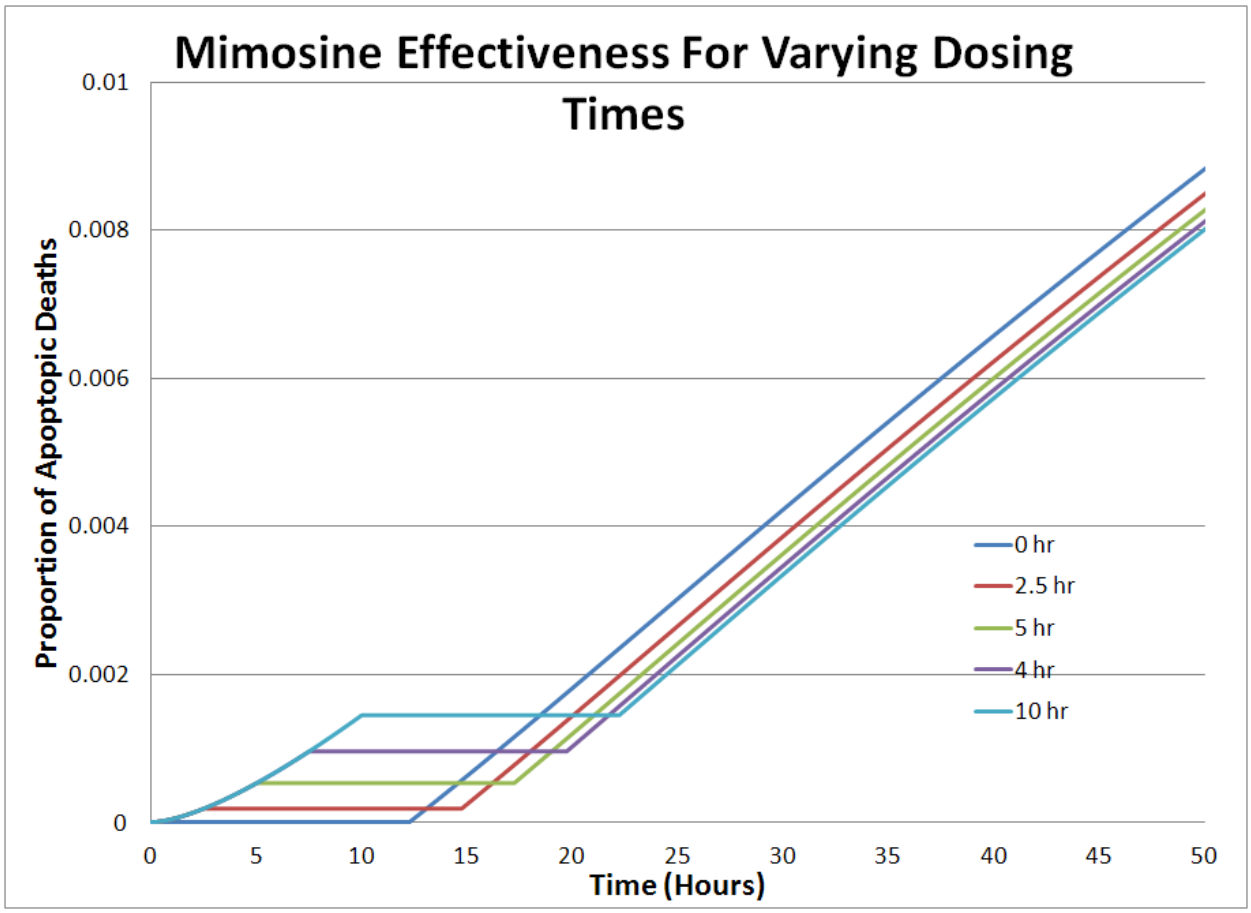

Figure 7-3. Cell-Cycle Inhibitor Effectiveness for Different Administration Times

7.3 PARP Inhibitors

For the HD model, PARP inhibitors were measured by the reduction of the concentration of PARP. We defined an inhibition rate k_{PARPi} that permanently removed PARP from the model. Once again, the model produced results that were not supported by the literature. In one study (Bhat, Ramachandra, J., & Ray, 2004), the researchers found that PARP inhibition using 3-amino benzamide (3-AB) reduced the repair rate of human epidermal keratinocytes by 66%. Whereas the HD model did predict a reduction in the concentration of killed cells early on (<15 hours), the PARP inhibitors ultimately resulted in an increase in cellular death in our model when compared to untreated individuals. Looking back at the model, this probably resulted from not having a toxicodynamic model for vesicants that accounted for the rate at which HD is metabolized. Nor did we have a model that differentiated between necrotic and apoptotic cell death. With the GVM, we are now accounting for PARP inhibitors by first including a pharmacokinetic model for PARP and then using the concentration of PARP inhibitors to scale the concentration of PARP in the body.

For the pharmacokinetic model we turn to a study conducted by Rolf W. Sparidans (Sparidans, Martensa, Iersel, Hartigh, Schellensa, & Beijnena, 2011) where plasma concentrations of the PARP inhibitor olaparib were measured in a human, following a 50mg dose. The result for this study is shown in Figure 7-4 along with the corresponding quadratic fit.

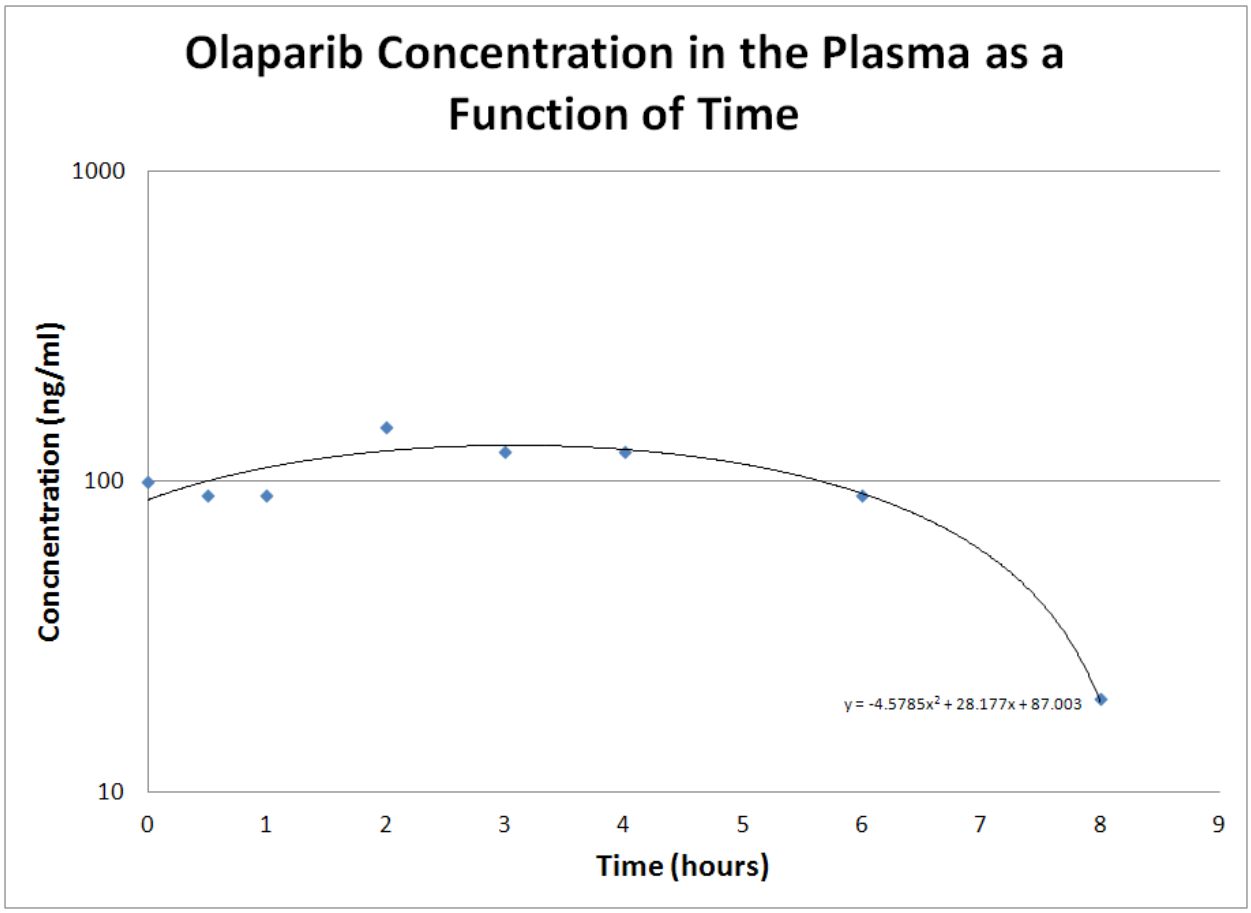

Figure 7-4. PARP Concentrations in the Plasma Following a 50mg dose

The PARP inhibitor concentrations remain relatively flat for the first six hours before experiencing a rapid drop-off in concentration. The equation for PARP inhibitor concentration (in ng/mL) is given by:

$$PARPIn = -4.6 * (t - t_{admin})^2 + 28.2 * (t - t_{admin}) + 87 \quad (7\text{-}5)$$

where t_{admin} is the time at which the PARP inhibitor is given. Using this model, an individual will get approximately 8 hours of protection from a single dosing of PARP inhibitors. We next defined a parameter $PARPIn_{eff}$, which represents the efficacy of PARP inhibitors. Using the study performed by Bhat et al., we set the value of $PARPIn_{eff}$, so that there would be a 66% reduction in PARP levels when PARP inhibitors are at their highest concentrations. We do this by first normalizing Equation 6-5 to have a maximum value of 1.0, as shown in Figure 7-5.

This modifies Equation (7-5) to:

$$PARPIn = -0.03 * (t - t_{admin})^2 + 0.19 * (t - t_{admin}) + 0.58 \quad (7\text{-}6)$$

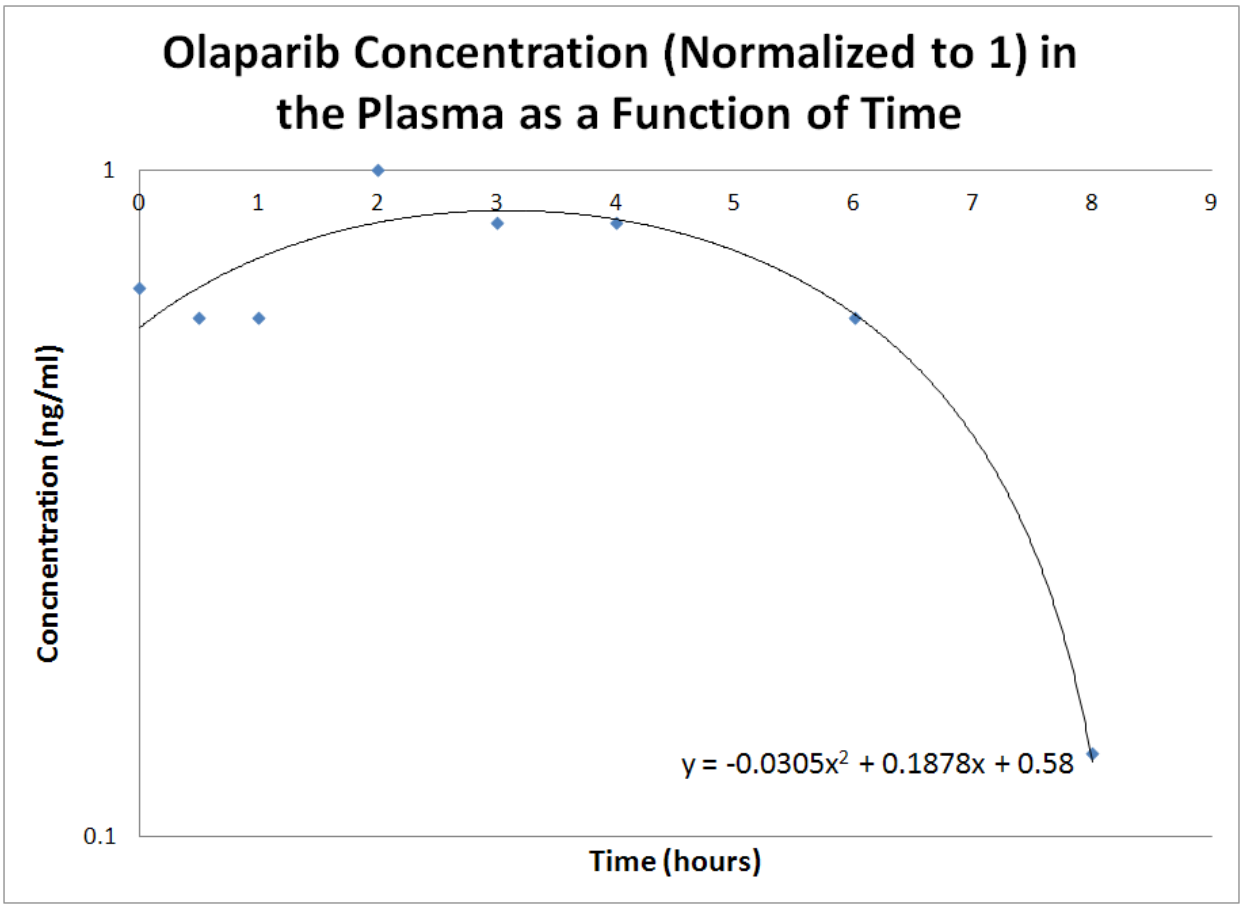

Figure 7-5. PARP Concentrations (Normalized to 1) in the Plasma Following a 50mg Dose

The concentration of PARP can now be modeled as:

$$PARP = (1 - PARP_{eff} * PARP_{conc}) * 5.91 * N_{I,x} \qquad (7\text{-}7)$$

The model prediction for PARP inhibitor effectiveness for three different dosing times is shown in Figure 7-6. Notice that PARP inhibitors have the opposite effect of cell-cycle inhibitors; they actually work to reduce the percentage of necrotic cell death, while increasing the percentage of apoptotic cells. This is consistent with the model and with the known injury mechanism for vesicants. Also, PARP inhibitors are predicted to be more effective with delayed treatment times, as the 8-hour window of protection is most beneficial when PARP would be most active. One interesting fact about the model is that if you delay the dosing long enough, PARP inhibitors actually increase the percentage of necrotic cells. This is probably due to NAD+ concentrations that are directly correlated with PARP concentrations in this model. Keeping PARP levels low at a time when NAD+ levels are low leads to an increase in necrotic cell death. We have no evidence to support this trend, so for this implementation we recommend keeping the PARP inhibitor dosing at less than 10 hours.

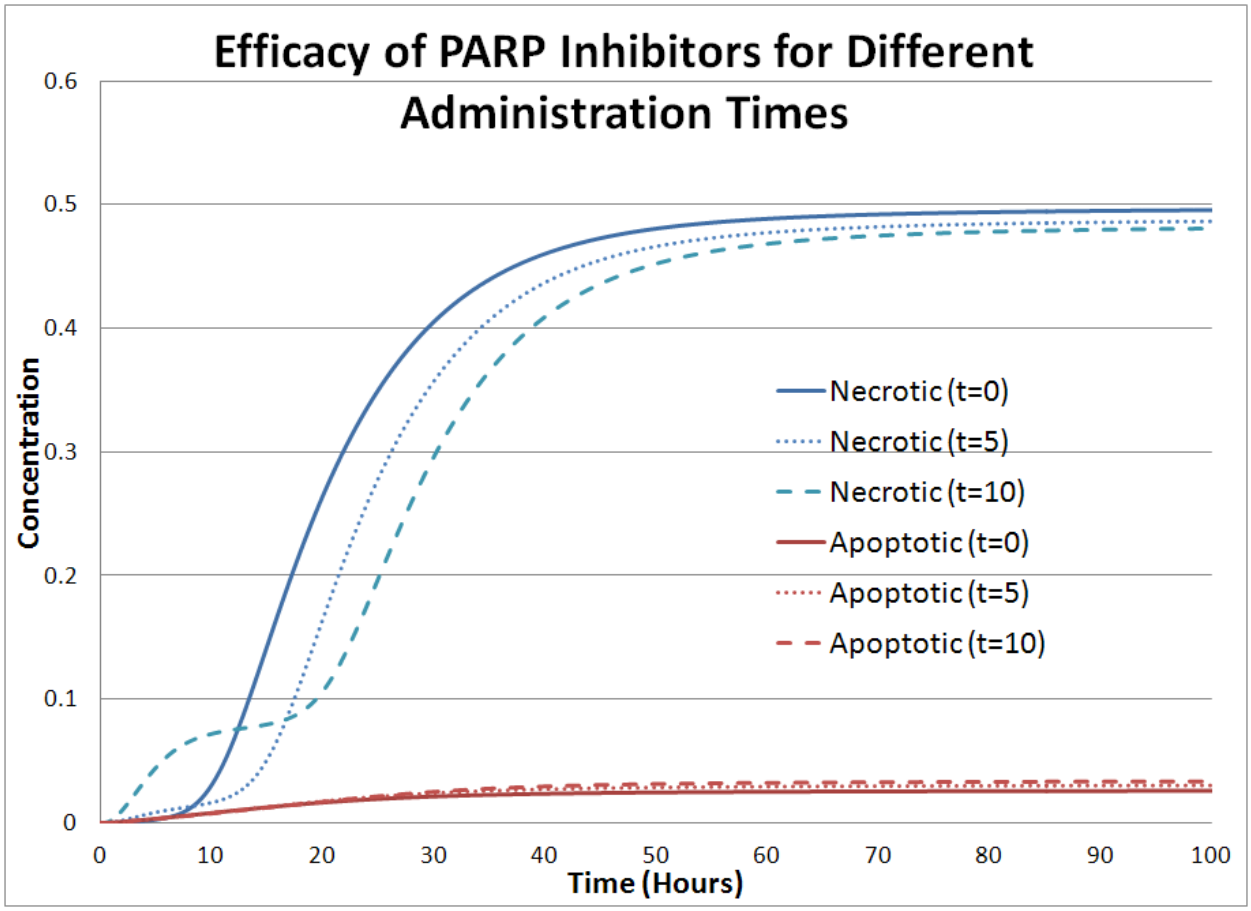

Figure 7-6. PARP Inhibitor Effectiveness for Three Different Dosing Times

7.4 Protease Inhibitors

We did a comprehensive review of protease inhibitors when developing the HD model, but once again, accounted for the effect of protease inhibitors by defining another set of rate equations. We designed these equations to irreversibly lower the concentration of protease. For the GVM, we can model protease inhibitors the same way we model PARP inhibitors, by first starting with a toxicokinetic model for protease concentration, normalizing it to 1.0, and then defining a maximum efficacy for the protease inhibitor. Unfortunately, we have not yet found a study measuring the pharmacokinetics of protease inhibitors in the literature, so we had to assume that the concentration of protease inhibitors follows a similar trend as the concentration of PARP inhibitors.

This would make the concentration of protease inhibitors (in ng/mL) equal to:

$$Prot_{conc} = -0.03 * (t - t_{admin})^2 + 0.19 * (t - t_{admin}) + 0.58 \qquad (7\text{-}8)$$

We will continue our literature search and attempt to find a pharmacokinetic study of protease inhibitors in humans, in order to update this portion of the model.

To fit the maximum efficacy of protease inhibitors we can turn to several studies. One study on protease inhibitor efficacy against inhaled HD in rats showed a significant benefit when

aprotinin was used to irreversibly bind with protease (Anderson, 2009). Aprotinin-treated rats showed a 50-percentage point decrease in bronchial injuries and a 45-percentage point difference in edema, effectively eliminating severe respiratory effects from the animals.

Another study conducted *in vivo* using a mouse ear model, tested the protective efficacies of multiple protease inhibitors (Casillas, Therapeutic Approaches to Dermatotoxicity by Sulfur Mustard I. Modulation of Sulfur Mustard-induced Cutaneous Injury in the Mouse Ear Vesicant Model, 2000). Of the five protease inhibitors tested, only one (peptide phosphonate) showed significant reduction of edema (16% reduction from positive control), but none had significant reduction in subepidermal blisters, epidermal necrosis, or contralateral epidermal necrosis. One point of note is that the protease inhibitors were only used as pretreatment. Looking back at our model output (and the measured protease levels it was based on) it is apparent that protese levels take several hours to rise. Several hours to several days are needed for dead cells to accumulate, which would result in blistering. It is possible that protease inhibitors are simply not beneficial as prophylaxis, much like PARP inhibitors and cell-cycle inhibitors.

One other study looked at the efficacy of using the protease inhibitor doxycycline (DOX) against HD and using nitrogen mustard against human bronchial epithelial cells *in vitro* (Rappeneau, 2000). Two treatment strategies were considered in this study, one with immediate co-treatment and one with 2.5 to 90-minutes delayed treatment. For the delayed treatment model, the researchers looked at treatment using NAC alone and NAC in combination with DOX. The benefits of NAC alone against HD were mainly seen in the first 5-10 minutes, with a peak protection factor of 1.6 taking place 2.5 minutes post-exposure. Also, DOX on its own had a protection factor of 1.3. However, NAC combined with DOX offered a protection factor of 2.0 that peaked at 2.5-minutes post-exposure. but there was still significant protection with the combination treatment if administered within 60-minutes.

We decided to use the Rappeneau, et. al. study, as it was conducted on human cell cultures. Additionally, the toxicokinetic model will handle the time-dependent differences in efficacy. A peak protection factor of 1.3 is obtained using Berkeley Madonna to derive a value for $Prot_{eff}$ used in the equation below:

$$\boldsymbol{Protease} = (1 - Prot_{eff} * Prot_{conc})\mathbf{35.6} * \boldsymbol{e^{-3.4*ATP}} \qquad \textbf{(7-9)}$$

We need to make the comparison at the time of peak protease inhibitor concentration in order to correctly use the *in vitro* data. If protease inhibitors are administered at the time of exposure, the peak concentration time is at approximately three hours. The value for $Prot_{eff}$ that results in a 33% decrease in necrotic cells at three hours is 0.33.

Figure 7-7 shows the concentration of necrotic cells using three different administration times of protease inhibitors. The model predicts an initial benefit from protease inhibitors but little efficacy as time goes on. At this point, we are going to use the model to predict the efficacy of continuous dosings of protease inhibitors every 12 hours, for a 48-hour period.

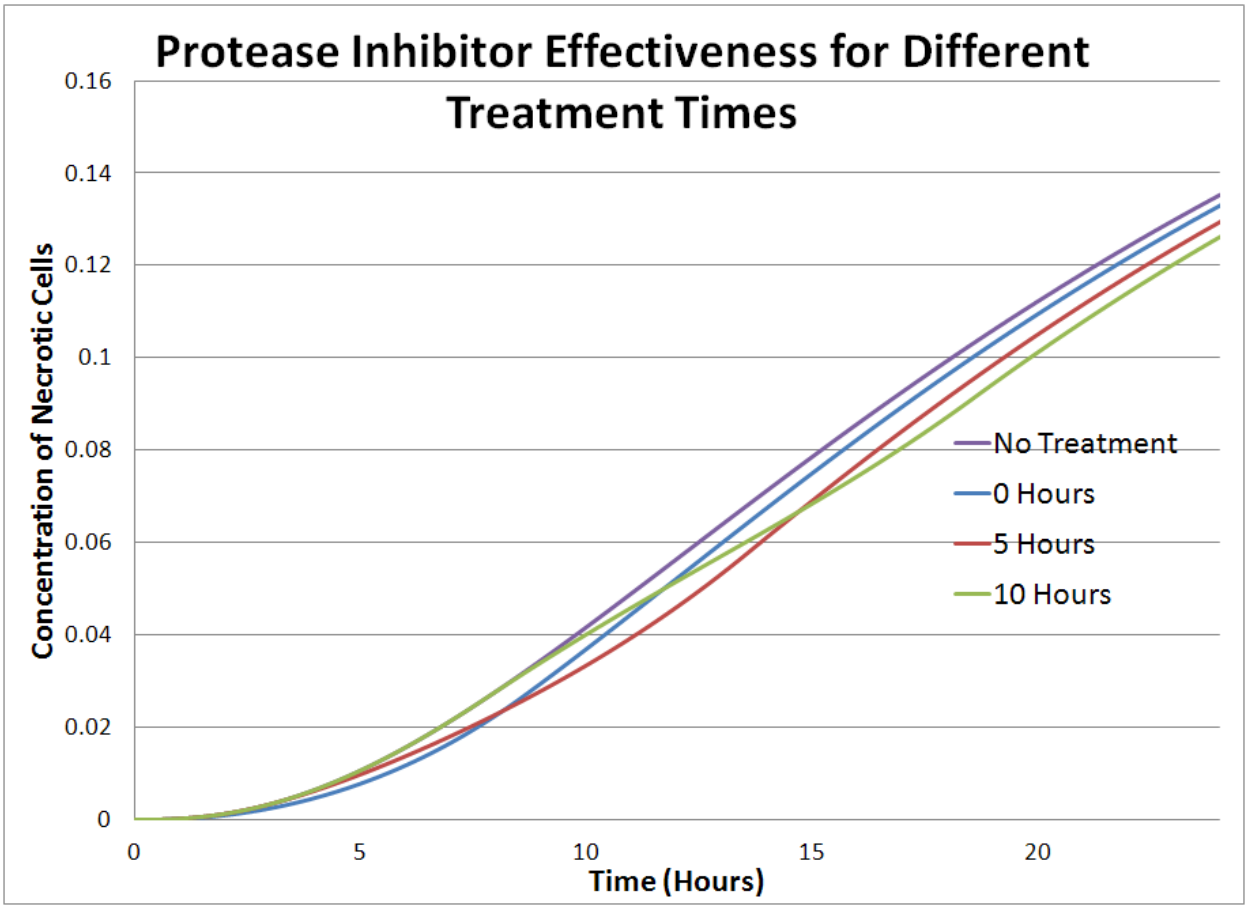

Figure 7-7. Protease Inhibitor Effectiveness for Three Different Treatment Times

Figure 7-8 shows the effectiveness of protease inhibitors when given regularly over a 48-hour period. Although we did see an increased efficacy prediction from the model, the benefit was not substantial. However, we do not have data to verify whether or not this is a valid conclusion.

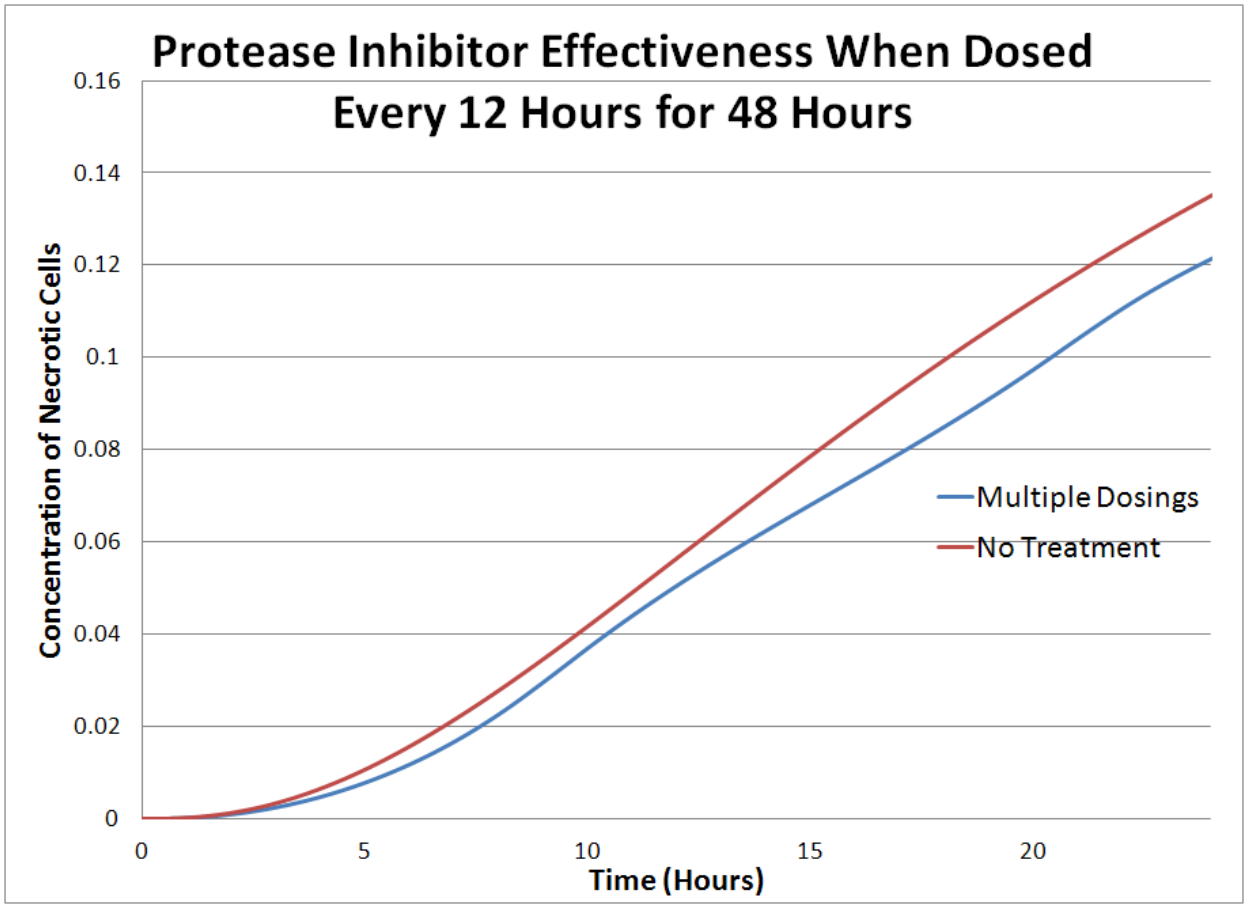

Figure 7-8. Protease Inhibitor Effectiveness for Multiple Dosings

7.5 Anti-inflammatories

For the HD model, we developed a pharmacokinetic and pharmacodynamic model of anti-inflammatory effectiveness using the published literature. There is a significant amount of literature on anti-inflammatory effectiveness as it's the only countermeasure being considered that was actually used against human vesicant exposures. There are two significant departures from the HD model, however. First, there's the fact that we used the anti-inflammatory toxicokinetic model to modify the rate equations for anti-inflammatories. Once again, we are no longer using rate equations for the underlying biological processes. Secondly, the inflammatory response model developed for HD was not based on any published data, a limitation that we corrected in the GVM. However, we reused the anti-inflammatory model that was developed, since the efficacy and concentration profiles for anti-inflammatories were well founded; we did change the implementation.

The equation for anti-inflammatory efficacy defines a rate of change in anti-inflammatory concentration (x). Using these parameters and an input dose ($AInlam_{dose}$) in mg, we defined the equation for the concentration of effective anti-inflammatories to be:

$$AInflam_{conc} = AInflam_{dose} * e^{-x*t} \quad \textbf{(7-10)}$$

For the GVM we will modify that equation to account for administration time (t_{admin}), as shown below:

$$AInflam_{conc} = AIinflam_{dose} * e^{-x*(t-t_{admin})} \quad \textbf{(7-11)}$$

In the HD model, we also derived parameter values for the anti-inflammatories olvanil and indomethacin, as shown in Table 7-4.

Table 7-4. Rate of Change for the Anti-Inflammatories Olvanil and Indomethacin

	x
Olvanil	.1
Indomethacin	.1

In the HD model we then used these values to define a rate of anti-inflammatory effectiveness, k_{inflam}. However, we will use the anti-inflammatory concentration in a manner similar to PARP and protease inhibitors by first normalizing the concentration to 1 and getting the following equation:

$$AInflam_{conc} = e^{-x*(t-t_{admin})} \quad \textbf{(7-12)}$$

We then modified the equation for inflammatory cell concentration to get:

$$Inflam = \left(1 - AInflam_{eff} * Inflam_{conc}\right) * 0.98 * \exp(N_i^2) \quad \textbf{(7-13)}$$

where $AInflam_{eff}$ is the efficacy of the anti-inflammatory. We then revisit the study performed by Robert Casillas et al. (Casillas, 2000) that was used to define the rate parameters in the HD model, to define the value of $AInflam_{eff}$. Casillas showed that there was a significant reduction in edema (19% and 23% at 24 hours post-exposure for olvanil and indomethacin, respectively) when the anti-inflammatories were applied topically at 10 minutes post-exposure. Since edema is a function of necrotic cell death in our percutaneous model, we can use these results to fit a value for I_{eff} in the GVM. The resulting values are shown in Table 7-5.

Table 7-5. Efficacies for the Anti-Inflammatories Olvanil and Indomethacin

	***AInflam*$_{eff}$**
Olvanil	1.1
Indomethacin	1.3

The model's prediction of anti-inflammatory effectiveness, administering a dosing every 12 hours for 48 hours is shown in Figure 7-9. The model predicts a significant decrease in necrotic cell death, following anti-inflammatory application. This decrease is larger than we've seen with other countermeasures included in this model, except for scavengers. Continued application of anti-inflammatories would lead to an even greater reduction in necrotic cells, unlike other treatments included in this model.

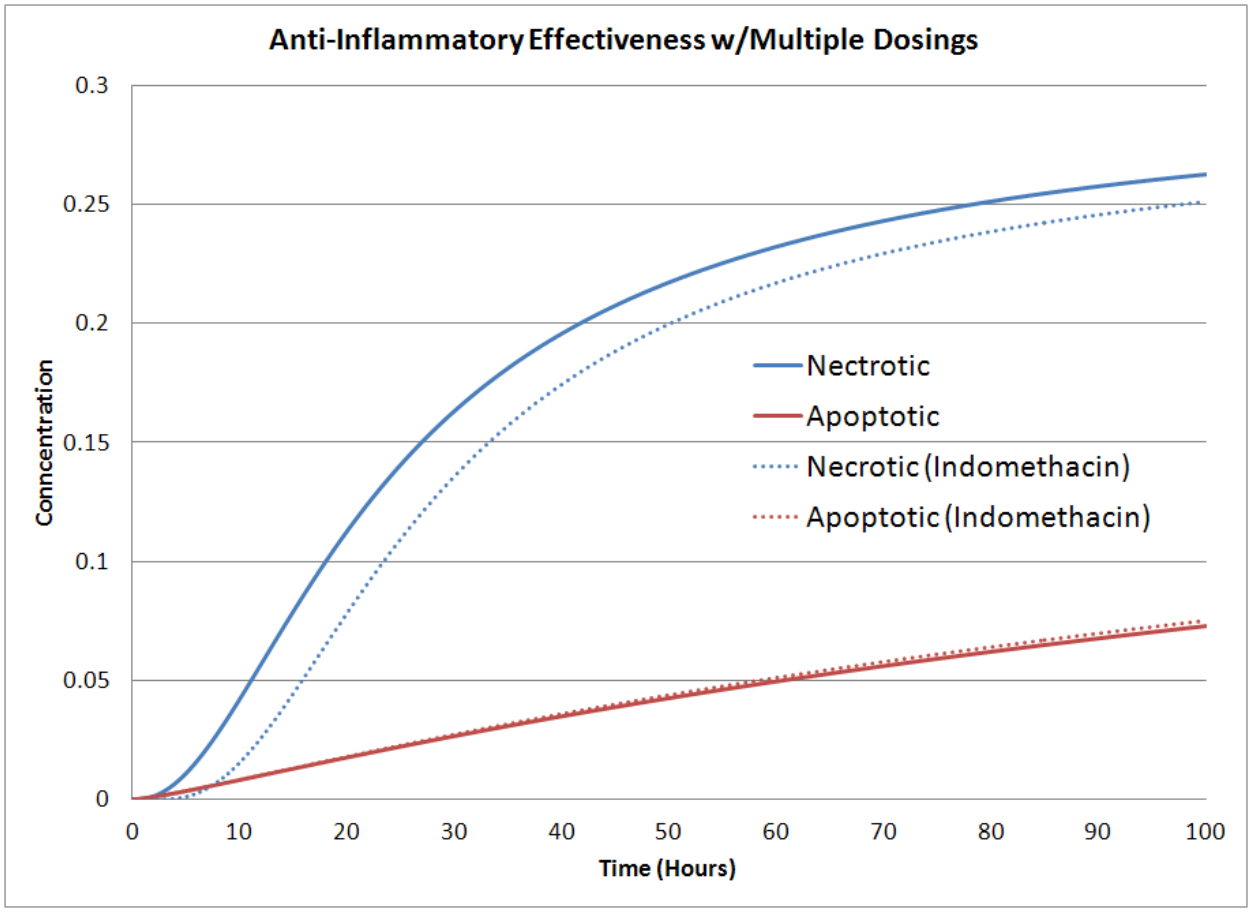

Figure 7-9. Anti-Inflammatory Effectiveness for Multiple Dosings

7.6 British Anti-Lewisite (BAL)

BAL is an incredibly efficacious heavy-metal chelating agent that works very well against arsenic compounds, like lewisite. We have not found any modern studies that measure the effectiveness of BAL against lewisite, but that is likely because early studies have proven that the countermeasure is nearly 100% effective if administered early. One experiment in rabbits showed a near complete recovery using a 5% solution of BAL, against enough lewisite to destroy the eyes of rabbits. Similar experiments were conducted on rabbits with percutaneous exposures to lewisite and even on human volunteers (Waters & Stock, 1945). The only downside to BAL is that nearly 50% of patients exhibit side effects after receiving a 5mg/kg dose intramuscularly (Klassen, 2002). In 34 humans given intramuscular BAL doses of 3.6 to 5.5 mg/kg, there were some observed side effects (mainly headaches and nausea), but all subjects recovered after two

hours with no cumulative toxicity by multiple injections (Sulzberger, Baer, & Kanof, 1946). We have not found any evidence to suggest that BAL is not 100% effective at reducing the dose of lewisite from the time of administration. Nor will continued administration will lead to anything outside of mild side effects, most of which are likely not even operationally relevant.

Due to these assumptions, our model for BAL is included in the following equations:

$$D_o = 0, t \geq BAL_{admin} \quad \textbf{(7-14)}$$

$$D_i = 0, t \geq BAL_{admin} \quad \textbf{(7-15)}$$

$$D_p = 0, t \geq BAL_{admin} \quad \textbf{(7-16)}$$

$$D_s = 0, t \geq BAL_{admin} \quad \textbf{(7-17)}$$

To conclude, BAL completely removes the dose from the eyes, lungs, skin, and systemic system from the moment it is administered.

This page is intentionally left blank.

Section 8.

Example Problem

For illustrative purposes we now present a walk-through of the model. The scenario is as follows:

An individual is exposed to HD via a line-source located upwind. The attack sets off a detector and the alarm goes out within seconds. The individual, however, was instantly exposed to 100 mg of liquid HD and a 10 mg/m3 concentration of HD vapor for five minutes, before putting on his mask. Two minutes later, he is in full MOPP gear. The individual does not decontaminate his skin or his eyes. The resulting injury to the eyes, lungs, and skin are shown in Figure 8-1.

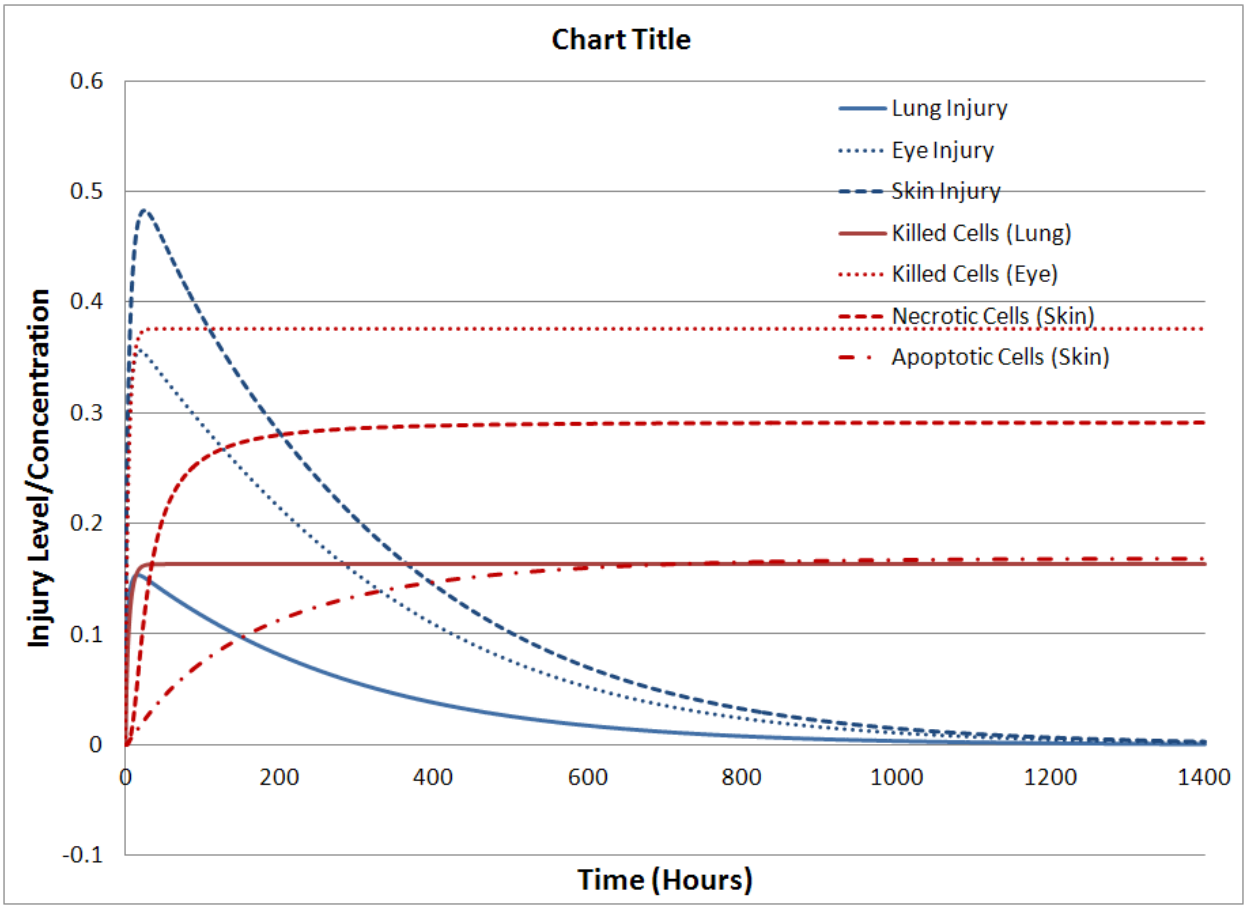

Figure 8-1. Eye, Lung, and Skin Injury Levels and Killed Cell Concentrations for Combined Exposure

The model predicts that the individual will be in the middle of the lowest percutaneous dose band from AMedP-8(C), on the border of the 2nd and 3rd ocular dose band, and on the border of the lowest inhalation dose band. This means that the individual will reach Severity Level 1, for

skin effects in 36 hours; reach Severity Level 1 in four hours and Severity Level 2 in six hours, for ocular effects, and no respiratory symptoms; but, the individual would reach Severity Level 1 for upper GI effects at 8 hours. The GSH suppression level is so low that there is no risk of becoming a fatality.

We assume that the individual did not have NAC before exposure, so there is no therapeutic effect from bioscavengers. However, if the individual was given NAC before exposure, the concentration of killed cells in the lungs would have been reduced from 0.16 to 0.12, no longer making him an inhalation casualty.

At one hour, the individual receives: 100 mg of cell-cycle inhibitors, a single dosing of PARP inhibitors, protease inhibitors, and anti-inflammatories. The cell-cycle inhibitors have a very minor effect on the concentration of killed cells in the eye (the value drops from 0.38 to 0.36), but this is enough to put him in the lowest dosage band for ocular injuries, avoiding a Severity Level 2 injury. The combination of medications have a greater effect on the skin, reducing the concentration of necrotic cells from 0.31 to 0.23, but this decrease is not enough to move the individual out of the first dose band and we will still have mild skin effects.

The same type of analysis can be done for different exposures and combinations of medications, but the end result should always relate to the AMedP-8(C) dosage bands and the lethality equation for systemic dose.

Section 9.

Summary of Assumptions and Limitations

The following is a summary of assumptions and limitations of the GVM and its underlying data sources.

1. Exposure
2. The model uses the same percutaneous toxicokinetic model for all vesicants. However, different vesicants will have different rates of evaporation and diffusion that should be addressed by the model. We will aim to account for these differences in the third year, as the models undergo verification and validation and are transitioned into useable source code.
3. We have not yet implemented a toxicokinetic model for inhalation and ocular exposures.
4. The model does not consider ingestion or intravenous exposure.
5. The only sink for vesicants in the lungs and eyes is healthy cells. We do not consider GSH suppression or other potential metabolic routes for these two models.
6. We assume that the three nitrogen mustards have the same toxicity. We assume that lewisite has the same toxicity as HD.
7. Injury and lethality
8. We assume that PARP concentration is solely dependent on the concentration of injured cells.
9. We assume that NAD+ concentration is solely dependent on the concentration of PARP.
10. We assume that that ATP concentration is solely dependent on the concentration of NAD+.
11. We assume that protease concentration is solely dependent on the concentration of ATP.
12. We assume that inflammatory response is solely dependent on the concentration of injured cells.
13. We assume that apoptotic cell death is solely dependent on mitotic division. There is evidence that this may not be the case, but we have yet to find data on which to base a different mechanism.
14. We assume that necrotic cell death is solely dependent on the depletion of ATP.
15. We assume that the concentration of necrotic cells is an indicator of severity of injury.
16. We assume that necrotic cell concentration can be used to determine inhalation fatalities.
17. We assume that GSH suppression can be used to determine systemic fatalities.
18. Treatment
19. We have not yet developed a true pharmacokinetic model for protease inhibitors. We used the PARP inhibitor model. This is a limitation that we would like to revisit, as we begin implementation of the models.

20. We assume that BAL is 100% effective, from the moment it is administered. A pharmacokinetic model of BAL would likely show a difference in BAL effectiveness as a function of time.
21. Several data sources for countermeasure effectiveness come from *in vivo* experiments. The model should be calibrated to *in vitro* data, when available. We will continue our literature review to see if there is better data available for the models.

Section 10.

Conclusions and Recommendations

When we set out to create a generic vesicant model, we assumed that we could start from the HD framework and refit all of the parameters for each vesicant of interest. We quickly realized that we would be doubling our parameter space with each new agent and that we would not have a truly "generic" model of vesicant exposures. In order to truly make the model generic, we needed to revisit all of the literature and decouple the biological processes from the effecting agent. This paper represents all of the work that went into that process.

We believe we have a better model, as a result of the redesign. All of the biological process models are based on published studies using human cell exposures. We reduced our rate equations down to four and our rate parameters down to three, with only one of them being intrinsically tied to the vesicant.

While improving on the model's design, we added several sub-models to the injury mechanism that allowed us to better quantify the effect of medical countermeasures. We added a toxicokinetic model for percutaneous exposure that accounts for vesicant diffusion through the skin, evaporation into the atmosphere, and the effect of metabolizing agents. We included a distinction between necrotic and apoptotic cell death, to better understand the effects of countermeasures. We included glutathione suppression and systemic distribution, to account for percutaneous fatalities.

We also documented our equation development and fitting processes, so we can quickly incorporate new data as it becomes available. This model requires significant amounts of data. We hope that a continued interest in toxicodynamic models will lead to new studies aimed at capturing the biological processes, resulting from vesicant exposure and reporting the data in a way that is beneficial to the model.

The true benefit of this model is that it provides a mechanism for postulating the therapeutic effects of current, proposed, and future countermeasures, aimed at combating vesicant exposures. It can and should be refined in the future, as we begin the process of publishing the model in peer-reviewed literature and presenting it at conferences. We believe this model represents a great starting point in modeling the effect of vesicant exposures and countermeasures; yet, there remains room for further development. There are mechanisms of injury that likely have not yet been discovered, countermeasures that have not yet been proposed, and data sources that have not yet been studied. But, the framework was created to be scalable, and it is our intention to improve this model as researchers continue to study the effects of vesicants and their countermeasures.

This page is intentionally left blank.

Section 11.

Works Cited

(NATO), N. A. (December 2007). AMedP-8 (B), Volume I-III: Medical Planning Guide for the Estimation of NBC Battle Casualties. STANAG 2475, 2476, 2477: North Atlantic Treaty Organization.

Amir, A., Turetz, J., Chapman, S., Fishbeine, E., Meshulam, J., Sahar, R., et al. (2000). Beneficial Effects of Topical Anti-inflammatory Drugs against Sulfur Mustard-induced Ocular Lesions in Rabbits. Journal of Applied Toxicology , 109-114.

Anderson, D. R. (2009). Evaluation of protease inhibitors and an antioxidant for treatment of sulfur mustard-induced toxic lung injury. Toxicology , 41–46.

Arfsten, D. P. (2003). Impact of 30-day Oral Dosing with N-Acetyl-L-Cysteine on Sprague-Dawley Rat Physiology. Wright-Patterson AFB: Naval Health Research Center.

Atkins, K. B., Lodhim, I. J., Hurley, L. L., & Hinshaw, D. B. (2000). N-Acetylcysteine and Endothelial Cell Injury by Sulfur Mustard. Journal of Applied Toxicology , 125-128.

ATSDR. (2009). Toxicology Curriculum-Module Two-Lecture Notes. Retrieved October 4, 2011, from Agency for Toxic Substances and Disease Registry: www.atsdr.cdc.gov/training/toxmanual/modules/2/lecturenotes.html

Babin, M. E., et.al. (2000). Systemic Administration of Candidate Antivesicants to Protect against Topically Applied Sulfur Mustard in the Mouse Ear Vesicant Model. Journal of Applied Toxicology , 141-144.

Balai-Mood, M. (2005). The pharmacology, toxicology, and medical treatment of sulfur mustard poisoning. Fundamental & Clinical Pharmacology , 19, 297-315.

Bhat, K. B., et.al. (2000). Role of Poly(ADP–ribose) Polymerase (PARP) in DNA Repair in Sulfur Mustard-exposed Normal Human Epidermal Keratinocytes (NHEK). Journal of Applied Toxicology, 20, 13-17.

Bhat, K., Ramachandra, B., J., B., & Ray, R. (2004). Poly (ADP-Ribose) Polymerase is Involved in the Repair of DNA Damage Due to Sulfur Mustard by a Mechanism Other Than DNA Ligase I Activation. Lincoln University: Department of Chemistry, Lincoln University.

Bobb, L. A. (2005). N-Acetyl-L-Cysteine as prophylaxis against sulfur mustard. Military Medicine , 170 (1), 52.

Casillas, R. P. (2000). Therapeutic Approaches to Dermatotoxicity by Sulfur Mustard I. Modulation of Sulfur Mustard-induced Cutaneous Injury in the Mouse Ear Vesicant Model. Journal of Applied Toxicology , 145-151.

Centers for Disease Control and Prevention (CDC). (2010, Aug 26). NIOSH Workplace Safety and Health Topic. Retrieved Oct 10, 2011, from Skin Exposures and Effects: www.cdc.gov/niosh/topics/skin/

ChemBase. (n.d.). Mimosine. Retrieved 10 20, 2011, from Chemical Compound Database: http://www.chembase.com/cbid_3862.htm

Command, U. A. (2005). Potential Military Chemical/Biological Agents and Compounds (FM 3-11.9). Ft. Monroe: US Army Training and Doctrine Command.

Cowan, F. M. (1993). Putative roles of inflammation in the dermatopathology of sulfur mustard. Cell Biol. Toxicol. , 201-213.

Dannenberg, A. M. (1993). Role of Cytokines and Reactive Oxygen Intermediatesin the Inflammatory Response Produced by Su1lfur Mustard. Baltimore: U.S. Army Medical, Research and Development Command.

Debiaka, M., Keheb, K., & Bürkle, A. (2009). Role of poly(ADP-ribose) polymerase in sulfur mustard toxicity. Toxicology , 20-25.

Dickson, M. , et.al. (2009). Development of cell-cycle inhibitors for cancer therapy. Current Oncologyy , 36-43.

Dire, D. (2010). CBRNE-Vesicants, Mustard-Hd, Hn1-3, H. Retrieved October 4, 2011, from emedicine: http://emedicine.medscape.com/article/832060-overview

EPA. (2007). Acute Exposure Guideling Levels (AEGLs) for Nitrogen Mustard. Interim Paper.

EPA. (2003). Acute Exposure Guideling Levels for Selected Airborne Chemicals: Volume 3. Washington DC: The National Academy Press.

Gietema, J. e. (2006). A phase I study assessing the safety and pharmacokinetics of the thrombospondin-1-mimetic angiogenesis inhibitor ABT-510 with gemcitabine and cisplatin in patients with solid tumors. Annals of Oncology , 1320-1327.

Glasgow, B. (2005, Oct 12). Medrounds. Retrieved Oct 10, 2011, from Ocular Pathology Study Guide: http://www.medrounds.org/ocular-pathology-study-guide/2005/10/anatomy-of-eye-study-guide-for.html

Greenberg, S., Kamath, P., Petrali, J., Hamilton, T., Garfield, J., & Garlick, J. A. (2006). Characterization of the Initial Response of Engineered Human Skin to Sulfur Mustard. Toxicological Sciences , 549-557.

Hinshaw, D. B., Lodhi, I. J., Hurley, L. L., Atkins, K. B., & Dabrowska, M. I. (1999). Activation of Poly [ADP-Ribose] Polymerase in Endothelial Cells and Keratinocytes: Role in an in Vitro Model of Sulfur Mustard-Mediated Vesication. Toxicology and Applied Pharmacology , 17-29.

Jin, X. R. (2004). Studies on mustard-stimulated proteases and inhibitors in human epidermal keratinocytes (HEK): Development of antivesicant drugs. Silver Spring: Department of Biology, Division of Experimental Therapeutics, Walter Reed Army Institute of Research.

Kehe, K., et.al. (2008). Inhibition of polu(ADP-ribose) polymerase (PARP) influences the mode of sulfur mustard (SM)-induced cell death in HaCaT cells. Arch. Toxicol. , 82, 461-470.

Kehe, K., & Szinicz, L. (2005). Medical aspects of sulphur mustard poisoning. Toxicology , 198-209.

Kehe, K., Balszuweit, F., Steinritz, D., & Thiermann, H. (2009). Molecular toxicology of sulfur mustard-induced cutaneous inflammation and blistering. Toxicology , 12-19.

Kehea, K. T. (2009). Acute effects of sulfur mustard injury—Munich experiences. Toxicology , 3-8.

Klassen, C. (2002). Heavy metals and heavy metal antagonists. In J. Hardman, & L. Limbird, Goodman and Gilman's The Pharmacological Basis of Therapeutics (pp. 1851-1875). New York: McGraw-Hill.

Krude, T. (1999). Mimosine Arrests Proliferating Human Cells before Onset of DNA Replication in a Dose-Dependent Manner. Exp. Cell Res. , 247 (1), 148-159.

Kumar, O., Sugendran, K., & Vijayarghavan, R. (2001). Protective effect of various antioxidants on the toxicity of sulphur mustard administered to mice by inhalation or percutaneous routes. Chemico-Biological Interactions , 1-12.

Lomash, V., Deb, U., Rai, R., Jadhav, S. E., R.Vijayaraghavan, & S.C.Pant. (2011). Designing of mouse model: A new approach for studying sulphur mustard-induced skin lesions. Burns .

Meier, H. M. (1998). Alterations in human lymphocyte DNA caused by sulfur mustard can be mitigated by selective inhibitors of poly(ADP-ribose) polymerase. Biochim Biophys Acta. , 1404 (3), 367-76.

Monteiro-Riviere, N., & Inman, A. (1997). Ultrastructural Characterization of Sulfur Mustard–Induced Vesication in Isolated Perfused Porcine Skin. Microscopy Research and Technique , 37, 229-241.

Murray, J. D. (1993). Mathematical Biology, Volume 2. Berlin: Springer-Verlag.

NCI. (2011). SEER Training Modules. Retrieved October 4, 2011, from National Cancer Institute: training.seer.cancer.gov/melanoma/anatomy/layers.html

Nicotera, P., & Melino, G. (2004). Regulation of the apoptosis–necrosis switch. Oncogene , 2757-2765.

North Atlantic Treaty Organization (NATO). (February 2010). AMedP-8 (C) NATO Planning Guide for the Estimation of CBRN Casualties: Ratification Draft 1. North Atlantic Treaty Organization: STANAG 2475.

Overton JH, K. J. (2001). Dosimetry modeling of inhaled formaldehyde: the human respiratory tract. Toxicol Sci , 122-134.

Piskunova, T. e. (2008). Deficiency in Poly(ADP-ribose) Polymerase-1 (PARP-1) Accelerates Aging and Spontaneous Carcinogenesis in Mice. Current Gerontology and Geriatrics Research , 2008, 754190.

Pita, R., & Vidal-Asensi, S. (2010). Cutaneous and Systemic Toxicology of Vesicant (Blister) Warfare Agents. Actas Dermosifiliogr , 7-18.

Powers, J. C. (1999). Biochemical Markers and Synthetic Protease Inhibitors in Animal Models of Sulfur Mustard Vesication. Fort Detrick: US Army Medical Research and Materiel Command.

Ramalingam, S. S. (2010). Phase 1 and Pharmacokinetic Study of Everolimus, a Mammalian Target of Rapamycin Inhibitor, in Combination With Docetaxel for Recurrent/Refractory Nonsmall Cell Lung Cancer. Cancer.

Rappeneau, S. B.-S.-H. (2000). Efficient protection of human bronchial epithelial cells against sulfur and nitrogen mustard cytotoxicity using drug combinations. Toxicological Sciences , 58, 153-160.

Ray, R. e. (2005). Antivesicant strategies based on DNA repair and apoptosis. APG, MD: US Army Medical Research Institute of Chemical Defense.

Ray, R., Benton, B. J., Anderson, D. R., Byers, S. L., & Petrali, J. P. (2000). Intervention of Sulfur Mustard Toxicity by Downregulation of Cell Proliferation and Metabolic Rates. Journal of Applied Toxicology , 87-91.

Riviere, & al., e. (1994). Toxicokinetics of topical sulfur mustard penetration, disposition, and vascular toxicity in isolation perfused porcine skin. Toicology. And Applied Pharmacology , 135, 25034.

Riviere, J., & al, e. (2001). Use of Methyl Salicylate as a Simulant to Predict the Percutaneous Absorption of Sulfur Mustard. Journal of Applied Toxicology , 91-99.

Riviere, J., & Monteiro-Riviere, N. (1991). The isolated perfused porcine skin flap as an in vitro model for percutaneous absorption and cutaneous toxicology. CRC Critical Reviews in. Toxicology , 21, 329-344.

Rodriguez, J., Reeves, G. I., & McClellan, G. (2011). A Model of Medical Countermeasures for Sulfur Mustard Exposure. DTRA Technical Report ARA-TR-11-SEASSP-000721-004.

S.M., B. S. (1989). Toxicodynamics of sulphur mustard. Journal of Clinical Pharmacology, Therapy, and Toxicology. , 27, 419-435.

Sawer, T. W., & Hamilton, M. G. (1999). Effect of Intracellular Calcium Modulation on Sulfur Mustard Cytotoxicity in Cultured Human Neonatal Keratinocytes. Toxicology in Vitro , 149-157.

Sawyer, T. H. (2000). Effect of intracellular calcium modulation on sulfur mustard cytotoxicity in cultured human neonatal keratinocytes. Toxicology In Vitro. , 14 (2), 149-157.

SEER Training: Layers of the Skin. (n.d.). Retrieved October 4, 2011, from National Cancer Institute: http://training.seer.cancer.gov/melanoma/anatomy/layers.html

Shakarjian, M. P., Heck, D. E., Gray, J. P., Sinko, P. J., Gordon, M. K., Casillas, R. P., et al. (2010). Review: Mechanisms Mediating the Vesicant Actions of Sulfur Mustard after Cutaneous Exposure. Toxicological Sciences , 5-19.

Sharma, M., Vijayaraghavan, R., & Agrawal, O. P. (2010). Comparative Toxic Effect of Nitrogen Mustards (HN-1, HN-2, and HN-3) and Sulfur Mustard on Hematological and Biochemical Variables and Their Protection by DRDE-07 and Its Analogues. International Journal of Toxicology , 1-11.

Simbulan-Rosenthal, C. M., Ray, R., Benton, B., Soeda, E., Daher, A., Anderson, D., et al. (2006). Calmodulin mediates sulfur mustard toxicity in human keratinocytes. Toxicology , 21-35.

Smith, W. J. (2009). Therapeutic Options to Treat Sulfur Mustard Poisoning - The Road Ahead. Toxicology , 70-73.

Smith, W. S. (1993). Cytometric Analysis of DNA Changes Induced by sulfur Mustard. APG, MD: U.S. Army Medical Research Institute of Chemical Defense.

Smitha, K. J. (1997). Histopathologic features seen with different animal models following cutaneous sulfur mustard exposure. Journal of Dermatological Science , 126-135.

Somani, S., & Babu, S. (1989). Toxicodynamics of sulphur mustard. Journal of Clinical Pharmacology, Therapy and Toxicology. , 27, 419-435.

Sparidans, R. W., Martensa, I., Iersel, L. B.-v., Hartigh, J. d., Schellensa, J. H., & Beijnena, J. H. (2011). Liquid chromatography–tandem mass spectrometric assay for the PARP-1 inhibitor olaparib in combination with the nitrogen mustard melphalan in human plasma. Journal of Chromatography , 1851-1856.

Sulzberger, M., Baer, R., & Kanof, A. (1946). Clinical uses of 2,3-dimercaptopropanol (BAL): Studies on the toxicity of BAL on percutaneous and parenteral administration. J Clin , 474-479.

Tewari-Singh, N. R. (2009). Inflammatory Biomarkers of Sulfur Mustard Analog 2-Chloroethyl Ethyl Sulfide–Induced Skin Injury in SKH-1 Hairless Mice. Toxicological Sciences , 108, 194-206.

Thallinger, C. e. (2007). Comparison of a Treatment Strategy Combining CCI-779 Plus DTIC Versus DTIC Monotreatment in Human Melanoma in SCID Mice. Journal of Investigative Dermatology , 2411-2417.

USAMRICD. (Feb 2007). Medical Management of Chemical Casualties Handbook: Fourth Edition. APG, MD: U.S. Army Medical Research Institute of Chemical Defense (USAMRICD).

Vilensky, J. A., & Redman, K. (2003). British anti-Lewisite (Dimercaprol): An Amazing History. Annals of Emergency Medicine, 378-383.

Waters, L., & Stock, C. (1945). British anti-Lewisite. Science , 601-606.

Weinberger, B. e. (2011). Sulfur mustard-induced pulmonary injury: Therapeutic approaches to mitigating toxicity. Pulmonary Pharmacology & Therapeutics , 24, 92-99.

Weltin, D., Aupeix, K., Iltis, C., Cuikrot, J. M., Dufour, P., Marchal, J., et al. (1996). N-Acetylcysteine Protects Lymphocytes from Nitrogen Mustard-Induced Apoptosis. Biochemical Pharmacology , 1123-1129.

Williams, P., Carver, M., & Riviere, J. (1990). A physiologically relevant pharmacokinetic model of xenobiotic percutaneous absorption utilizing the isolated perfused porcine skin flap (IPPSF). J. Pharm. Sci., , 79, 305-311.

Wormser, U. L. (2000). Reduced sulfur mustard-induced skin toxicity in cyclooxygenase-2 knockout and celecoxib-treated mice. Toxicol. Appl. , 40-47.

Wouters, B. G. (2009). Cell death after irradiation: how, when and why cells die. In M. Joiner, & A. van der Kogel, Basic Clinical Radiobiology, 4th ed. (pp. 27-40). London, England: Hodder Arnold.

Yourick, J. e. (1995). Reduction of erythema in hairless guinea pigs after cutaneous sulfur mustard vapor exposure by pretreatment with niacinamide, promethazine and indomethacin. J Appl Toxicol , 15 (2), 133-8.

Section 12.

Definitions, Acronyms, and Abbreviations

1xLD50	A dose that is 1.0 times the LD50
ADP	Adenosine Diphosphate
AEBSF	4-(2-Aminoethyl) benzenesulfonyl fluoride hydrochloride
AMedP-8	Allied Medical Publication 8
ARA	Applied Research Associates, Inc.
ATP	Adenosine Triphosphate
ARDS	Acute Respiratory Distress Syndrome
BAL	British anti-Lewisite
BAPTA	1,2-bis(o-aminophenoxy)ethane-N,N,N',N'-tetraacetic acid
CB	Chemical and Biological
CBD	Chemical and Biological Defense
CDC	Centers for Disease Control
DoD	Department of Defense
DTRA	Defense Threat Reduction Agency
EPA	Environmental Protection Agency
Gryphon	Gryphon Scientific, LLC
GSH	Glutathione
GVM	Generic Vesicant Model
HD	Sulfur Mustard
HN-1, HN-2. HN-3	Nitrogen Mustard Analogues
JPEO-CBD	Joint Program Executive Office for Chemical/Biological Defense
JPM-IS	Joint Program Manager-Information Systems
JSTO	Joint Science and Technology Office
LD50	Median lethal dose
LDX	Dose causing X% mortality
MCM	Medical Countermeasure
NAC	N-acetylcysteine
OP	Organophosphate

NAD+	Nicotinamide Adenine Dinucleotide
PARP	Poly(ADP-ribose) polymerase
PBPK/PD	Physiology Based Pharmacokinetic/Pharmacodynamic
RD	Research & Development
RD-CBI	Information Systems Capability Development Division
SM	Sulfur Mustard
TBD	To Be Determined
TK/TD	Toxicokinetic/Toxicodynamic
USAMRICD	US Army Medical Research Institute for Chemical Defense
USAMRIID	US Army Medical Research Institute for Infectious Disease

Section 13.

Percutaneous Source Code

```
METHOD RK4

STARTTIME = 0
STOPTIME=1400
DT = 0.02

{Exposure calculations}
Vapor = 0 ;Average concentration in mg/m3
Liquid = 100 ;Average concentration in mg/m2
Tmask = 1/60
Tmopp= 1/60
CF = 1.2
Sexposed=.93
BreathingRate=0.9


Skin=BasalEpidermis+Dermis

d/dt(Evaporated) = k48*Surface
init Evaporated = 0

d/dt(Surface) = IF TIME <= Tmask THEN Vapor*CF -k48*Surface- k49*Surface+ k94*StratumCorneum
ELSE IF TIME <=Tmopp THEN Vapor*CF*Sexposed -k48*Surface- k49*Surface+ k94*StratumCorneum
ELSE  -k48*Surface- k49*Surface+ k94*StratumCorneum
init Surface = Liquid

d/dt(StratumCorneum) = k49*Surface+k29*BasalEpidermis-k92*StratumCorneum-k94*StratumCorneum
init StratumCorneum= 0

d/dt(BasalEpidermis) = k92*StratumCorneum+k32*Dermis-k23*BasalEpidermis-
k29*BasalEpidermis+k22_2*Metabolites-k2_22*BasalEpidermis
init BasalEpidermis= 0

d/dt(Dermis) = k23*BasalEpidermis+k13*Vascular+k53*Fat-a_k31*exp(-b_k31*TIME)*Dermis-
k32*Dermis-k35*Dermis
init Dermis= 0

d/dt(Fat) = k35*Dermis-k53*Fat
init Fat= 0

d/dt(Metabolites) = -k22_2*Metabolites+k2_22*BasalEpidermis
init Metabolites = 0

d/dt(Vascular)=a_k31*exp(-b_k31*TIME)*Dermis-k13*Vascular
init Vascular=0

k48=0.34*60
k49=0.25*60
k94=0.23*60
k92=0.26*60
```

```
k29=0.22*60
k23=0.24*60
k32=0.12*60
a_k31 = 0.33*60
b_k31=0.0001*60
k13=0.12*60
k35=0.0058*60
k53=0.0060*60
k2_22 = 0.12*60
k22_2 = 0.007*60



d/dt(Systemic) = Dermis*(exp(-TIME/taob)-exp(-TIME/taod))
init Systemic = 0
taob = 39
taod = 0.7

;Equations for Skin Injury
d/dt(NN) = k_split*(1-NN)*NN*fcc - k_bind*Skin*NN+k_repair*PARP*NAD*NI
init NN=1.0

SkinInjury = 1-NN
d/dt(NI) = k_bind*Skin*NN - k_repair*PARP*NAD*NI - k_kill*Protease*Inflam*Ca*NI - k_split*(1-NI)*NI*fcc
init NI = 0.0

CC = IF TIME< AdminTime THEN 0 ELSE Dcc*a*exp(-b*(TIME-AdminTime))
Dcc=0
a = 20
b = 0.49
fCC = IF CC < CCDose THEN 1 ELSE 0
CCDose = 0.1
AdminTime=1

d/dt(NKN) = k_kill*Protease*Inflam*Ca*NI
init NKN = 0.0

d/dt(NKA) = k_split*(1-NI)*NI*fcc
init NKA = 0.0

TotalInjury = NKA+NKN

A =1.5*NAD
PARP = (1-PARPi*PARPic)*5.9088*NI
;PARPi = .66
PARPi=0
PARPic = -0.03*(TIME-tparpadmin)^2+.19*(TIME-tparpadmin)+0.58
limit PARPic >= 0

tparpadmin=0

NAD =1.0827*EXP(-.511*PARP)

Protease = (1-Proteff*Protconc)*35.6*exp(-3.4*A)
Protconc1 = -0.03*(TIME-tprotadmin1)^2+.19*(TIME-tprotadmin1)+0.58
Protconc2= -0.03*(TIME-tprotadmin2)^2+.19*(TIME-tprotadmin2)+0.58
```

```
Protconc3 = -0.03*(TIME-tprotadmin3)^2+.19*(TIME-tprotadmin3)+0.58
Protconc4= -0.03*(TIME-tprotadmin4)^2+.19*(TIME-tprotadmin4)+0.58
Protconc5= -0.03*(TIME-tprotadmin5)^2+.19*(TIME-tprotadmin5)+0.58
limit Protconc1 >= 0
limit Protconc2 >= 0

limit Protconc3 >= 0
limit Protconc4 >= 0
limit Protconc5 >= 0
Protconc = Protconc1+Protconc2+Protconc3+Protconc4+Protconc5

tprotadmin1=0
tprotadmin2=12
tprotadmin3=24
tprotadmin4=36
tprotadmin5=48

;Proteff=0.33
Proteff = 0

Inflam = (1-Ieff*Iconc)*.9811*exp(0.0638*NI)
limit Inflam >=0
Iconc1 = exp(-xinflam*TIME-tinflamadmin1)
Iconc2 = exp(-xinflam*TIME-tinflamadmin2)
Iconc3 = exp(-xinflam*TIME-tinflamadmin3)
Iconc4 = exp(-xinflam*TIME-tinflamadmin4)
Iconc5 = exp(-xinflam*TIME-tinflamadmin5)
Iconc = Iconc1 +Iconc2+Iconc3+Iconc4+Iconc5
Ieff = 1.1
xinflam=.1
tinflamadmin1=0
tinflamadmin2=24
tinflamadmin3=48
tinflamadmin4=72
tinflamadmin5=96
Idose=1
Ca = 1

GSH = 1.25*exp(-.007*Systemic)

k_split = 0.004
k_bind = 0.04
k_repair = 0.003
k_kill = 0.003
```

This page is intentionally left blank.

Section 14.

Ocular Source Code

```
METHOD RK4

STARTTIME = 0
STOPTIME=1400
DT = 0.02

{Exposure calculations}
Vapor =100 ;Average concentration in mg/m3
Liquid = 0 ;Average concentration in mg/m2
Tmask = 1/60
Tmopp= 1/60
CF = 1.2
Sexposed=.93
BreathingRate=0.9

d/dt(Ocular) = IF TIME < Tmask THEN Vapor - k_bind*Ocular*NN else - k_bind*Ocular*NN
init Ocular = 0

;Equations for Eye Injury
d/dt(NN) = k_split*(1-NN)*NN - k_bind*Ocular*NN+k_repair*PARP*NAD*NI
init NN=1.0

EyeInjury = 1-NN
d/dt(NI) = k_bind*Ocular*NN - k_repair*PARP*NAD*NI - k_kill*Protease*Inflam*Ca*NI - k_split*(1-NI)*NI
init NI = 0.0

d/dt(NKN) = k_kill*Protease*Inflam*Ca*NI
init NKN = 0.0

d/dt(NKA) = k_split*(1-NI)*NI
init NKA = 0.0

TotalInjury = NKA+NKN

A =1.5*NAD
PARP =5.9088*NI

NAD =1.0827*EXP(-.511*PARP)

Protease = 35.6*exp(-3.4*A)

Inflam = .9811*exp(0.0638*NI)

Ca = 1

k_split = 0.004
k_bind = 0.4
k_repair = 10
k_kill = 5.8
```

This page is intentionally left blank.

Section 15.

Inhalation Source Code

```
METHOD RK4

STARTTIME = 0
STOPTIME=1400
DT = 0.02

{Exposure calculations}
Vapor = 100 ;Average concentration in mg/m3
Liquid = 0 ;Average concentration in mg/m2
Tmask = 10/60
Tmopp= 2/60
CF = 1.2
Sexposed=.93
BreathingRate=0.9

d/dt(Inhaled) = IF TIME < Tmask THEN Vapor*BreathingRate - NACreduction *k_bind*Inhaled*NN else -
NACreduction *k_bind*Inhaled*NN
init Inhaled = 0

NACreduction = 1

;Equations for Inhalation Injury
d/dt(NN) = k_split*(1-NN)*NN - k_bind*Inhaled*NN+k_repair*PARP*NAD*NI
init NN=1.0

LungInjury = 1-NN
d/dt(NI) = k_bind*Inhaled*NN - k_repair*PARP*NAD*NI - k_kill*Protease*Inflam*Ca*NI - k_split*(1-NI)*NI
init NI = 0.0

d/dt(NKN) = k_kill*Protease*Inflam*Ca*NI
init NKN = 0.0

d/dt(NKA) = k_split*(1-NI)*NI
init NKA = 0.0

TotalInjury = NKA+NKN

A =1.5*NAD
PARP =5.9088*NI

NAD =1.0827*EXP(-.511*PARP)

Protease = 35.6*exp(-3.4*A)

Inflam = .9811*exp(0.0638*NI)

Ca = 1

k_split = 0.004
k_bind = 0.35
```

k_repair = 10
k_kill = 2

Appendix A.

Inhalation and Ocular Model

This Appendix preserves the work done for inhalation and ocular injury modeling.

A.1 Exposures

A.1.1 Inhalation

Inhalation dosage is defined as the integral of the vapor concentration (C) from the start of exposure (t_0), until the time a mask (t_{mask}) is donned or until the end of the exposure (t_f), whichever is lower. The inhalation dose is the dosage, times the breathing rate (b). Therefore, the inhalation dose is defined as:

$$\frac{d}{dt}D_i = b * \int_0^{T_{mask}} C\ dt \qquad \textit{(A-1)}$$

Figure A-1 shows the inhaled dose as a function of time, for an individual (breathing at a rate of 0.015 m^3/min) exposed to 1 mg/m^3 of vesicant vapor, until the mask is donned at 2 minutes. As you can see, exposure to a constant vapor results in a constant increase in inhaled dose, until the mask is donned.

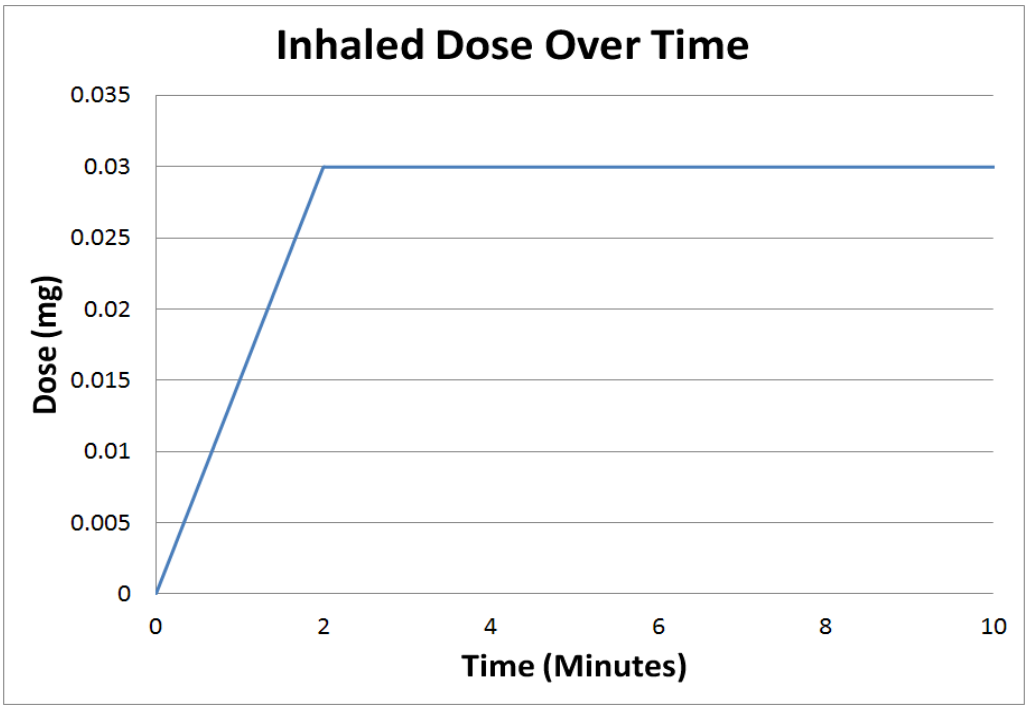

Figure A-1. Inhaled Dose Over Time for a Constant Exposure and Breathing Rate

Note that inhaled liquid droplets are not included in the model at this time. An inhaled liquid droplet model for HD has been developed for the Joint Effects Model (JEM) and could be used in the front-end for the final implementation of the GVM.

A.1.2 Ocular

Ocular dose is simply the integral of the vapor concentration (C) from the start of exposure (t_0), until the time a mask (t_{mask}) is donned or until the end of the exposure (t_f), whichever is lower. There is no modification for breathing rate when considering ocular exposures. Therefore, the ocular dose is defined by;

$$\frac{d}{dt}D_o = \int_0^{T_{mask}} C\,dt \qquad \textit{(A-2)}$$

Figure A-2 shows the ocular dose as a function of time, for an individual exposed to 1 mg/m^3 of vesicant vapor, until the mask is donned at 2 minutes. As you can see, exposure to a constant vapor results in a constant increase in inhaled dose, until the mask is donned.

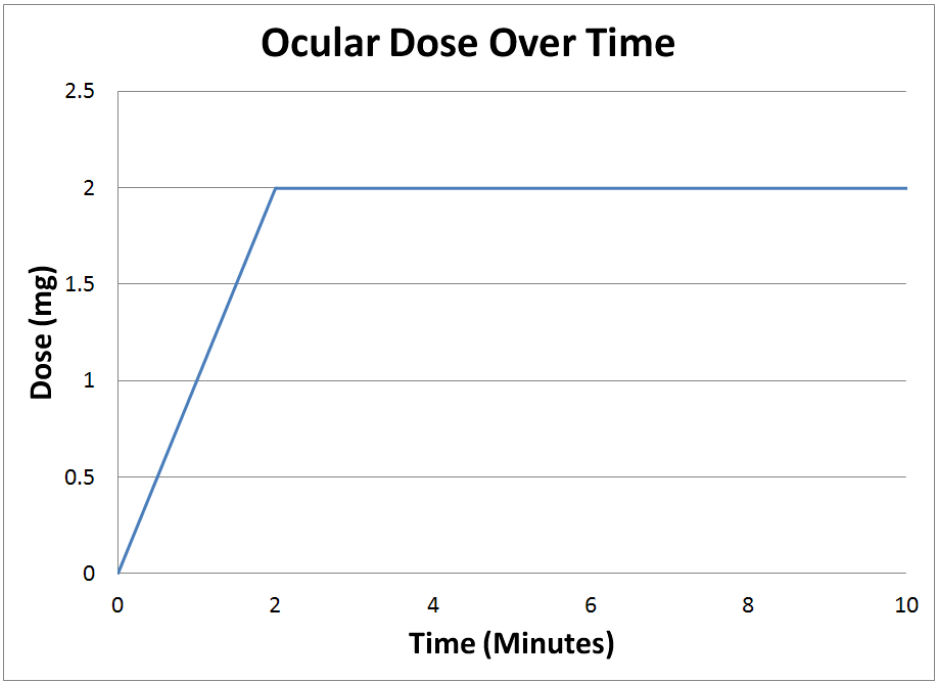

Figure A-2. Ocular Dose Over Time for a Constant Exposure and Breathing Rate

At the time of this report, we have no model for liquid ocular exposure. For the foreseeable future, ocular doses will only be from vapor exposures.

A.2 Using Ocular and Inhaled Doses

Inhaled dose is used by calculating the dose as a function of time and subtracting the rate at which the vesicant attacks healthy cells. This modifies equation (A-3)as shown below:

$$\frac{d}{dt}D_i = \int_0^{\mathrm{T_{mask}}} \mathrm{C\ dt} * \mathrm{b} - \mathrm{k_{bind}} * \mathrm{N_{N,i}} * \mathrm{D_i} \qquad \textit{(A-3)}$$

Note some changes in variable names in equation (A-3)when compared to the original HD document. For clarification, we specify the proportion of normal, healthy cells in the lung as $N_{N,i}$. The other term introduced above, k_{bind}, is the rate at which the vesicant binds with, and fragments, the DNA in normal, healthy cells. We fit this parameter in the original HD model, but we will be revisiting all fits in the GVM.

Ocular dose is used by calculating the dose as a function of time and subtracting the rate at which the vesicant attacks healthy cells. This modifies equation (A-3) as shown below:

$$\frac{d}{dt}D_o = \int_0^{\mathrm{T_{mask}}} \mathrm{C\ dt} - \mathrm{k_{bind}} * \mathrm{N_{N,o}} * \mathrm{D_o} \qquad \textit{(A-4)}$$

Once again, note some changes in variable names in equation (A-4), when compared to the original HD document. For clarification, we specify the proportion of normal, healthy cells in the eye as $N_{N,o}$.

A.3 Injury Model

For ocular and inhalation exposures we are using the same injury mechanism used for the HD model: DNA alkalization and its effects. We did make two significant changes, however, as follows:

1. We included the depletion of ATP and correlated that value with a pathway to necrotic cell death.
2. It is now the depletion of ATP in the cell that signals protease, kills the cells, and begins the vesication process. In the HD model, it was the depletion of NAD+ that directly signaled protease release.

These changes were made to better fit the revised injury mechanism of vesicants, as presented in the previous section and to better incorporate the beneficial effects of countermeasures. Looking at the figure below, it is apparent that the new framework would better account for PARP inhibitors. PARP inhibitor would slow the depletion of NAD+ and ATP, thereby slowing the release of protease. This would result in the main path to necrosis occurring during the attempted mitosis of injured cells. In the percutaneous model, which we present below, attempted mitosis of injured cells leads to apoptotic cell death, which is more in agreement with the known injury mechanism presented in the previous section. We believe it is beneficial to achieve that level of fidelity for the percutaneous exposures, due to the wider dose range of toxic skin exposures and the fact that blistering, which results from necrotic death, is a significant endpoint for skin exposures. Additionally, we have data that supports a necrosis/apoptosis model for skin injuries, but not for ocular and lung injuries.

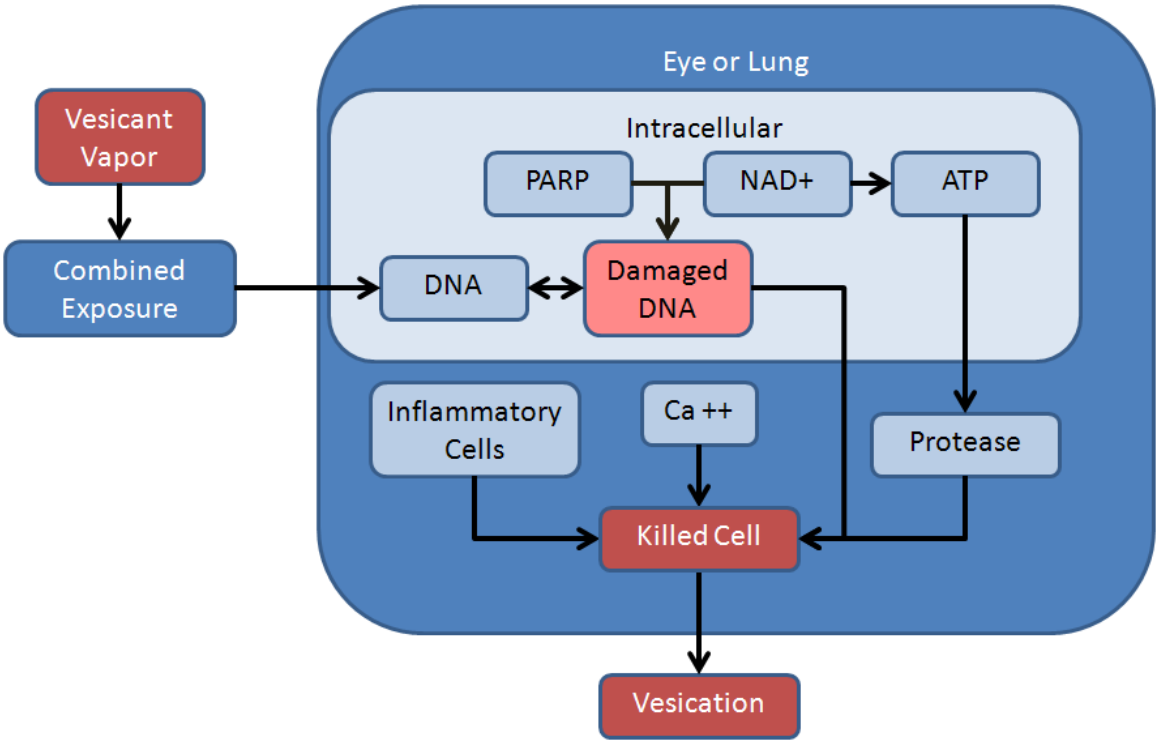

Figure A-3. GVM Model Framework for Ocular and Inhalation Exposures

A.4 Proportion of Healthy Cells

Given the above statements, we can draw the system diagram for $N_{N,L}$ and $N_{N,O,}$ shown inFigure A-4.

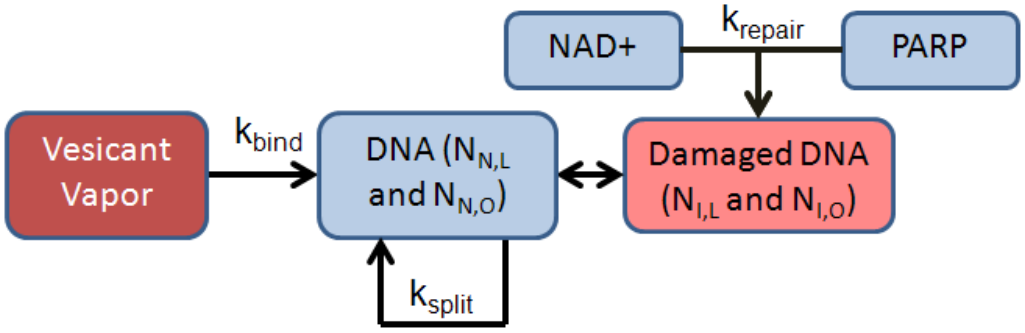

Figure A-4. Proportion of Healthy Cells in the Lungs ($N_{N,L}$) and Eyes ($N_{N,O}$)

The equations that describe the above diagram are:

$$\frac{d}{dt}N_{N,L} = k_{split} * (1 - N_{N,L}) * N_{N,L} - k_{bind} * D_i * N_{N,L} + k_{repair} * PARP_L * NAD_L * N_{I,L} \quad (A\text{-}5)$$

$$\frac{d}{dt}N_{N,O} = k_{split} * (1 - N_{N,O}) * N_{N,O} - k_{bind} * D_o * N_{N,O} + k_{repair} * PARP_O * NAD_O * N_{I,O} \quad (A\text{-}6)$$

Where:

1. D_i and D_o are the inhaled and ocular doses, respectively, given in milligrams and described in Section 5,
2. k_{split} is the rate of mitotic division, given in min^{-1},
3. k_{bind} is the rate vesicant binds with the DNA in healthy, normal cells in min^{-1},
4. k_{repair} is the rate of DNA repair, given in min^{-1}, and
5. NAD_L and NAD_o are the relative concentrations of NAD+ and PARP in the lungs and eyes, respectively, and are defined by the equations in Section 6.2.1.

A.5 Proportion of Injured Cells

Given the above statements, we can draw the system diagram for $N_{I,L}$ and $N_{I,O}$, shown in Figure A-5.

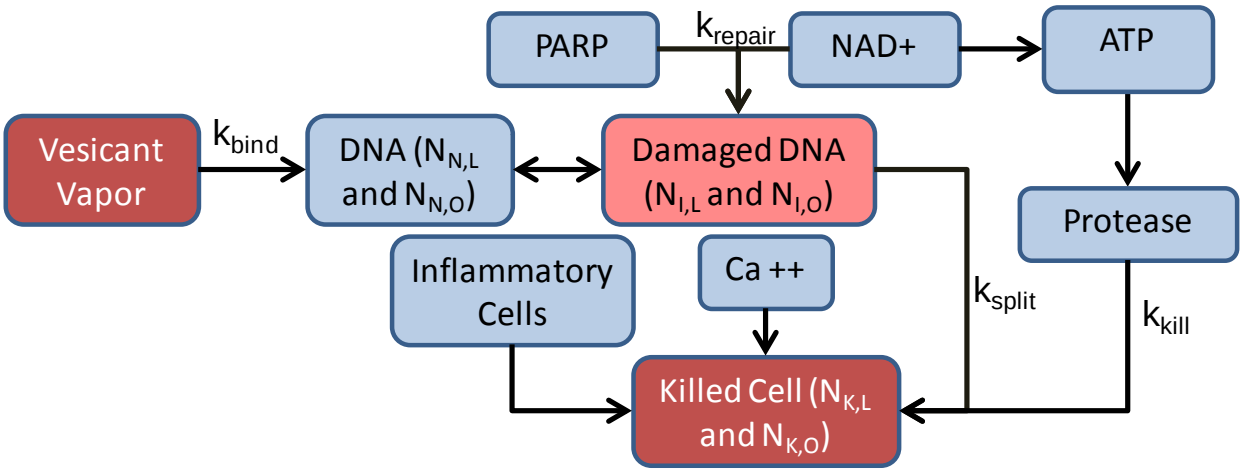

Figure A-5. Proportion of Injured Cells in the Lungs ($N_{N,L}$) and Eyes ($N_{N,O}$)

The equations that describe the above diagram are:

$$\frac{d}{dt}N_{I,L} = k_{bind} * N_{N,L} * D_i - k_{repair} * N_{I,L} * NAD * PARP - k_{kill} * Prot * Ca * Inf * N_{I,L} - k_{split} * (1 - N_{I,L}) * N_{I,L} \quad (A\text{-}7)$$

$$\frac{d}{dt}N_{I,O} = k_{bind} * N_{N,O} * D_o - k_{repair} * N_{I,O} * NAD * PARP - k_{kill} * Prot * Ca * Inf * N_{I,O} - k_{split} * (1 - N_{I,O}) * N_{I,O} \quad (A\text{-}8)$$

Where:

1. D_i and D_o are the inhaled and ocular doses, respectively, given in milligrams,
2. k_{split} is the rate of mitotic division, given in min^{-1},
3. k_{bind} is the rate vesicant binds with the DNA in healthy, normal cells in min^{-1},
4. k_{repair} is the rate of DNA repair, given in min^{-1},
5. k_{kill} is the rate of DNA death, given in min^{-1}, and
6. NAD, PARP, Prot, Ca, and Inf are the relative concentrations of NAD+, PARP, protease, calcium ions, and inflammatory cells, respectively, as defined in section 6.2.

A.6 Proportion of Necrotic Cells

We can draw a system diagram for necrotic cell death in the lungs and eyes, as shown in Figure A-6.

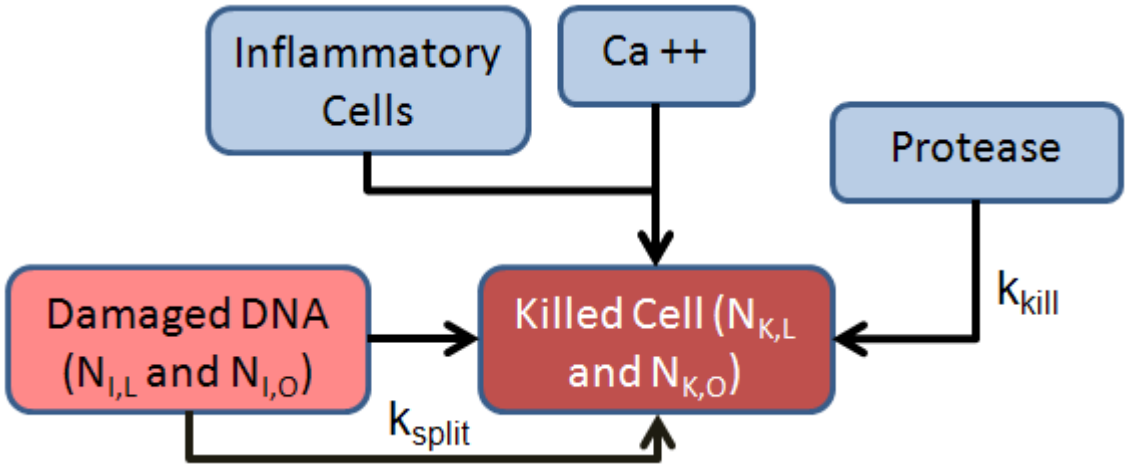

Figure A-6. Proportion of Necrotic Cells in the Lungs ($N_{K,L}$) and Eyes ($N_{K,O}$)

The equations that describes the above diagram are:

$$\frac{d}{dt}N_{K,L} = k_{split} * (1 - N_{I,L}) * N_{I,L} + k_{kill} * Prot * Ca * Inflam * N_{I,L} \quad \textit{(A-9)}$$

$$\frac{d}{dt}N_{K,O} = k_{split} * (1 - N_{I,O}) * N_{I,O} + k_{kill} * Prot * Ca * Inflam * N_{I,O} \quad \textit{(A-10)}$$

Where:

1. k_{split} is the rate of mitotic division, given in min^{-1}, and
2. k_{kill} is the rate of necrotic cell death, given in min^{-1}

A.7 The Repair Rate, Kill Rate, and HD Binding Rate for Ocular Exposures

For ocular exposures, we assumed that the mitotic division rate is still 0.004 hr^{-1}, since we found no data that supported changing the rate. We assumed that the other values could change,

due to differences in the cellular structure of the eye. Holding that value constant, we fit a 10mg/m^3 exposure for ten minutes to the highest ocular dose band in AMedP-8 (C). At that dose band, ocular injury peaks at 11 hours and recovers at 672 hours. The curves corresponding to our fit can be seen in Figure A-7. The values that correspond to the curve are tabulated in Table A-1.

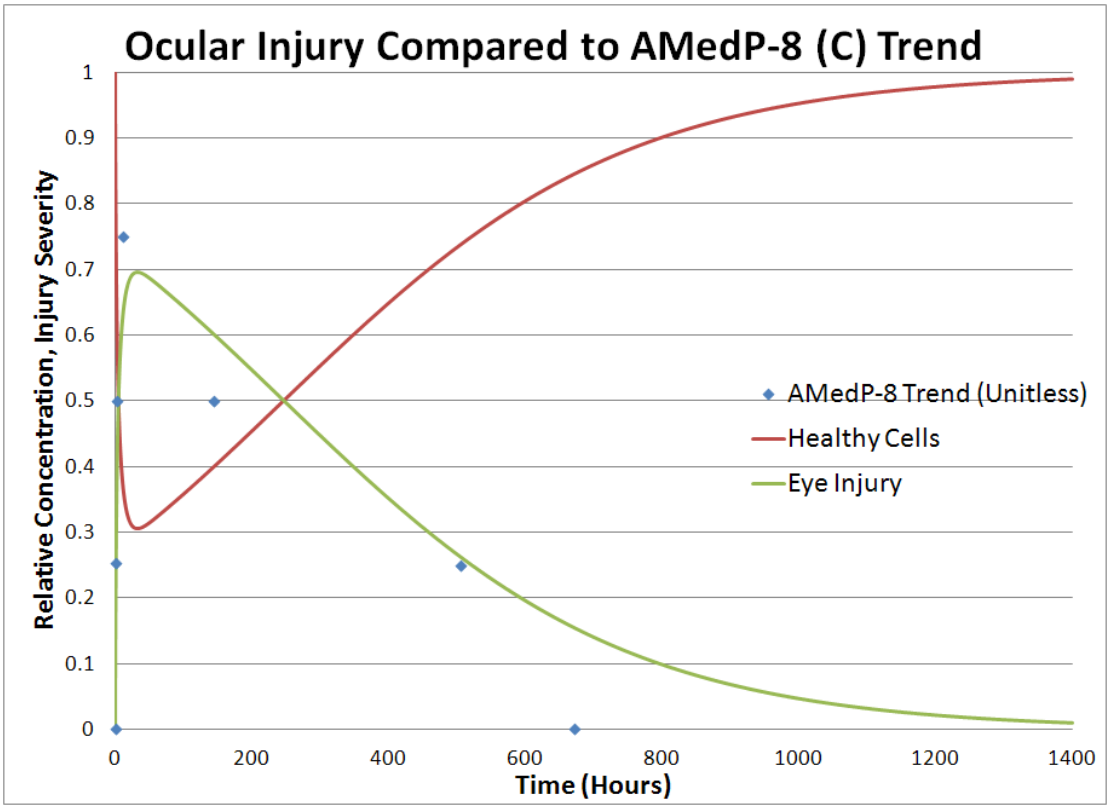

Figure A-7. Ocular Model Output for HD Compared to AMedP-8 (C)

Table A-1. HD Ocular Values for k_{bind}, k_{repair}, and k_{kill}

k_{bind} (hr^{-1})	k_{repair} (hr^{-1})	k_{kill} (hr^{-1})
0.4	10.0	5.8

Note the higher values for k_{bind}, k_{repair}, and k_{kill}, compared to the percutaneous exposure. This is due to the earlier peak time (11 hours vs. 24 hours) and the lower dosage (100 mg vs. 180 mg) used in the fit.

A.8 The Repair Rate, Kill Rate, and HD Binding Rate for Inhalation Exposures

For inhalation exposures we also assumed that the mitotic division rate is still 0.004 hr^{-1}, since we found no data that supported changing the rate. We assumed that the other values could change, due to differences in the cellular structure of the lung. Holding that value constant, we fit a 25 mg/m^3 exposure for 10 minutes to the 150-250 mg/m^3 inhalation dose band in AMedP-8

(C). At that dose band, lung injury peaks at 36 hours and recovers at 1008 hours. The curves corresponding to our fit can be seen in Figure A-8. The values that correspond to the curve are tabulated in Table A-2.

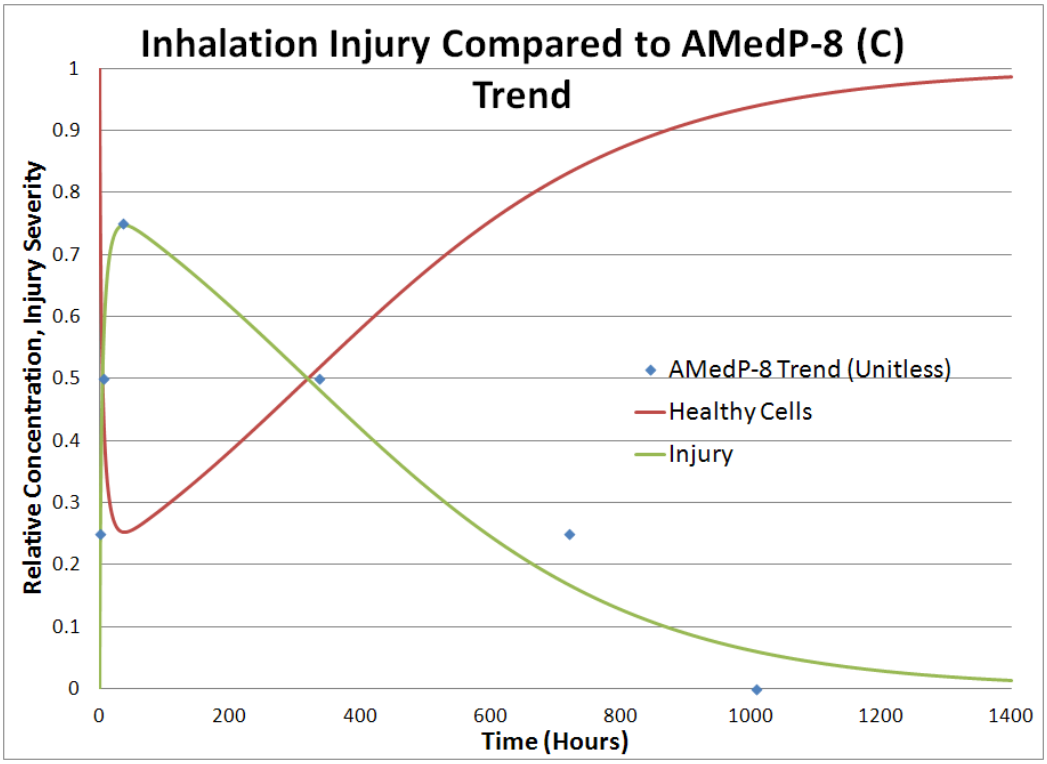

Figure A-8. Ocular Model Output for HD Compared to AMedP-8 (C)

Table A-2 – HD Inhalation Values for k_{bind}, k_{repair}, and k_{kill}

k_{bind} (hr^{-1})	k_{repair} (hr^{-1})	k_{kill} (hr^{-1})
0.35	10.0	2

Note that the values for k_{bind} and k_{repair} are equal to the ocular values and k_{kill} is the only different value. This is due to the slower recover time (1008 hours vs. 672 hours) used in the fit.

DEPARTMENT OF DEFENSE

DEFENSE THREAT REDUCTION
AGENCY
8725 JOHN J. KINGMAN ROAD
STOP 6201
FORT BELVOIR, VA 22060
ATTN: C. KILEY

DEFENSE TECHNICAL
INFORMATION CENTER
8725 JOHN J. KINGMAN ROAD,
SUITE 0944
FT. BELVOIR, VA 22060-6201
ATTN: DTIC/OCA

DEPARTMENT OF DEFENSE CONTRACTORS

QUANTERION SOLUTIONS, INC.
1680 TEXAS STREET, SE
KIRTLAND AFB, NM 87117-5669
ATTN: DTRIAC